# NATIONAL ADVISORY COMMITTEE FOR AERONAUTICS

**TECHNICAL NOTE**
No. 1520

# DE-ICING EFFECTIVENESS OF EXTERNAL ELECTRIC HEATERS FOR PROPELLER BLADES

By James P. Lewis

Flight Propulsion Research Laboratory
Cleveland, Ohio


Washington
February 1948

NATIONAL ADVISORY COMMITTEE FOR AERONAUTICS

TECHNICAL NOTE No. 1520

# DE-ICING EFFECTIVENESS OF EXTERNAL ELECTRIC HEATERS FOR PROPELLER BLADES

By James P. Lewis

## SUMMARY

An investigation has been conducted in the NACA Cleveland icing research tunnel to determine the icing protection provided by external rubber-clad blade heaters at several icing, heating, and propeller operating conditions. Data are presented to show the effect of propeller speed, ambient-air temperature, liquid-water concentration, heating-power density, duration of heating, and total cycle times on the power requirements and de-icing performance of the blade heaters. A comparison is made of the results of the icing-tunnel investigation with the results obtained during a flight investigation in natural icing conditions. The maximum ice-covered area on the blade was determined and also the maximum heated area required.

Power densities of $4\frac{1}{2}$ to 10 watts per square inch were required for effective cyclic de-icing with the best chordwise power distribution approaching uniformity. Cyclic heating times of approximately 24 seconds were required for effective de-icing at the conditions investigated with a ratio of heat-on to total cycle time of 1:4 giving the best performance. A mean rate of rise of the heater-surface temperature of approximately 1.1° F per second was obtained.

## INTRODUCTION

An investigation of the icing protection provided by electrically heated, external, rubber-clad propeller-blade heaters has been conducted in the NACA Cleveland icing research tunnel. The objectives of the investigation were to determine the icing protection provided by the blade heaters and the effect of several icing, heating, and propeller operating conditions on the heater performance. Several methods of obtaining icing protection for propellers have been proposed, including the use of alcohol or

other freezing-point depressants, internal electric blade heaters, and hot-gas de-icing. Flight investigations and theoretical analyses (references 1 and 2) have indicated that electric power requirements for ice prevention using continuously heated blade heaters exceed that which is readily available on current aircraft. The present investigation was primarily concerned with cyclic or intermittent blade heating as a practical system for use with current aircraft generators providing possible power and weight economies.

Data are presented to show the effect of propeller speed, air temperature, liquid-water concentration, heating-power distribution, and the duration of heat-on and heat-off time on the blade-heater power requirements and performance. The evaluation of the icing protection of the blade heaters in terms of the propeller aerodynamic performance was planned as part of the program. The performance measurements, however, were inconclusive because of critical and undetermined variations of the tunnel air velocity and the variations of thrust and torque measurements were of the same order of magnitude as the accuracy of the instrumentation.

A comparison is made of the results of the tunnel investigation with the performance of similar blade heaters during a flight investigation in natural icing conditions.

The conditions of the tunnel investigation were as follows: propeller speeds, 675 and 925 rpm at blade angles of 35° and 25°, respectively; air temperature, 2°, 11°, and 21° F, with corresponding liquid-water concentration of 0.2, 0.4, and 0.9 gram per cubic meter, respectively; total power per blade, 675 to 2110 watts; power density, 3.5 to 9 watts per square inch; heat-on time, 12 to 24 seconds, with ratios of heat-on time to total cycle time, 1:4 and 1:8.

## APPARATUS AND INSTRUMENTATION

The propeller on which the investigation was conducted was mounted on a modified airplane fuselage located in the diffuser section of the icing research tunnel. The location of the installation and of the water sprays, together with details of the setup, are shown in figure 1. The propeller, which was driven by an aircraft engine located in the airplane fuselage, was a 10-foot, 5-inch diameter, three-blade, hollow steel propeller having 614-101.5-21 blades. The blade-form characteristics are given in figure 2. Electric power for the blade heaters was supplied through autotransformers and an electronic timer and was conducted to the propeller through five circuits and a slip-ring assembly mounted at the rear of the propeller hub.

Propeller-blade heaters. - The blade heaters consisted of a series of parallel chromel ribbon heating elements laid radially over two layers of neoprene and covered with an outer layer of abrasion-resisting neoprene, the ribbons being separated by fabric insulation. Details of the heater construction are shown in figure 3. A view of the heaters before application of the outer layer is shown in figure 4(a) and the completed heater installation is shown in figure 4(b). The heated area was 45 inches long extending to 88 percent of the radius. The chordwise coverage extended to 38 and 46 percent of the chord on the camber and the thrust faces, respectively, at the 75-percent radius station.

The chromel ribbons were arranged in nine heating elements per blade; the two elements at the leading edge and a single element at the rear of the thrust face were 1/2 inch wide and the remaining six elements were 1 inch wide. The nominal resistances were 24 and 12 ohms for the narrow and wide elements, respectively. Power leads from the nine elements of each blade were connected at a terminal ring in a series-parallel arrangement to the five power supply circuits, thus permitting various combinations of the heating elements and power distributions. A diagram of the circuit for a typical power distribution is shown in figure 5.

Instrumentation. - Instrumentation was provided to measure the propeller rotational speed, ambient-air temperature, tunnel air velocity, blade-surface temperatures, power to the heating elements, and heat-on and cycle times.

The velocity distribution at the plane of the propeller was determined from a survey of the total and static pressures with the propeller removed. The average velocity at the 75-percent propeller radius station was based on the static-pressure drop through the contraction section of the tunnel, which was then used as an indication of the tunnel air velocity. The tunnel air temperature was indicated by two thermocouples mounted on the tunnel turning vanes on each side of the fuselage approximately 15 feet downstream of the propeller. The propeller speed was measured by a standard aircraft tachometer with an accuracy of ±3 percent.

Surface temperatures were measured by temperature-sensitive electric resistance gages that were similar to strain gages. The gages were constructed of 1.2 mil nickel wire and covered an area 3/8 by 7/16 inch. The gages were directly cemented to both the heated and unheated areas, in such a manner as to minimize strains due to propeller operation and were then covered with a thin coat of rubber cement as a protection against abrasion. A total of

40 gages was installed on two of the three blades. The installed gages are indicated in figure 4(b). A multiple-bridge circuit was used that was compensated by the method described in reference 3 to minimize slip-ring and contact-resistance errors. (See fig. 6.) Both indicating and film-recording galvanometers were provided to indicate bridge unbalance. Manual selector switches permitted the continuous recording of three temperatures and, in addition, a motor-driven selector switch provided successive records of all blade temperatures. The temperature gages were statically calibrated before and after installation on the blades. The accuracy of the gages before installation, and independent of the circuit, was approximately $\pm 1^{\circ}$ F but, because of the bridge circuit, the method of installation, and the nature of the calibration, the total accuracy of the system is estimated to be within $\pm 5^{\circ}$ F.

Observations of the rotating propeller were made by using a stroboscopic lighting system consisting of a battery of four flash lamps synchronized with the propeller. Photographs of the propeller ice formations were also made during rotation using this lighting system. As these photographs were unsuitable for reproduction, they were used only in the analysis of the heater performance. The locations of the flash lamps and the camera are shown in figure 1(c).

Water spray system. - Icing conditions were simulated by spraying water into the refrigerated tunnel air stream. A battery of 46 standard air-atomizing nozzles enclosed in a steam-heated fairing were located around the periphery of the tunnel immediately ahead of the contraction section. The spray water discharged perpendicularly to the air stream and was refrigerated to approximately $38^{\circ}$ F before discharge to assist in obtaining supercooled droplets.

Icing conditions in the tunnel were determined by the rotating cylinder method (reference 4). A survey of the liquid-water distribution was made using a grid consisting of six vertical cylinders spaced 23 inches apart. The cylinders were 2 inches in diameter and rotated about their axes at 12 rpm. The ice accretions on the cylinders at 48 points were measured by special type calipers. Droplet size was measured by two double rotating cylinder assemblies. The icing-survey equipment is shown in figure 7.

## CONDITIONS AND PROCEDURE

The physical parameters used in this investigation can be divided into three main groups: (1) propeller operating conditions, (2) icing conditions, and (3) blade-heating conditions.

Operating conditions. - From the velocity survey at the plane of the propeller, it was found that the highest velocity at 75 percent of the propeller radius and full tunnel airspeed was 150 miles per hour. The velocity distribution across the tunnel was fairly uniform for the first 50 percent of the propeller radius but the velocity then decreased sharply with a value at the propeller tip approximately 70 percent of that at the center. As most of the thrust of this propeller is developed in the portion of the blade beyond the 30-percent radius, the average velocity at the 75-percent radius was used as the test velocity. A nominal value of 120 miles per hour was held during the entire investigation. This velocity allowed a tunnel power reserve to compensate for tunnel icing and also allowed operation at advance diameter ratios of 1.1 and 1.4 for blade angles of 25° and 35° and propeller speeds of 925 and 675 rpm, respectively. The higher speed corresponds to a cruising condition for this propeller. The speed of 675 rpm, although rather low for this propeller, is representative of the low-speed range for large propellers on installations using a large speed-reduction ratio. In addition, the differential in speed and blade angle was expected to be great enough to show any significant changes in icing or heating requirements with these variables. Because of the nature of the velocity distribution, the shank end of the blades operated at small negative angles of attack; however, as the blade section at this region becomes nearly cylindrical, such negative angles would have a very slight effect on the propeller performance and the heat requirements and therefore would affect only the region over which heat is required. Icing of the tunnel is known to alter the velocity distribution and result in an increase in the velocity at the center of the propeller and further reduce the tip velocities. All investigations were made in fixed propeller pitch with manual throttle speed control.

Icing conditions. - The investigation was made at three different icing conditions that were defined by the ambient-air temperature, liquid-water concentration, and droplet size. The conditions used were at nominal air temperatures of 2°, 11°, and 21° F with corresponding liquid-water concentrations of 0.2, 0.4, and 0.9 gram per cubic meter, respectively. The indicated temperature of the tunnel air was maintained within ±1° F at operating conditions. The thermocouples used to measure the tunnel air temperature were incompletely shielded from the impinging water and the ice; hence, they did not give an accurate reading at all conditions. From a recent calibration of these unshielded thermocouples against completely shielded and isolated thermocouples, a correction was obtained that was applied to the data presented. The calibration also indicated the accuracy of the air-temperature measurements during icing conditions to be approximately ±3° F for temperatures below 25° F.

The variation of the liquid-water concentration with air temperature is shown in figure 8(a) and the radial distribution of liquid-water concentration is shown in figure 8(b). The values of liquid-water concentration recommended at the Mount Washington Observatory-Weather Bureau meeting of June 1945 and an envelope of values from numerous ground and flight observations are also shown in figure 8(a). The marked decrease in liquid-water concentration with decreasing air temperature (fig. 8(a)) for a constant input of spray water indicates that the amount of frozen-water particles increased with decreasing temperature. As shown in figure 8(b), the liquid-water concentration decreased toward the propeller tip, particularly at temperatures below 10° F.

An average volume maximum droplet size of 55 microns was found but no consistent variation with temperature was obtained. For the range of air temperatures from 0° to 32° F, droplet sizes of 15 to 30 microns were recommended at the Mount Washington Observatory-Weather Bureau meeting of June 1945. This difference between the recommended and the tunnel droplet size was, however, considered unimportant as the propeller airfoil section has a leading edge of very small radius. As indicated in reference 3, the blades would have a collection efficiency very close to 100 percent for all droplet sizes larger than those recommended. Collection efficiency is defined as the ratio of the cloud intercepted to the cloud available. Small variations in collection efficiency near 100 percent would, however, have an important effect in determining the chordwise extent of icing.

Although the liquid-water concentrations used in the tunnel were less than those recommended, they were considered to be representative of the moderate-to-light icing conditions normally encountered. The limited data given in reference 4, however, showed the greatest frequency occurring in the range of 0.1 to 0.6 gram per cubic meter. Time limitations prevented repeating the tunnel calibration of liquid-water concentration and distribution during or after the investigation. Visual observations of the spray cloud and the icing of the setup and the tunnel, together with readings of the water flow and the spray pressures, indicated, however, that the icing conditions remained reasonably constant throughout the research program.

Blade-heating conditions. - The heating-power distribution of the heaters is shown in figure 9. Not all configurations were investigated at all icing and operating conditions. The extent of investigation of each configuration was determined by the degree of icing protection obtained. Power densities greater than those used were prevented by the electrical limitations of the heaters

and the power circuit. Pattern 1 is an approximation of the heating power used in previous flight investigations. The other configurations were obtained by increasing both the chordwise coverage and the power densities. The powers listed in figure 9 are for a single blade only. It was desired to obtain controlled de-icing with cyclic heating by sufficiently melting the inner face of the ice during each cycle to allow the centrifugal forces to throw off the ice formations before they became large enough to shed automatically and cause damage or unbalance. The heating patterns were selected to obtain this result with maximum ice removal for minimum expenditure of energy and also to minimize the runback and refreezing of melted ice on the unheated areas. The radial variation of the heater coverage on the blade in percentage of chord is presented in figure 10. The location of the heater elements is also shown.

The duration of the heat-on and total cycle time was varied to obtain the following four combinations:

| Ratio of heat-on to total cycle time | Heat-on time (sec) | Total cycle time (sec) |
|---|---|---|
| 1:4 | 12 | 48 |
| | 24 | 96 |
| 1:8 | 12 | 96 |
| | 23 | 184 |

These times and cycles were selected on the basis of previous investigations, the estimated rate of temperature rise, and the estimated icing rate.

## RESULTS AND DISCUSSION

Ice formations on unheated blades, the results of cyclic de-icing, and a comparison of the results of the tunnel investigation with those obtained in flight are discussed.

Ice formation on unheated blade. - Typical ice-covered areas on both the thrust and camber face for the two propeller speeds at each of the three ambient-air temperatures are shown in figures 11 to 13. The maximum percentage of ice-covered element area on each of the nine heating elements during the unheated condition for the speed and the temperature conditions studied is presented in table I. These iced areas were determined from observations and photographs made during the unheated part of the heat cycle and during a few

icing studies. Observations indicated that the extent of the ice-covered areas did not change materially for icing periods greater than approximately 30 seconds, except at air temperatures of 21° and 2° F. At a temperature of 21° F, a large proportion of the droplets impinging on the blade did not freeze because of the high blade-surface temperature and an eroding effect was noticed on the small ice formations present. At the low temperature (2° F), the large percentage of frozen droplets in the spray cloud caused the initial ice formations to erode inward from the tip to approximately 50 percent of the blade radius within a period of about 3 to 5 minutes.

The data given in figures 11 to 13 and table I refer to the ice-covered element areas only and do not indicate the thickness of the ice formations. No direct measurements of the ice thickness were made for all conditions, but from visual observations and rough measurements a maximum ice thickness of approximately 3/8 inch after 3 minutes of icing was obtained at the leading edge of the shank end of the blade and gradually decreased towards the ice-free areas at the tip and trailing edge.

No great variation in the iced area was obtained for the conditions investigated. The effect of propeller speed on the iced area for the conditions of this investigation was negligible in most cases. A greater variation was due to the icing conditions (ambient-air temperature and liquid-water concentration). At the highest temperature and water concentration (21° F and 0.9 gram/cu m), a rough and irregular formation of glaze ice was obtained. At these conditions, the greatest variation in iced area with propeller speed was observed. The large variation was probably caused by the necessity of a smaller force to throw off the heavy wet ice formations and also by a sufficient difference in the kinetic temperature rise to cause a larger portion of the blade to be above a temperature of 32° F at the higher speed. At 11° F and 0.4 gram per cubic meter, the iced area on the camber face was only slightly less than at 21° F but the ice was harder, being more of a rime formation, and adhered strongly to the blade heater and the metal. On the thrust face, a decrease in the iced area was obtained with the greatest difference occurring at the lower speed. Lowering the temperature from 11° to 2° F again slightly decreased the ice-covered area on both faces. This ice was extremely hard and smooth.

It should be noted that the iced areas referred to in figures 11 to 13 and table I are the heater-element areas and do not include the unprotected area of the blade. Ice occurred as small deposits on the leading edge beyond the heater area and at the rearward edge of the heater at approximately 50-percent radius although very little was noted on the unprotected portion of the

blade. As previously indicated, the extent of the blade icing was determined from the area iced during the unheated part of the heat cycles and during a few icing studies and hence is not fully representative of a complete study of blade icing. In addition, the ice formations are typical for only this blade and would probably differ for other blade designs. From a consideration of the ice formations and the kinetic temperature rises obtained at the conditions investigated, there is a possibility that the ice formations which would be obtained at higher rotational speeds would be of a less serious nature both as to the area covered and the type of ice. Increasing the water concentration with the other conditions remaining the same would probably result in a thicker and different type of ice formation with very small change in the iced area.

The results given in figures 11 to 13 and table I show that the maximum chordwise extent of icing was found to cover a surface width on both faces of the blade varying from $6\frac{1}{2}$ inches at the shank to 3 inches at the tip end of the heater. The radial coverage varied from 85 to 100 percent of the blade radius.

Cyclic de-icing. - The results of a preliminary study of the power and the de-icing times required for an initial ice removal are shown in figure 14. Heat was applied after the blades had been allowed to ice for 3 minutes and the time to remove ice from the various areas was noted. Although there was not a close degree of consistency in the time for ice removal, the results do indicate limits for power density and de-icing times. For the conditions indicated on figure 14, a maximum de-icing time of approximately 40 seconds would be required at a power density of 3.5 watts per square inch. An upper limit for power density of approximately 8 to 9 watts per square inch is indicated with a corresponding de-icing time of 2 to 8 seconds. Raising the ambient-air temperature from 11° to 20° F reduced the heat-on time about one-half at the same power density. The data indicate a greater power or time requirement at 925 rpm than at 675 rpm for the same ambient-air temperature.

The results of the investigation of cyclic de-icing are presented in table II as the percentage of the heater area that was ice-covered for the different conditions. The data given in table II indicate the relative amount of de-icing obtained with each power-distribution pattern for each set of conditions averaged over the entire heated area.

When the heating cycle was changed from 12-96 to 24-96 with pattern 5 at 2° F, considerably better de-icing occurred on both

faces. At the 23-184 cycle, which had the same energy input as the 12-96 cycle, the de-icing with pattern 5 showed a considerable increase on the thrust face and very little change on the camber face. Pattern 5 gave better de-icing than pattern 9 under the same conditions at 2° F.

At an ambient-air temperature of 11° F and corresponding liquid-water content of 0.4 gram per cubic meter, the smallest ice-covered area was obtained with the 24-96 heating cycle, pattern 4 giving slightly better performance than patterns 8 and 9. At the 23-184 cycle, pattern 5 gave the best performance, particularly on the camber face. At both the 12-48 and 12-96 cycles, extremely poor results were obtained for all the patterns, particularly on the camber face. At 21° F, good de-icing was obtained for all distributions with the exception of pattern 2 at 675 rpm and the 12-96 cycle.

The de-icing effectiveness of each of the heater elements for several different conditions of propeller speed, ambient-air temperature, power density, heat-on time, and cycle time are presented in figure 15. The de-icing effectiveness was defined as $\left(100 - \frac{A_1}{A_2}\right)$ where $A_1$ is the percentage of ice-covered element area following heating and $A_2$ is the percentage of ice-covered element area previous to heating. These percentages were obtained from a close study of photographs taken during and after de-icing together with visual observations of the de-icing obtained. No general relation of de-icing effectiveness was obtained with any of the variables of propeller speed, ambient-air temperature, power density, and heat-on and cycle times. The maximum over-all effectiveness for all conditions was obtained with pattern 9 (fig. 15(i)). High effectiveness was also obtained with patterns 1 and 2 (patterns are the same as those shown in fig. 9) for a 12-96 cycle at an ambient-air temperature of 21° F (figs. 15(a) and (b)) and also with pattern 5 for the 23-184 cycle at 11° F (fig. 15(e)). In practically every case, the effectiveness on the camber face was considerably less than that obtained at the leading edge and the thrust face. Neither raising the power density at the rear of the heater and thus approaching a uniform distribution as in patterns 5 and 9 nor the use of an unsymmetrical distribution (pattern 5) gave complete ice removal on the camber face for all icing and speed conditions.

Photographs of typical residual ice formations are shown in figures 16 to 23. The chordwise limit of the heated area is

indicated on each photograph. The residual formations in some cases include ice formations formed after the final heating period. Successive layers of ice can be seen on many of the photographs resulting from the intermittent removal and rebuilding of ice. (See figs. 22(b) and 22(d).)

With optimum heating power density, heat-on time, and cycle time the following results were observed (table I and figs. 16 to 23): At an ambient-air temperature of 21° F, effective de-icing was obtained at the leading edge with power densities as low as $4\frac{1}{2}$ watts per square inch; both the 12-48 and 12-96 cycles gave effective de-icing. At 11° F, a power density of 7 to 9 watts per square inch was required for effective de-icing. Both the 24-96 and the 23-184 cycles gave good results at these power densities although slightly more efficient de-icing was obtained with the 96-second cycle time. Power densities of 7 to 9 watts per square inch were not completely effective at 2° F but it is estimated that a density of 10 watts per square inch would be satisfactory at this temperature. The best results at 2° F were obtained with the 24-96 and 23-184 cycles.

Typical curves of the time variation of blade temperature for several patterns, propeller speeds, heat-on times, cycle times, and icing conditions are shown in figures 24 to 31. The shape of the heating and cooling curves are very similar for the various radial and chordal positions, speed, heating, and icing conditions. As might be expected, the presence of ice formations precludes any correlation between the blade temperatures at various chordal positions except as affected by differences in local heating power densities.

A greater divergence in the shape of the cooling curves than in the heating curves was obtained for practically all conditions, possibly because new ice deposits were forming during the cooling period. From the time of heat cut-off, the temperatures dropped sharply for approximately 75 to 90 percent of the difference between the peak and the minimum temperature in a period approximately equal to the heat-on time. Thereafter the rate of cooling reduced quickly, the minimum temperatures being reached in a period two to three times the heating period. The rate of cooling increased as the surface temperature increased. In general, the temperatures at all points approached their minimum values in about the same period of time for each combination of heat-on and cycle time. In addition, the temperature at practically every point returned after each heat application to the value at the start of the cycle with

the exception of the curves in figure 31(a), which were initial cycles in which the initial injection of water disturbed the stabilized conditions by momentarily raising the ambient-air temperature.

The chordwise variation of the blade-surface-temperature increment during cyclic de-icing at four radial stations for the various conditions is presented in figure 32. The temperature increment is defined as the rise in blade-surface temperature from the application of heat at the start of the cycle to the maximum temperature obtained at the time of heat cut-off. Only a few values of temperature increment at the leading edge are presented because the gages at this position were quickly damaged by water erosion. Little change appears in the temperature increment at the four radial stations. This effect is probably due to the presence of ice, which would obscure most of the effects of kinetic heating or convective cooling and thus the local power density would have the dominant effect. As shown in figures 32(a) and 32(b), the increment for pattern 5 was fairly constant on the heated area and decreased sharply on the unheated area of the thrust face. For patterns 8 and 9, which had a nearly uniform power density over all the area, the increment was practically constant over the entire heater area. (See figs. 32(c), 32(d), and 32(e).) The inaccuracy of the air- and blade-temperature measurements preclude making any further correlation of the blade-temperature increment with icing or operating conditions.

Rates of blade-temperature rise were obtained by dividing the temperature increment by the heating time. Rates of rise of 0.5° to 2.4° F per second were obtained with a mean value of approximately 1.1° F per second occurring over a chordwise distance of 3 inches of heated area on each face of the blade. For the range of conditions investigated, the average rate of rise appeared independent of the air temperature.

Comparison of tunnel and flight results. - In order to establish the validity of the icing-tunnel data, a comparison was made between typical results obtained from a flight investigation in natural icing conditions and those obtained in the tunnel. Photographs of icing and de-icing obtained in flight are shown in figures 33 and 34.

The propeller used in the flight investigation was a three-blade, hollow, steel propeller of $12\frac{1}{2}$-foot diameter. The blades had extended trailing edges giving a maximum chord of 15 inches. The blade airfoil section and leading-edge radius were similar to those of the propeller used in the tunnel investigation. An external

rubber-clad electrical blade heater of the wire-inserted type was used. The heater was 49 inches long and $5\frac{3}{4}$ inches wide extending to 80 percent of the radius and to 19 percent of the maximum chord on both faces. A concentrated heating area $2\frac{3}{16}$ inches wide at 7.5 watts per square inch was centered on the leading edge and the remainder of the heater was at $3\frac{3}{4}$ watts per square inch. These densities were obtained by spacing the heating wires at 1/16- and 1/8-inch intervals, respectively. The heater was designed to operate at a power input of 1470 watts per blade at 110 volts.

The results shown in figure 33 were obtained at a true airspeed of 190 miles per hour; propeller speed, 955 rpm; ambient-air temperature, -10° F; liquid-water concentration, 0.1 gram per cubic meter; blade angle, 35°; droplet size, 11 microns. The formation shown in figure 33(a) was obtained after 8 minutes of icing. The ice appeared smooth and hard and was confined to the leading-edge area and extended to approximately the 75-percent-radius station. A similar type of ice, although covering a greater area, was obtained in the tunnel at 2° F and 0.2 gram per cubic meter. (See figs. 20(a) and 20(b).) Fairly good de-icing was obtained, as shown in figure 33(b). Small residual formations and a slight amount of runback at the shank end of the blade are evident.

Figure 34(a) shows the ice formation obtained after 16 minutes at the following conditions: true airspeed, 213 miles per hour; propeller speed, 1070 rpm; ambient-air temperature, 25° F; liquid-water concentration, 0.2 gram per cubic meter; blade angle, 34°; droplet size, 18 microns. A rough, irregular formation of semi-glaze ice was obtained. The formation was again confined fairly well to the leading edge although it covered a greater chordwise distance than at -10° F. A somewhat similar type of ice was obtained in the tunnel (figs. 17(a) to 17(d)). Complete de-icing was obtained upon the application of heat (fig. 34(b)).

In comparing the flight results with the tunnel data, several factors must be considered. Because the propeller used in flight had a greater diameter and operated at higher speeds, greater kinetic temperature rises were obtained than in the tunnel investigation. Hence the heating requirements may be less at similar icing conditions. The water concentration at the lower flight temperature (-10° F) was approximately equal to an extrapolation of the curve of tunnel conditions, but is considerably lower than either the envelope curve or values recently obtained at the same temperature. At the higher flight temperature (25° F), the liquid-water

concentration was approximately one-fifth that obtained in the tunnel. The droplet sizes encountered in flight were small enough to give a collection efficiency of 90 to 95 percent. Hence the impingement area was confined to a small region on the leading edge. The large droplets obtained in the tunnel resulted in practically 100-percent collection efficiency, which caused icing over a greater area. These considerations, together with the fact that small positive and negative angles of attack were obtained in the tunnel (resulting from the nonuniform velocity distribution), help to explain fairly adequately the differences in the extent and the location of the iced areas. Because the ice formations in flight were confined to the leading edge, the power density at this location (7.5 watts/sq in.) must be used in comparing the flight and the tunnel data. Approximately this same value was used in the tunnel investigations on the leading edge with the exception of patterns 1 and 9. In figure 14, it can be seen that ice removal at 20° F and 7.5 watts per square inch was obtained in 2 to 8 seconds.

The frequency with which any combination of liquid-water concentration, droplet size, and air temperature occurs in natural icing conditions is not fully known. The limited data in reference 2, however, indicate that the tunnel conditions are on the high side of the maximum frequency, whereas those cited from typical flight results are slightly low. The power and the heated area requirements shown by the tunnel data may therefore be slightly conservative; whereas those from flight may prove marginal in some cases.

## SUMMARY OF RESULTS

The results of this investigation of external rubber-clad blade heaters are summarized as follows:

1. The experimental heater area included the maximum ice-covered area for all the conditions investigated except for small areas at the blade tip and at the 50-percent radius on the camber face.

2. Heating pattern 9 gave the most effective over-all de-icing, whereas pattern 5 was only slightly less effective. All the patterns investigated left residual ice formations on the camber face at the rear margin of the heated area.

3. At an ambient-air temperature of 21° F, a power density of $4\frac{1}{2}$ watts per square inch gave satisfactory de-icing. Lowering the

ambient-air temperature to 11° F required an increase in power density of 7 to 9 watts per square inch. No effective de-icing was obtained at 2° F for the power densities investigated.

4. Cyclic heat-on times of 23 and 24 seconds gave the best de-icing through the range of conditions investigated. The 12-second heat-on time was effective only at ambient-air temperatures greater than 21° F. Total cycle times of 96 and 183 seconds were satisfactory. In most cases the best performance was obtained with a ratio of heat-on to total cycle time of 1:4.

## CONCLUSIONS

From this investigation, several significant conclusions can be drawn concerning the requirements for the design and the operation of an external rubber-clad electric blade heater. Due consideration must be given to the difference between the simulated and the natural icing conditions and to the special construction of the experimental heating element.

1. The maximum heated area should be at least equal to the maximum ice-covered area. The minimum required heated area cannot be exactly defined in the absence of more complete data concerning the frequency of icing conditions and the effects of residual ice formations on propeller performance. The radial extent of heating depends upon the kinetic temperature rise and, therefore, is a function of the propeller diameter, rotational speed, and forward velocity.

2. All the results showed a need for more heat on the rear margin of the heated area of the camber face indicating the optimum distribution to be one approaching chordwise uniformity.

3. The estimation is made that power densities of $4\frac{1}{2}$ to 10 watts per square inch are required for the temperature range of 21° to 2° F.

Flight Propulsion Research Laboratory,
National Advisory Committee for Aeronautics,
Cleveland, Ohio, September 3, 1947.

## REFERENCES

1. Scherrer, Richard, and Rodert, Lewis A.: Tests of Thermal-Electric De-Icing Equipment for Propellers. NACA ARR No. 4A20, 1944.

2. Scherrer, Richard: An Analytical Investigation of Thermal-Electric Means of Preventing Ice Formation on a Propeller Blade. NACA ACR No. 4H31, 1944.

3. Warshawsky, Isidore: A Multiple Bridge for Elimination of Contact-Resistance Errors in Resistance Strain-Gage Measurement. NACA TN No. 1031, 1946.

4. Vonnegut, B., Cunningham, R. M., and Katz, R. E.: Instruments for Measuring Atmospheric Factors Related to Ice Formations on Airplanes. M.I.T., Dept. Meteorology, De-Icing Res. Lab., April 1946.

TABLE I - MAXIMUM PERCENTAGE OF ELEMENT

AREA COVERED BY ICE ON UNHEATED BLADE

| Ambient-air temperature (°F) | Propeller speed (rpm) | Area covered by ice (percent) | | | | | | | | |
|---|---|---|---|---|---|---|---|---|---|---|
| | | Blade-heater element | | | | | | | | |
| | | Camber face | | | | Thrust face | | | | |
| | | 4 | 3 | 2 | 1 | 5 | 6 | 7 | 8 | 9 |
| 1 - 3 | 675 | 97 | 70 | 50 | 35 | 92 | 37 | 15 | 5 | 0 |
| 1 - 3 | 925 | 97 | 80 | 60 | 45 | 93 | 38 | 20 | 5 | 0 |
| 9 - 13 | 675 | 100 | 97 | 85 | 72 | 100 | 42 | 3 | 0 | 0 |
| 9 - 13 | 925 | 97 | 92 | 87 | 75 | 92 | 23 | 3 | 0 | 0 |
| 19 - 22 | 675 | 100 | 100 | 95 | 83 | 100 | 100 | 65 | 48 | 10 |
| 19 - 22 | 925 | 100 | 100 | 95 | 80 | 100 | 92 | 0 | 0 | 0 |

National Advisory Committee
for Aeronautics

TABLE II - RESULTS OF CYCLIC DE-ICING

NATIONAL ADVISORY
COMMITTEE FOR AERONAUTICS

| Heating cycle | | Heating pattern | Power per blade (watts) | Air temperature (°F) | Liquid-water concentration (gram/cu m) | Heater area covered by ice, percent | | | | | | | |
|---|---|---|---|---|---|---|---|---|---|---|---|---|---|
| | | | | | | Propeller speed, 675 rpm | | | | Propeller speed, 925 rpm | | | |
| | | | | | | Thrust face | | Camber face | | Thrust face | | Camber face | |
| Heat-on time (sec) | Total time (sec) | | | | | Unheated | Heated | Heated | Unheated | Unheated | Heated | Heated | Unheated |
| 12 | 48 | 2 | 775 | 11 | 0.4 | — | — | — | — | 0 | 26 | 37 | 60 |
| | | 2 | 775 | 21 | .9 | 24 | 5 | 0 | 15 | — | — | — | — |
| 12 | 96 | 1 | 675 | 21 | 0.9 | 7 | 1 | 0 | 10 | 2 | 8 | 0 | 17 |
| | | 2 | 775 | 21 | .9 | 4 | 21 | 26 | 29 | 0 | 3 | 0 | 8 |
| | | 3 | 900 | 11 | .4 | 0 | 16 | 28 | 48 | 0 | 27 | 21 | 44 |
| | | 5 | 1845 | 2 | .2 | — | — | — | — | 0 | 27 | 37 | — |
| | | 6 | 1450 | 11 | .4 | — | — | — | — | — | 10 | 44 | — |
| | | 7 | 1810 | 11 | .4 | — | — | — | — | — | 5 | 33 | — |
| | | 8 | 1935 | 11 | .4 | — | 9 | 38 | — | — | — | — | — |
| 24 | 96 | 2 | 775 | 2 | 0.2 | 0 | 16 | 24 | 43 | — | — | — | — |
| | | 4 | 1530 | 2 | .2 | — | — | — | — | 0 | 4 | 29 | 37 |
| | | 4 | 1530 | 11 | .4 | — | — | — | — | 2 | 2 | 10 | 49 |
| | | 5 | 1845 | 2 | .2 | — | — | — | — | 0 | 14 | 23 | — |
| | | 8 | 1935 | 11 | .4 | — | 10 | 18 | — | — | 14 | 19 | — |
| | | 9 | 2110 | 2 | .2 | 0 | 7 | 35 | — | 0 | 5 | 22 | — |
| | | 9 | 2110 | 11 | .4 | 0 | 10 | 15 | — | 0 | 6 | 12 | — |
| 23 | 184 | 4 | 1530 | 11 | 0.4 | — | — | — | — | 0 | 7 | 28 | 52 |
| | | 5 | 1845 | 2 | .2 | — | — | — | — | 0 | 3 | 19 | — |
| | | 5 | 1845 | 11 | .4 | — | — | — | — | 0 | 5 | 3 | — |
| | | 8 | 1935 | 11 | .4 | — | 10 | 30 | — | — | 12 | 28 | — |
| | | 9 | 2110 | 2 | .2 | 0 | 12 | 28 | — | 0 | 7 | 24 | — |
| | | 9 | 2110 | 11 | .4 | 0 | 9 | 20 | — | 0 | 8 | 21 | — |

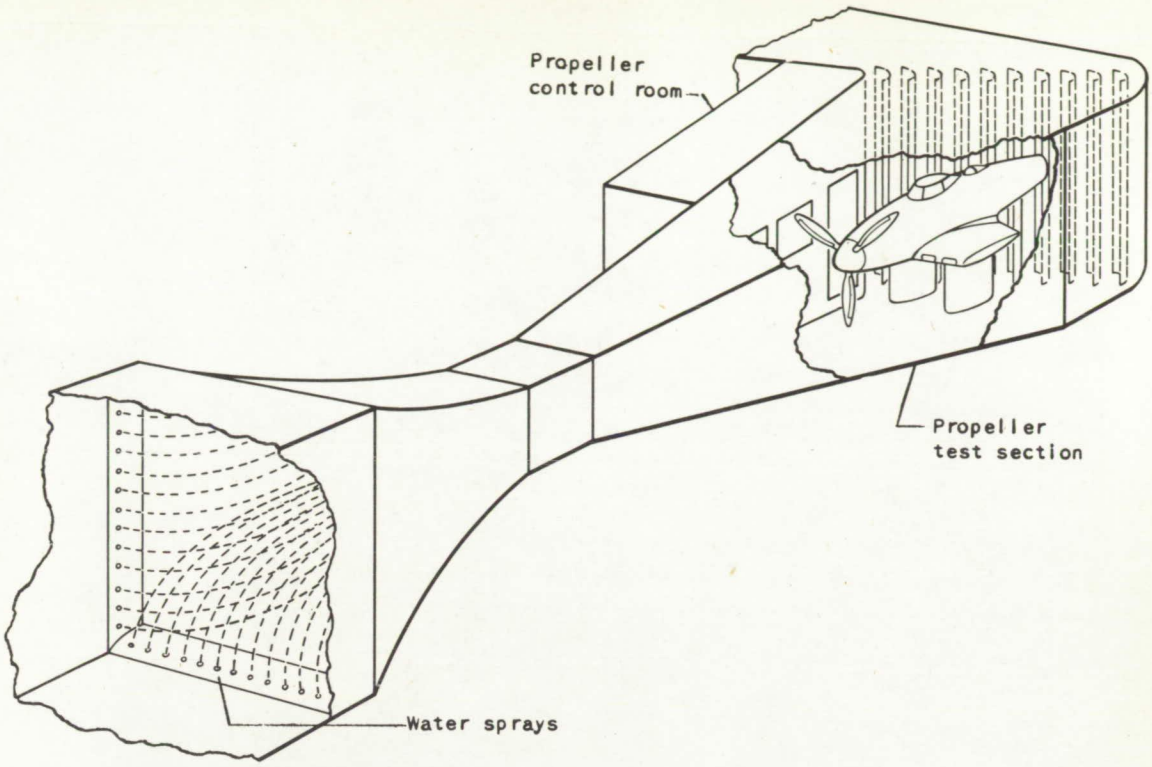


(a) Location of propeller setup and water sprays.

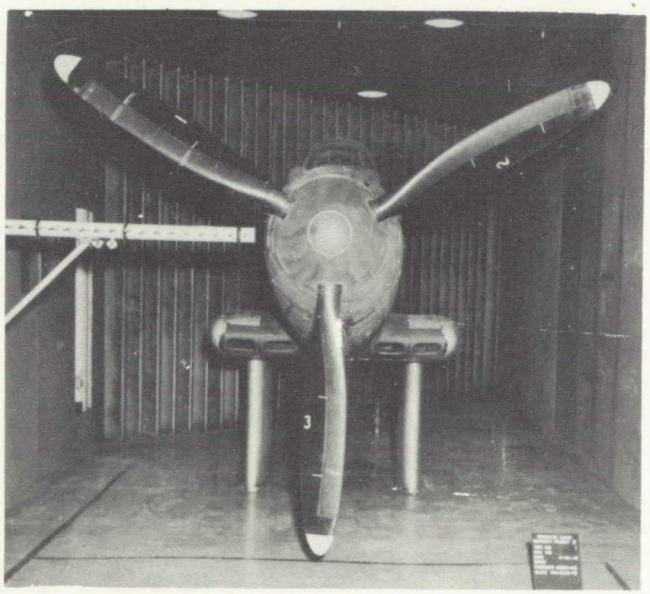

NACA
C-11370
7-9-43

(b) Setup in tunnel.

Figure 1. - Propeller-icing installation in icing research tunnel.

Page intentionally left blank

Page intentionally left blank

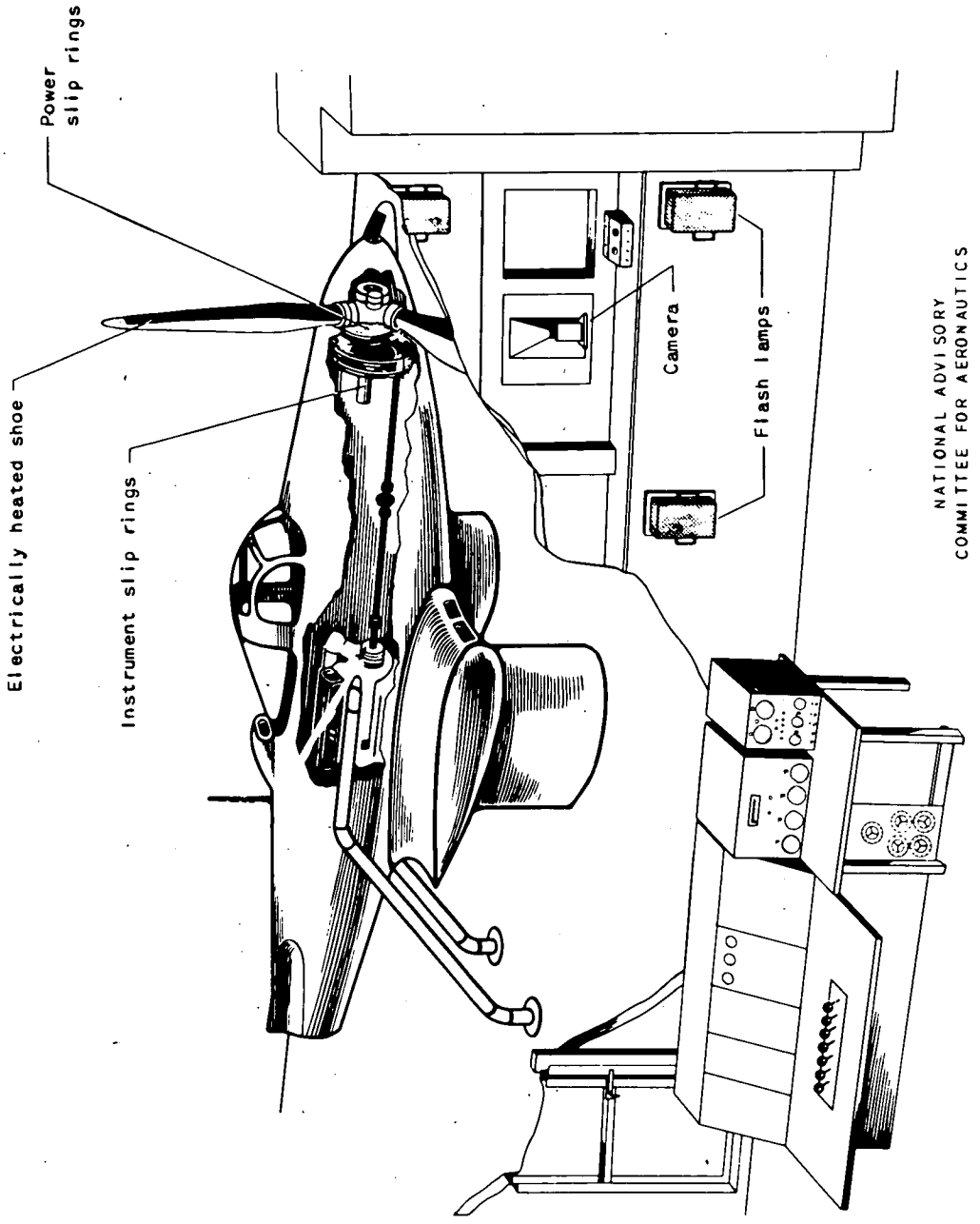


(c) Details of installation.

Figure 1. - Concluded. Propeller-icing installation in icing research tunnel.

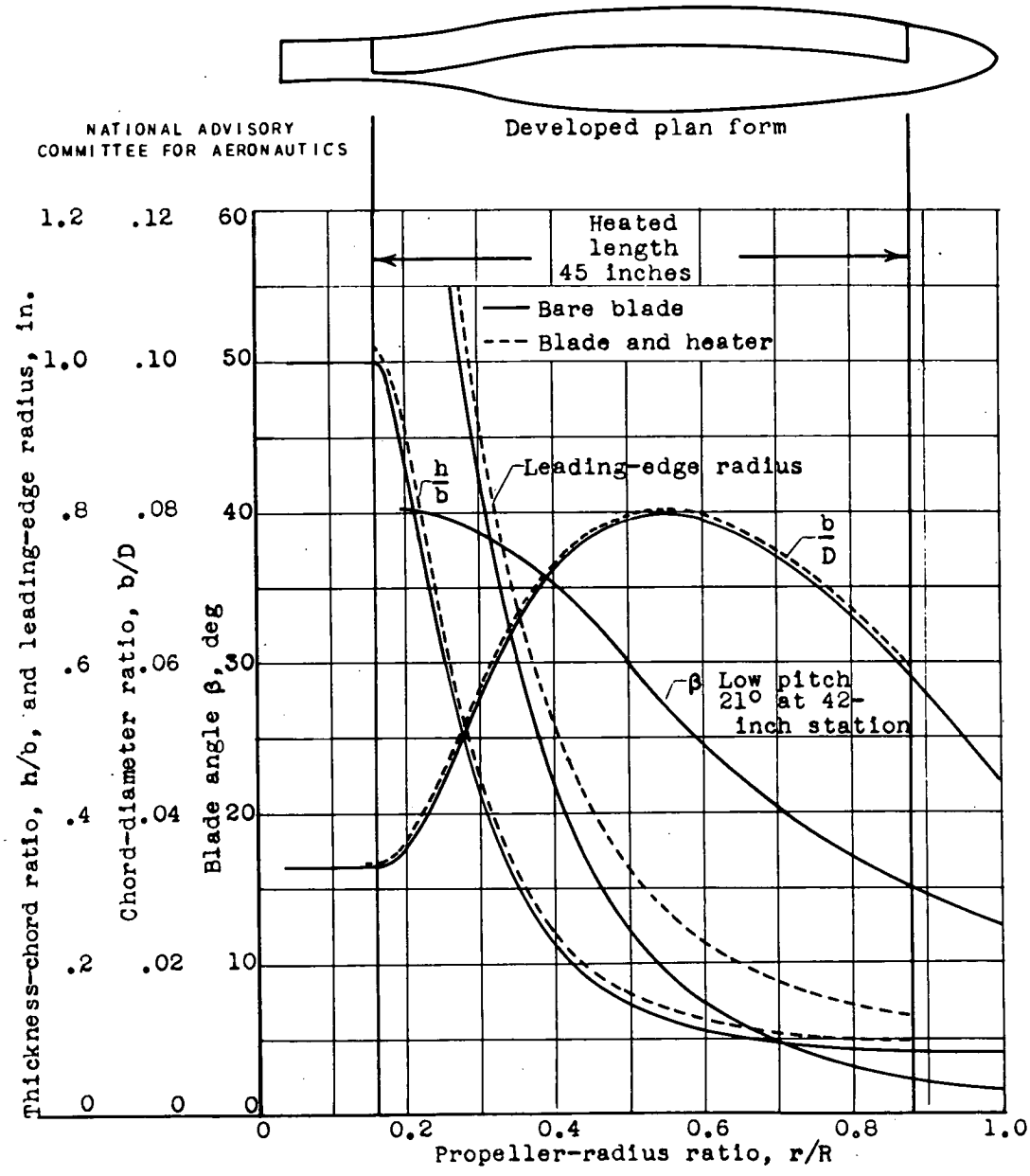


Figure 2. - Blade-form characteristics for propeller blade with external rubber-clad blade heater.

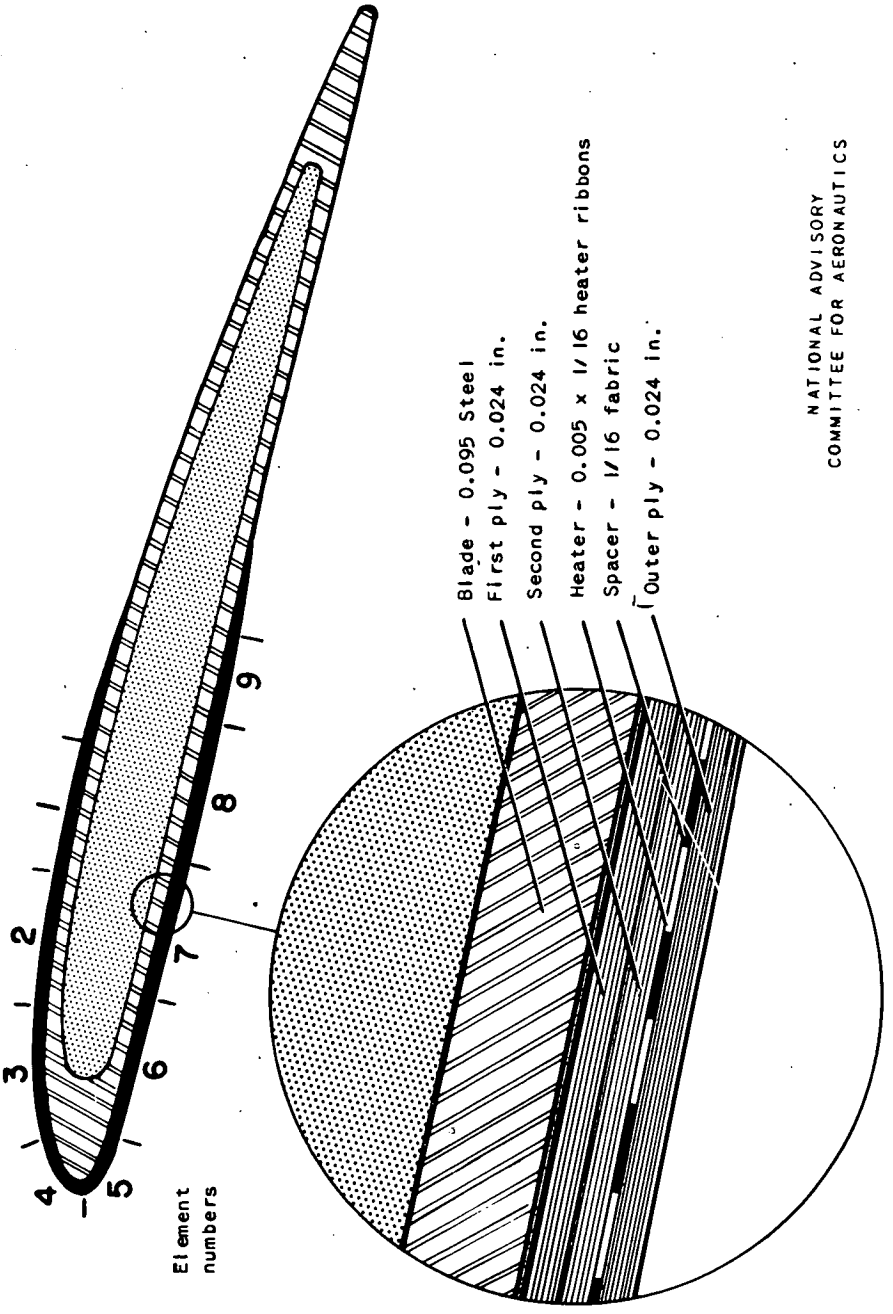


Figure 3. - Details of construction of electrical, external, rubber-clad propeller-blade heaters.

Page intentionally left blank

Page intentionally left blank

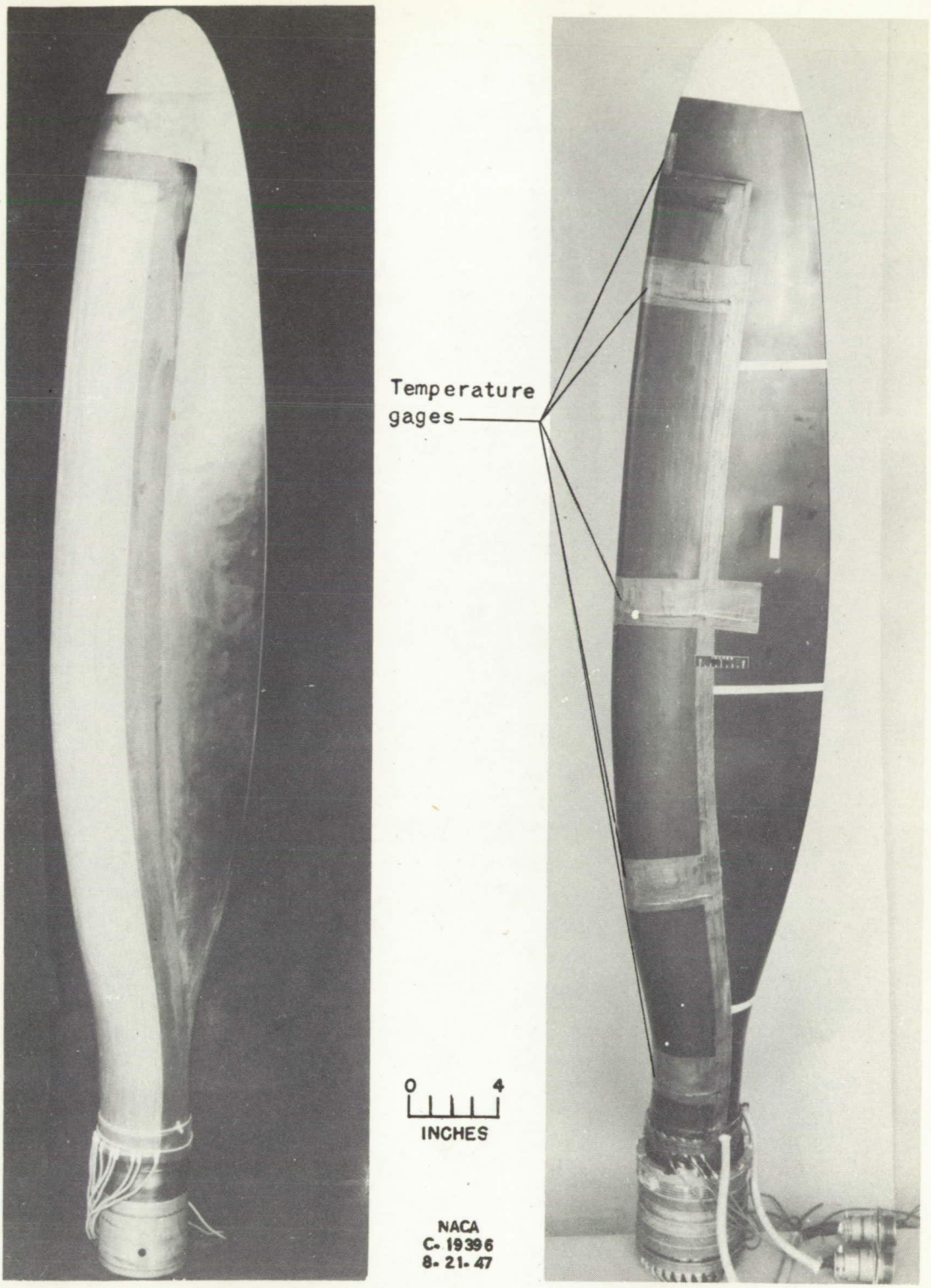


(a) Before installation of outer layer.

(b) Completed blade heater.

Figure 4. - Views of propeller blade with electric, external, rubber-clad propeller-blade heaters.

Page intentionally left blank

Page intentionally left blank

NATIONAL ADVISORY
COMMITTEE FOR AERONAUTICS

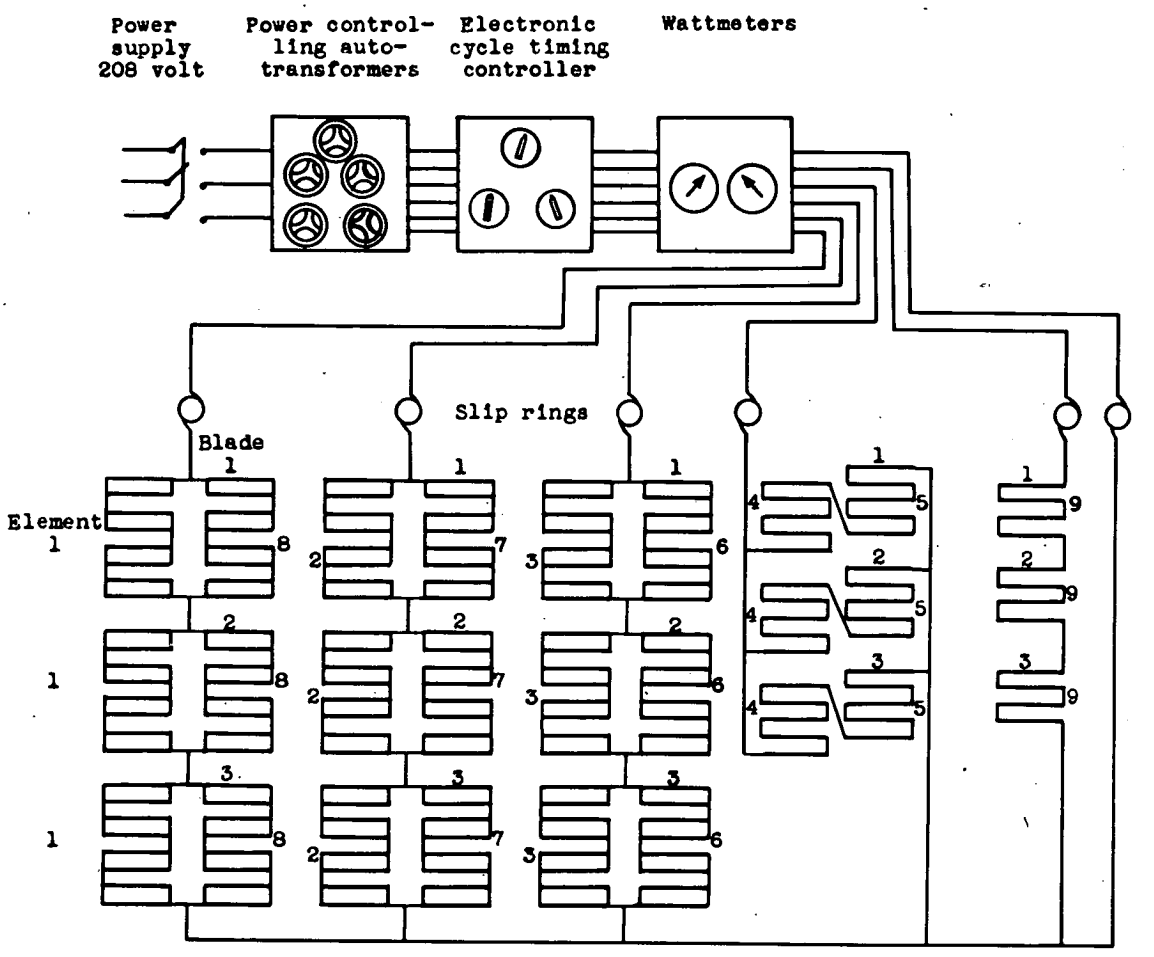


Figure 5. - Typical blade-heating circuit.

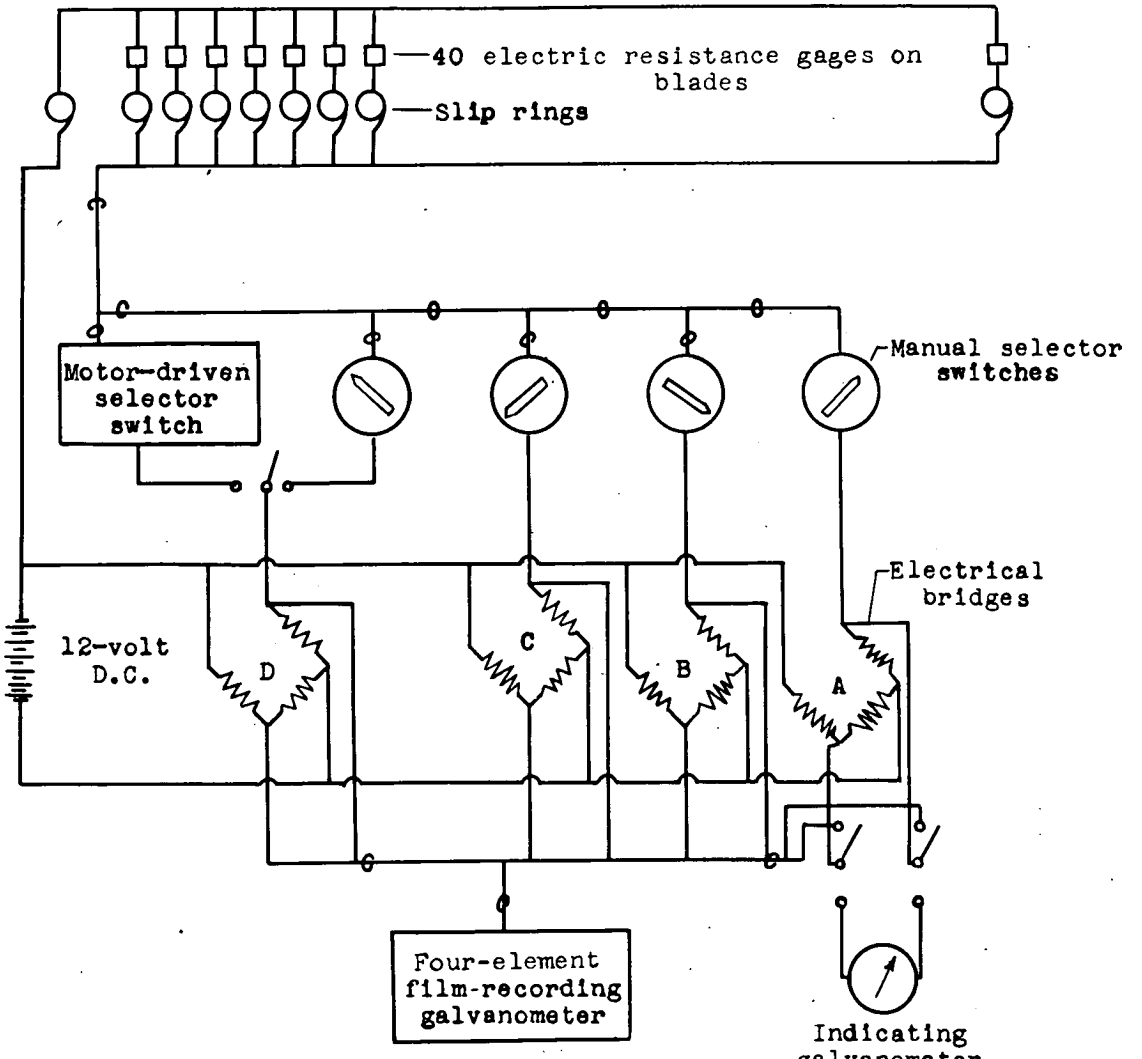


| Bridge | Elements connected | |
|---|---|---|
| A | 1 - 40 | Indicating and recording |
| B | 1 - 15 | On film recorder |
| C | 16 - 30 | On film recorder |
| D | 31 - 40 | On film recorder |
| | 1 - 40 | On motor switch |

NATIONAL ADVISORY COMMITTEE FOR AERONAUTICS

Figure 6. - Schematic diagram of blade-surface temperature-measuring system.

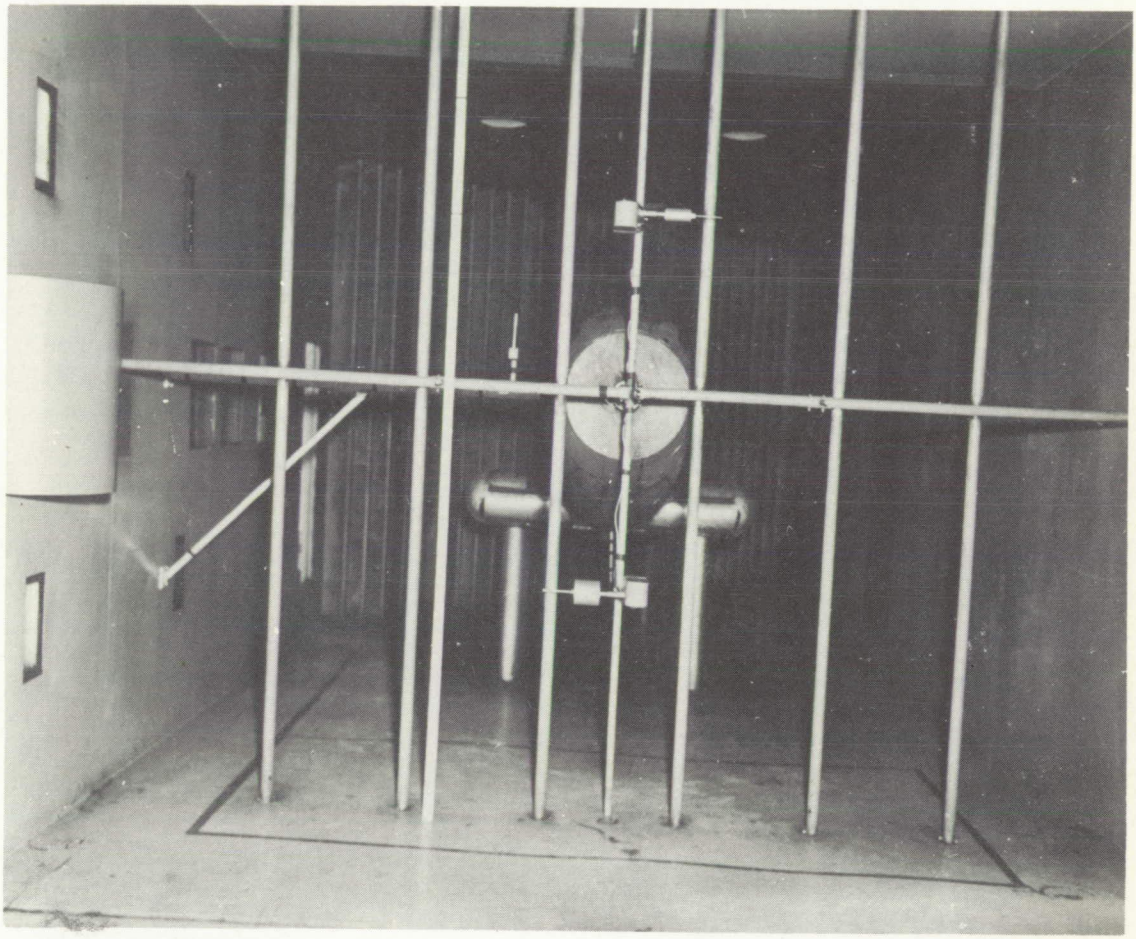

NACA
C-11579
7-27-45

Figure 7. - Icing-survey equipment for liquid-water concentrations and droplet-size measurements.

Page intentionally left blank

Page intentionally left blank

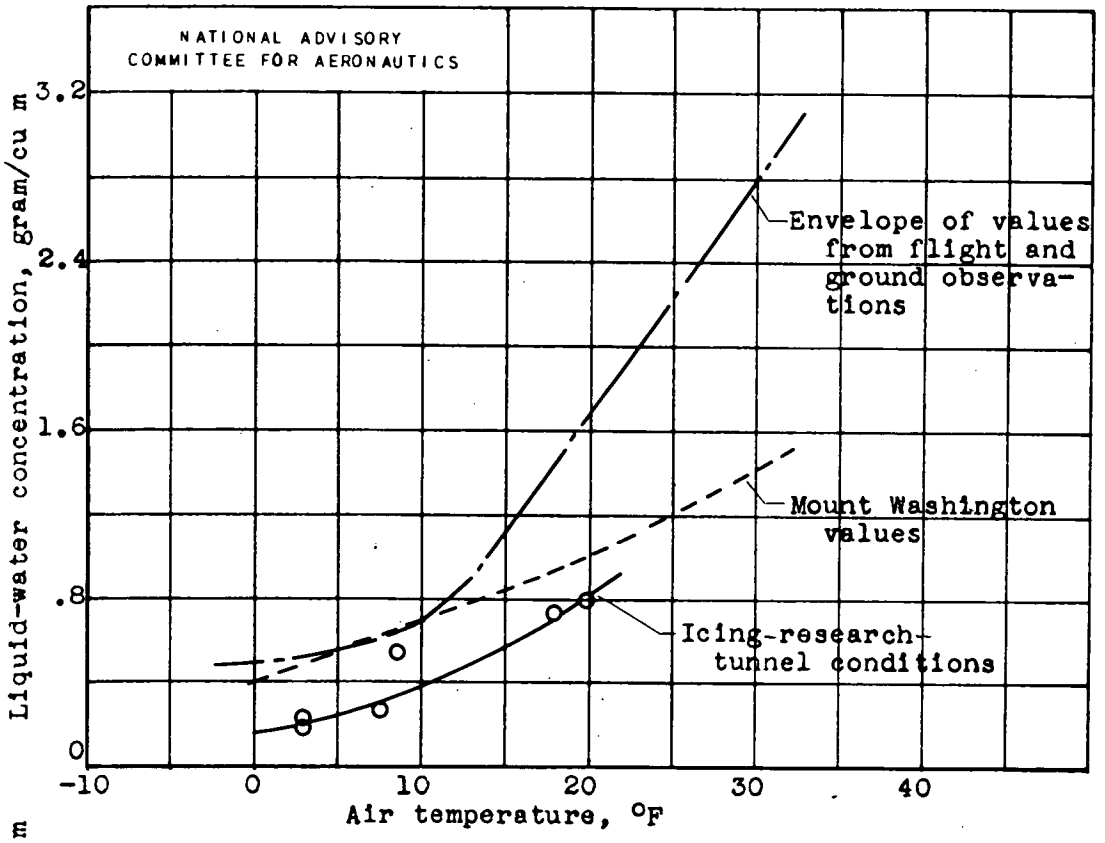


(a) Variation of liquid-water concentration with air temperature.

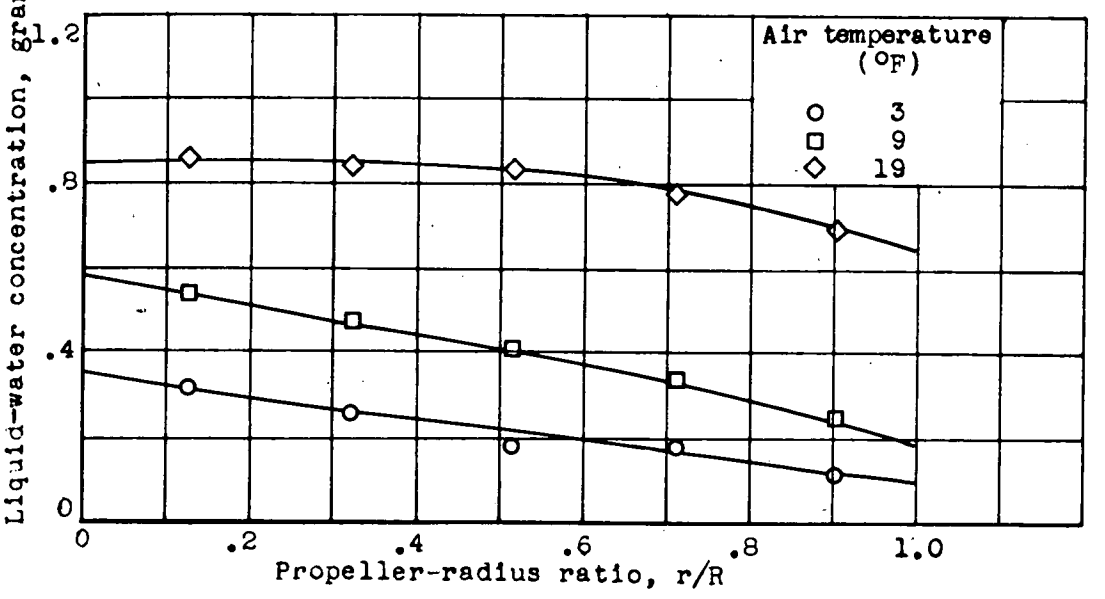


(b) Radial distribution of liquid-water concentration.

Figure 8. - Icing conditions for propeller-icing research.

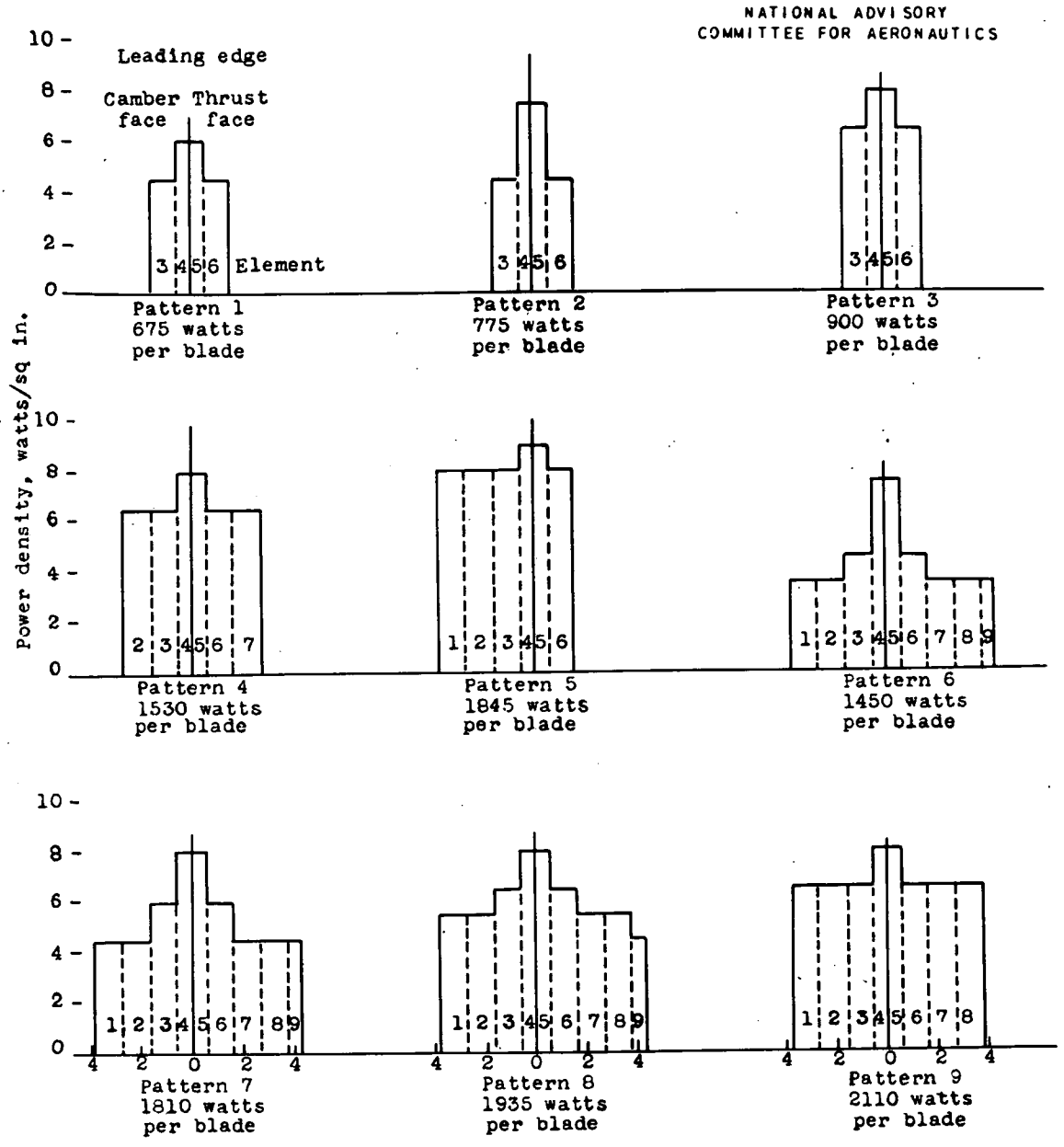


Figure 9. - Chordal-heating power distribution.

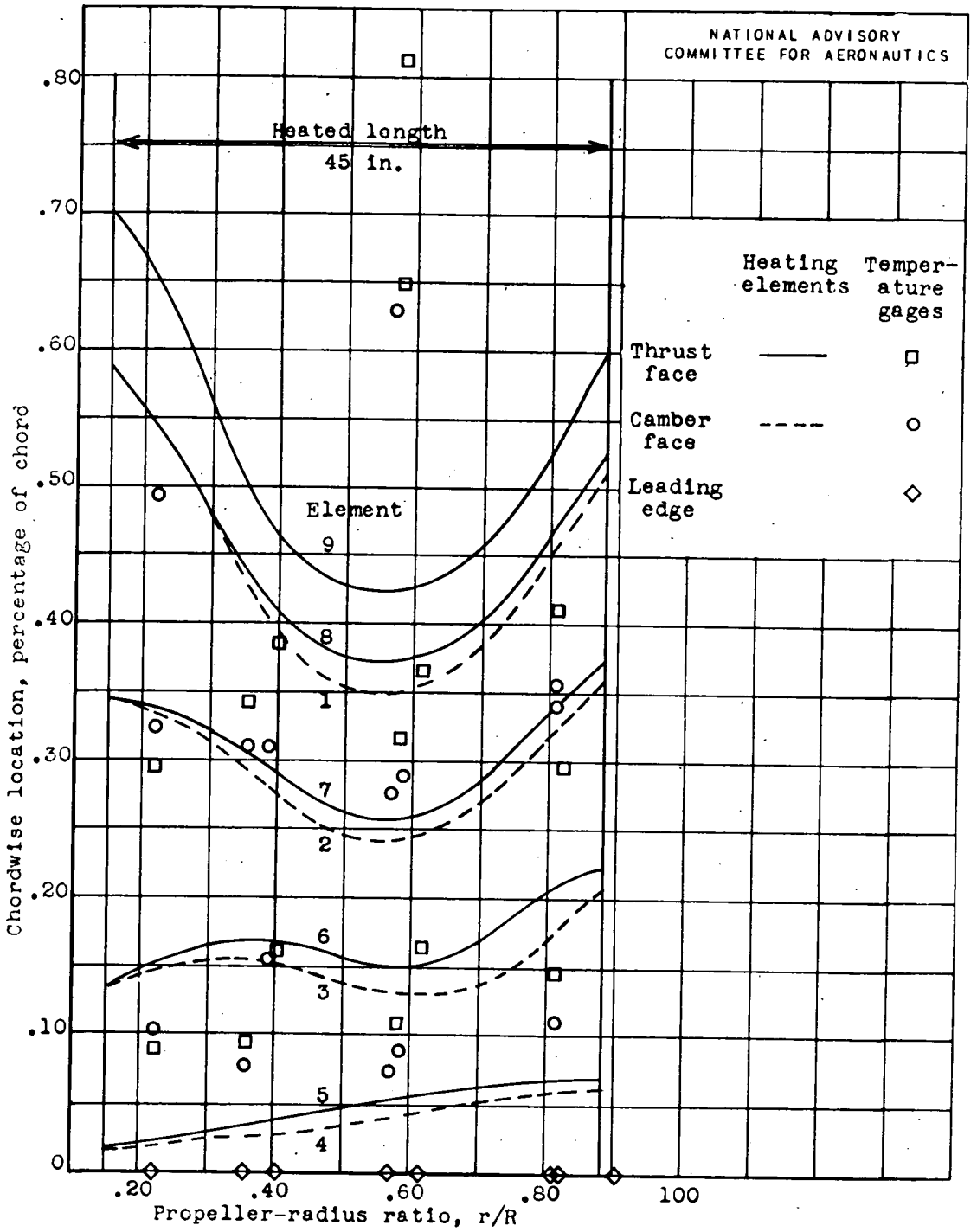


Figure 10. - Radial variation of chordwise-location heater elements and temperature gages.

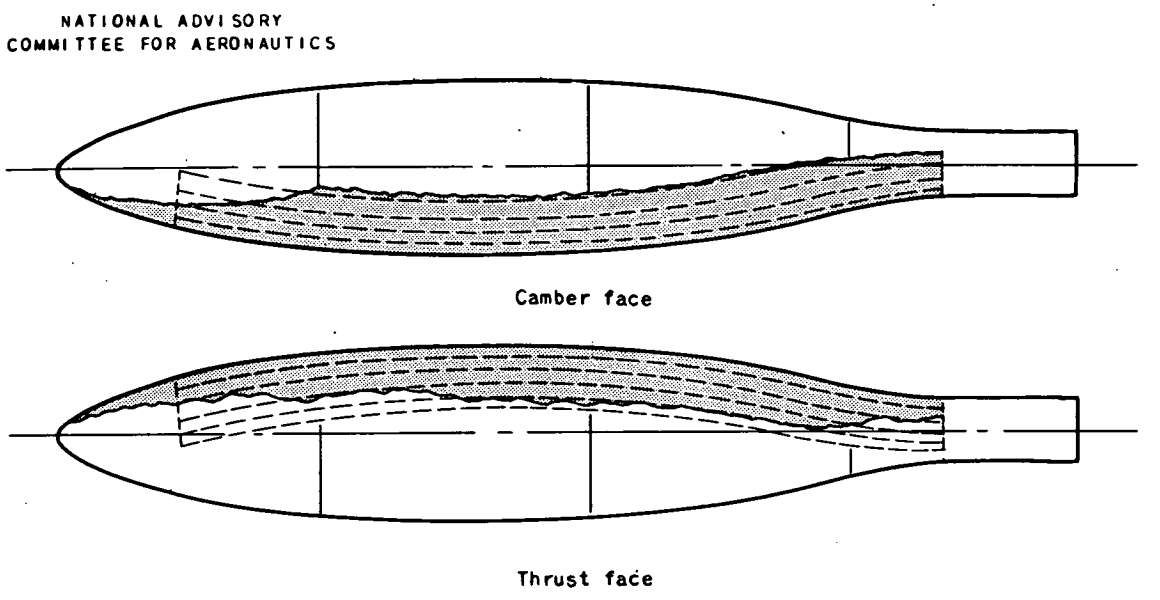


(a) Propeller speed, 675 rpm.

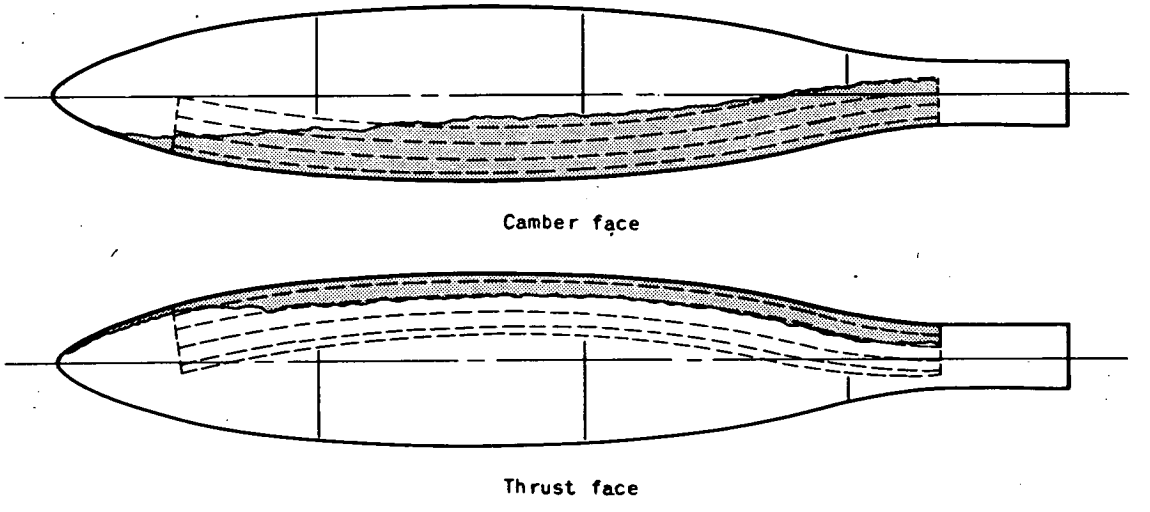


(b) Propeller speed, 925 rpm.

Figure 11. - Typical ice coverage obtained on unheated blade at ambient-air temperature of 21° F and liquid-water concentration of 0.9 gram per cubic meter.

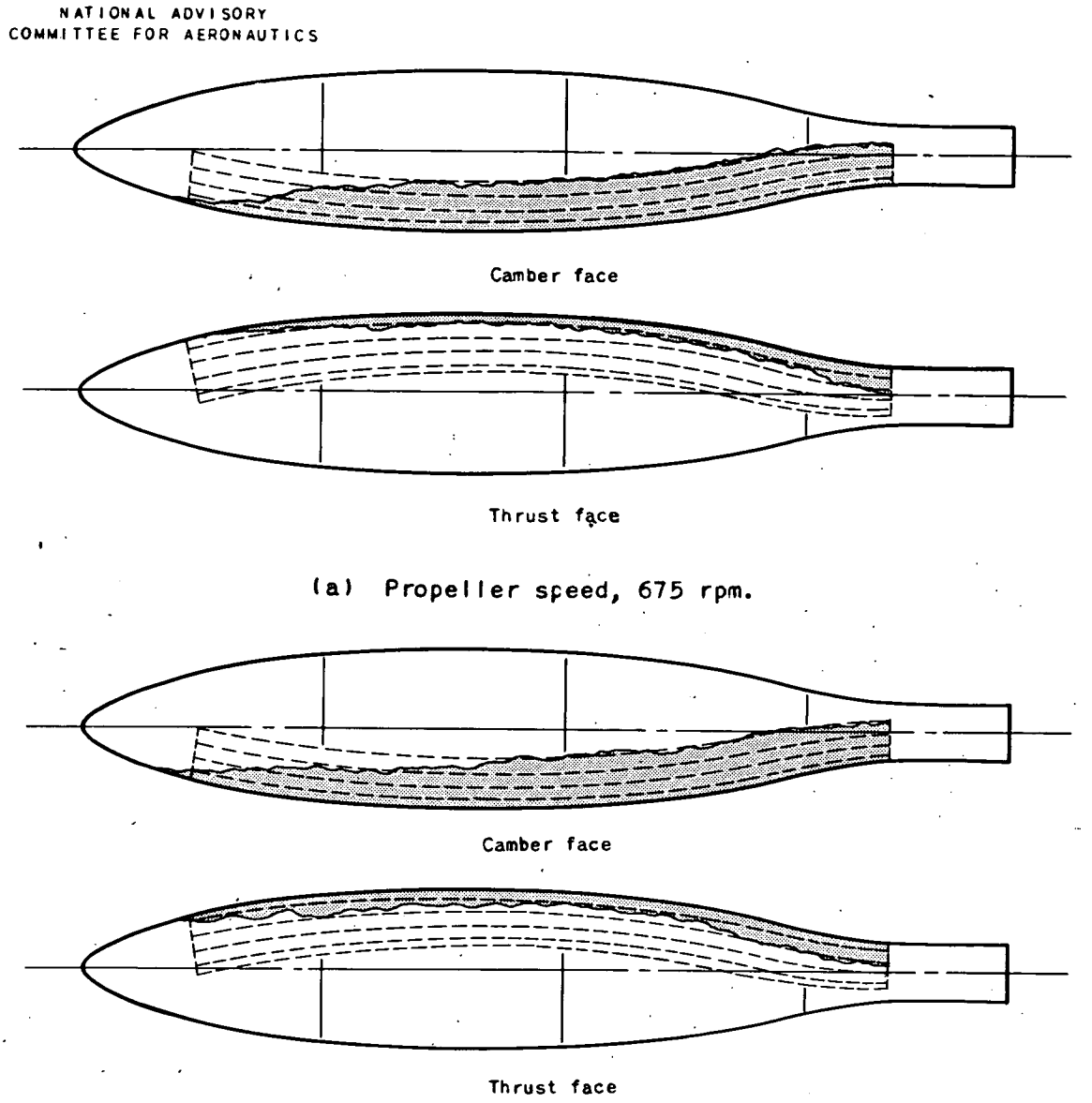


(a) Propeller speed, 675 rpm.

(b) Propeller speed, 925 rpm.

Figure 12. - Typical ice coverage obtained on unheated blade at ambient-air temperature of 11° F and liquid-water concentration of 0.4 gram per cubic meter.

NATIONAL ADVISORY
COMMITTEE FOR AERONAUTICS

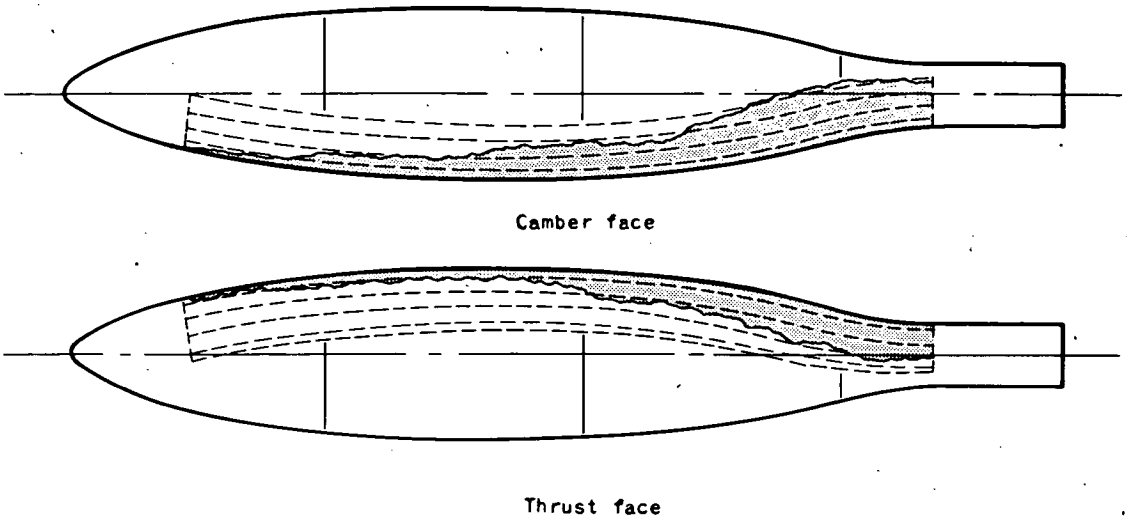


(a) Propeller speed, 675 rpm.

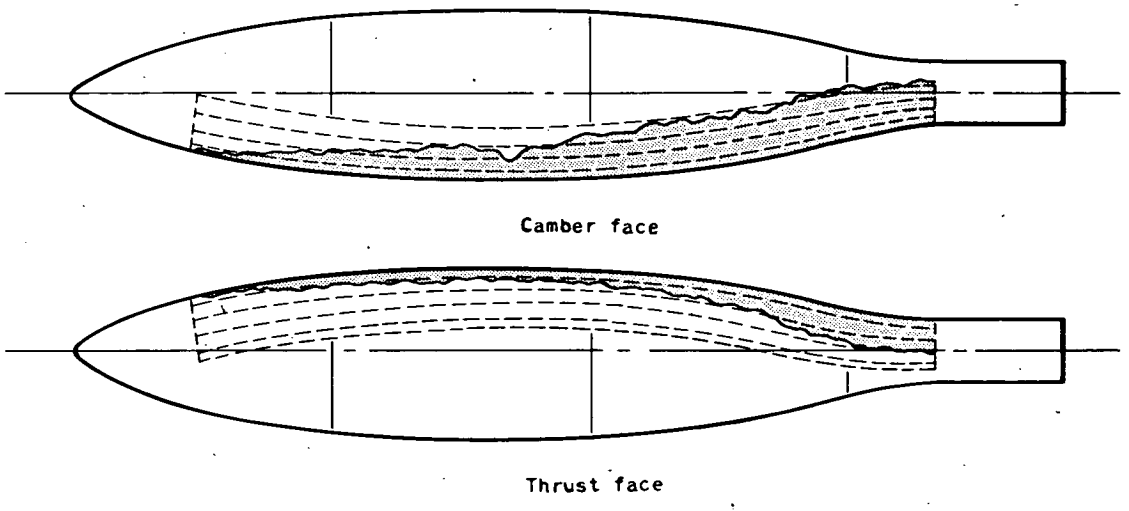


(b) Propeller speed, 925 rpm.

Figure 13. - Typical ice coverage obtained on unheated blade at ambient-air temperature of 2° F and liquid-water concentration of 0.2 gram per cubic meter.

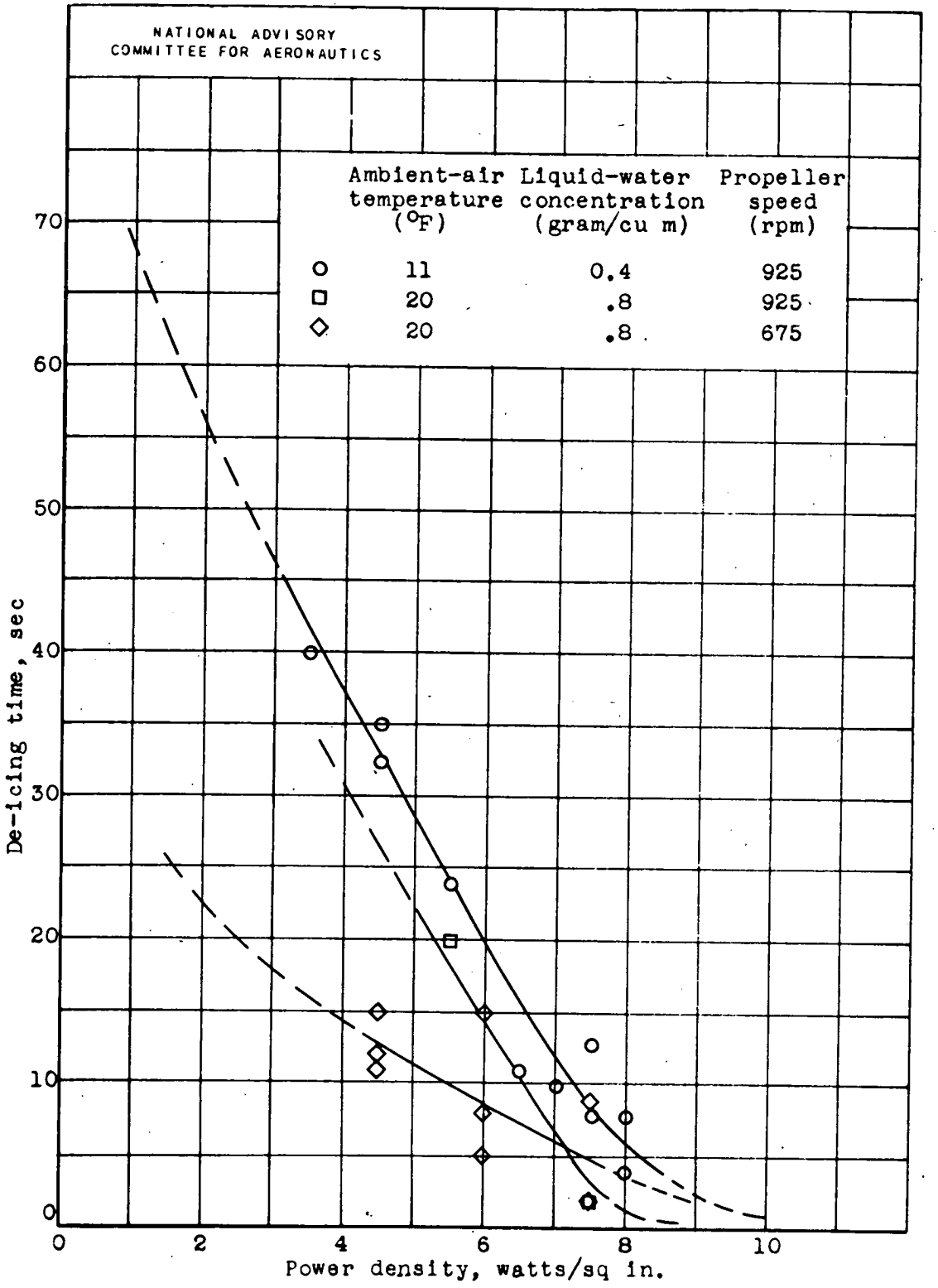


Figure 14. - Variation of de-icing time with power density at several icing and propeller-speed conditions.

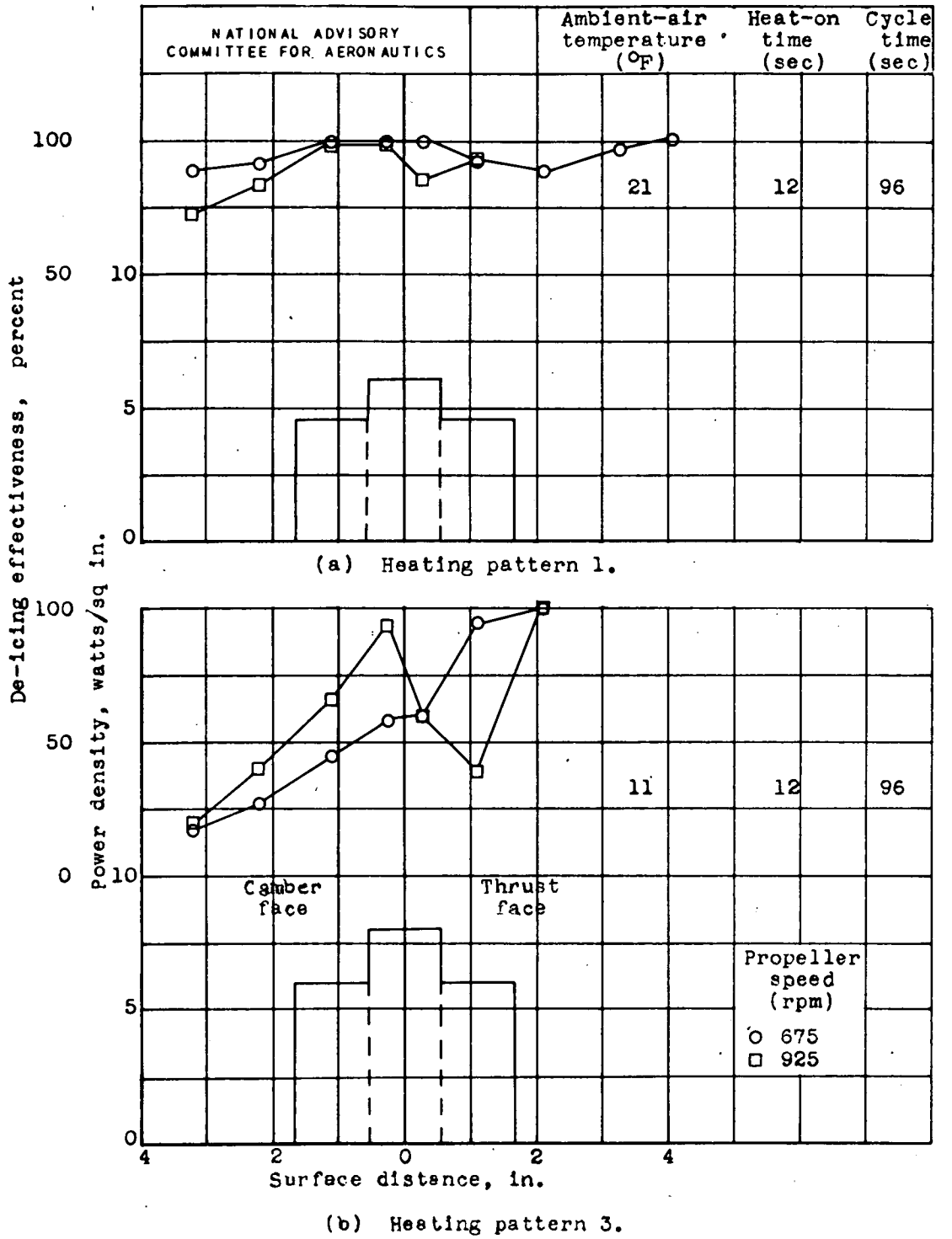


Figure 15. - Variation of de-icing effectiveness at various conditions.

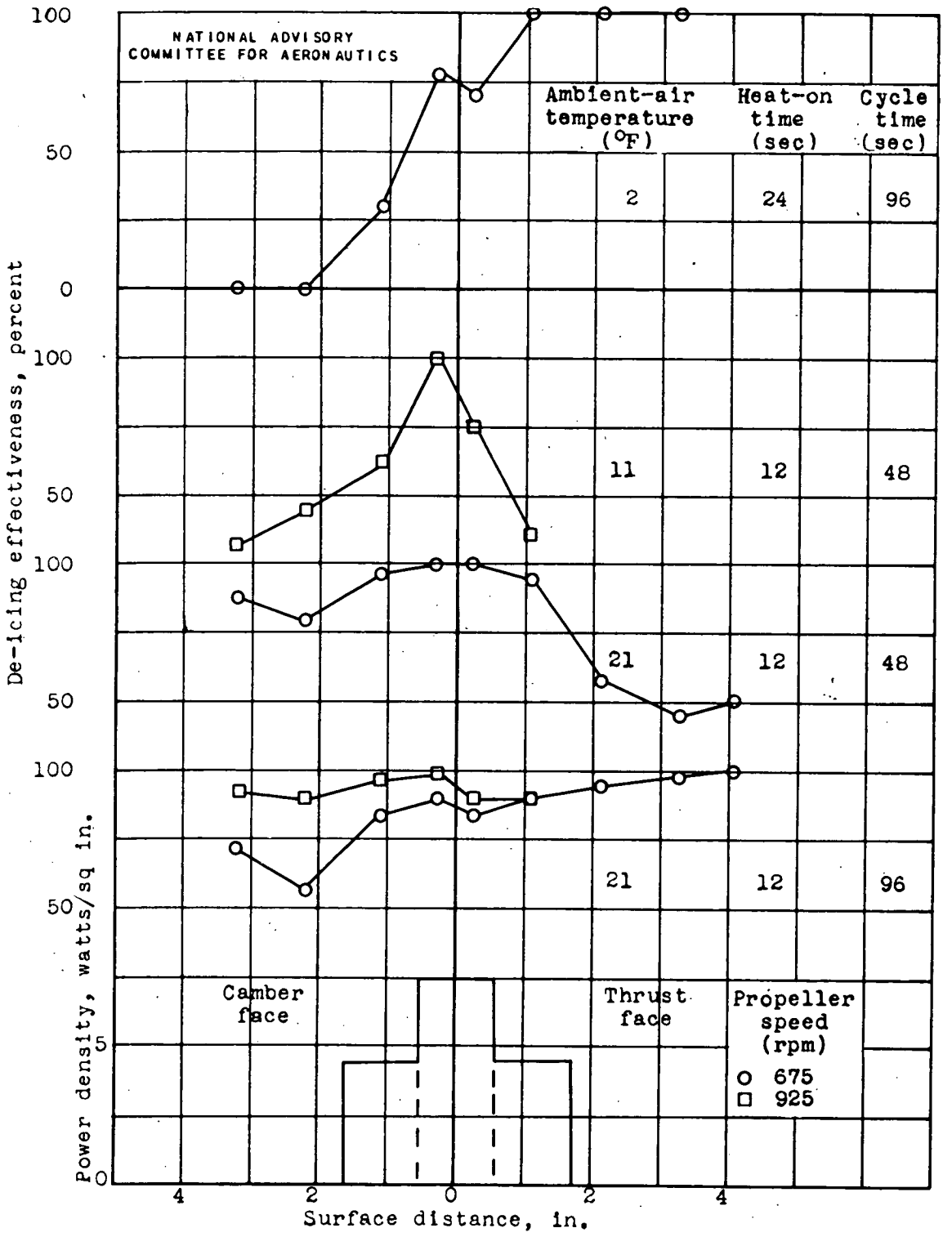


(c) Heating pattern 2.

Figure 15. - Continued. Variation of de-icing effectiveness at various conditions.

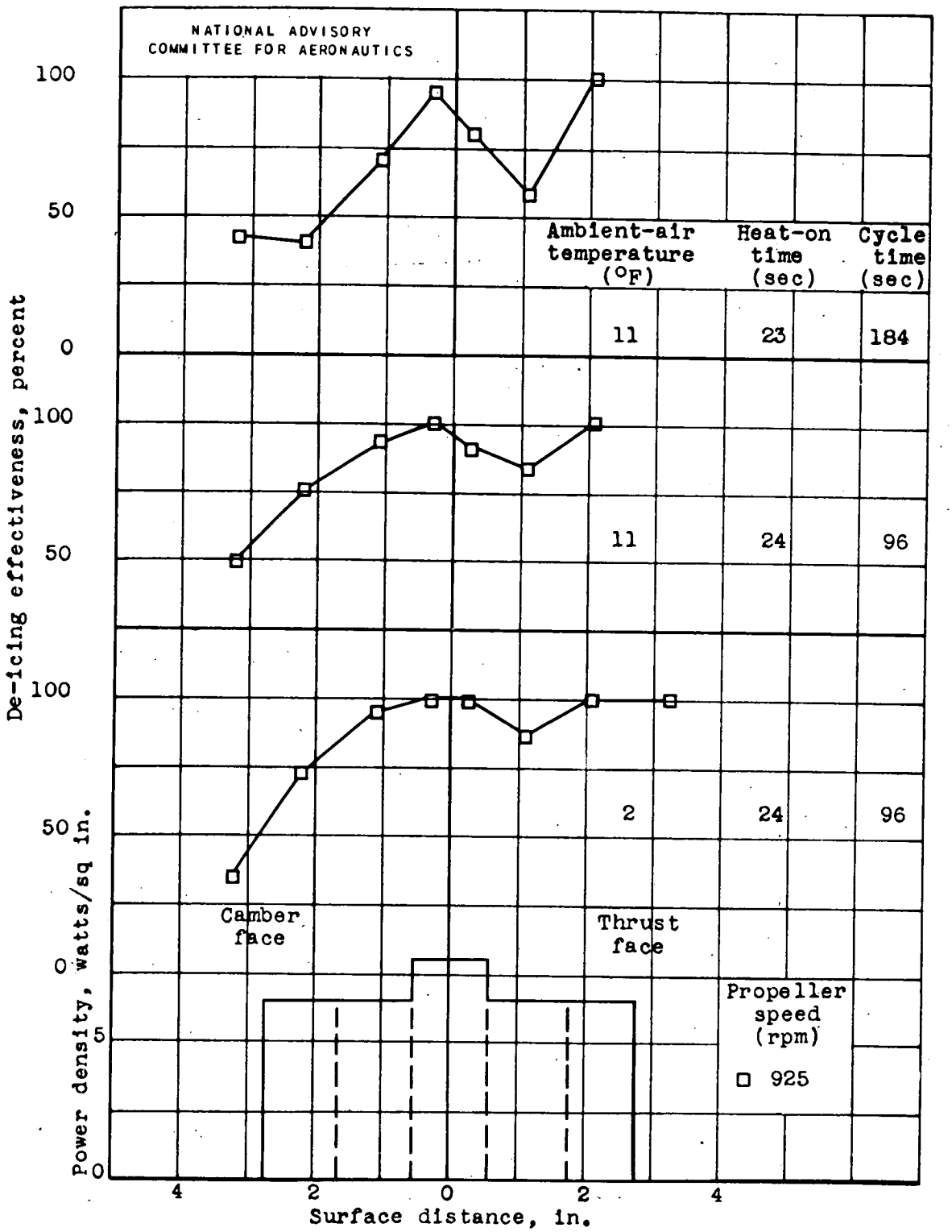


(d) Heating pattern 4.

Figure 15. - Continued. Variation of de-icing effectiveness at various conditions.

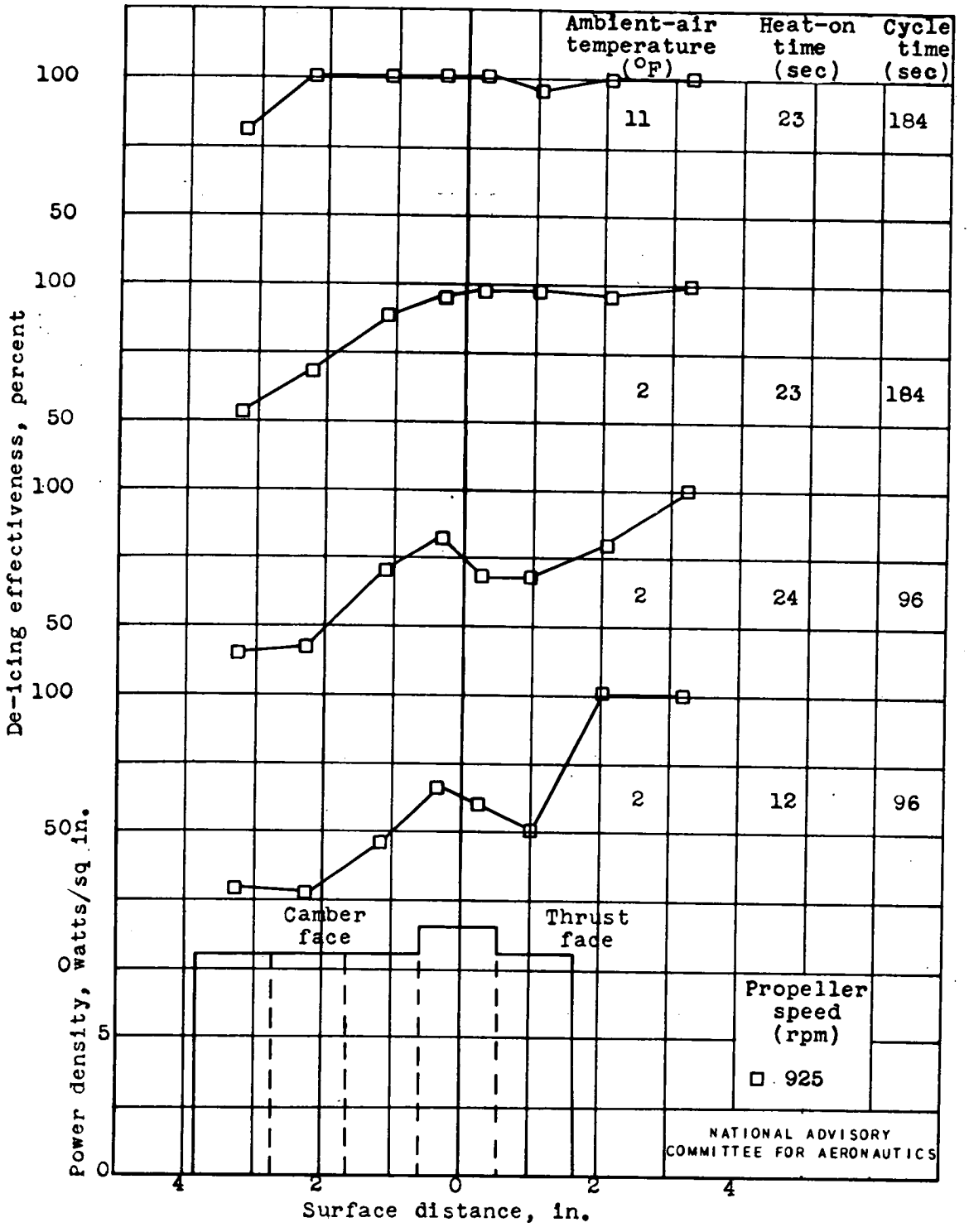


(e) Heating pattern 5.

Figure 15. - Continued. Variation of de-icing effectiveness at various conditions.

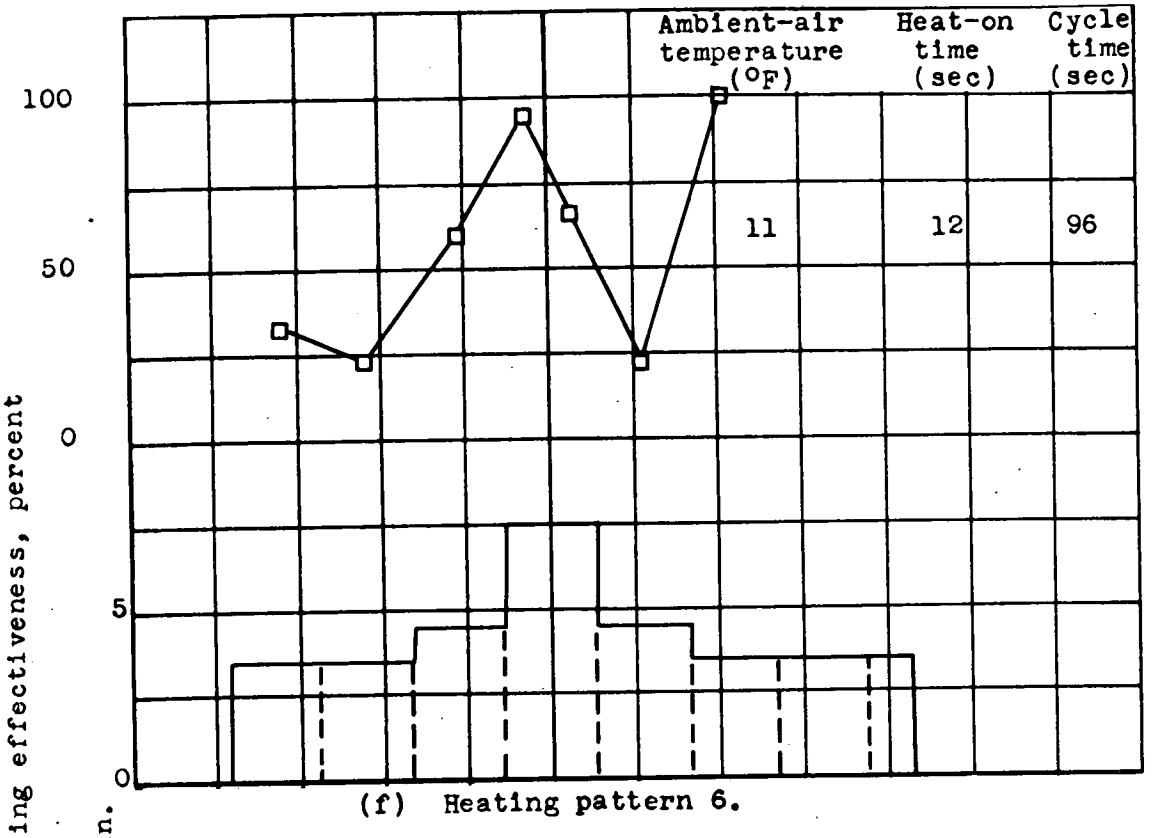


(f) Heating pattern 6.

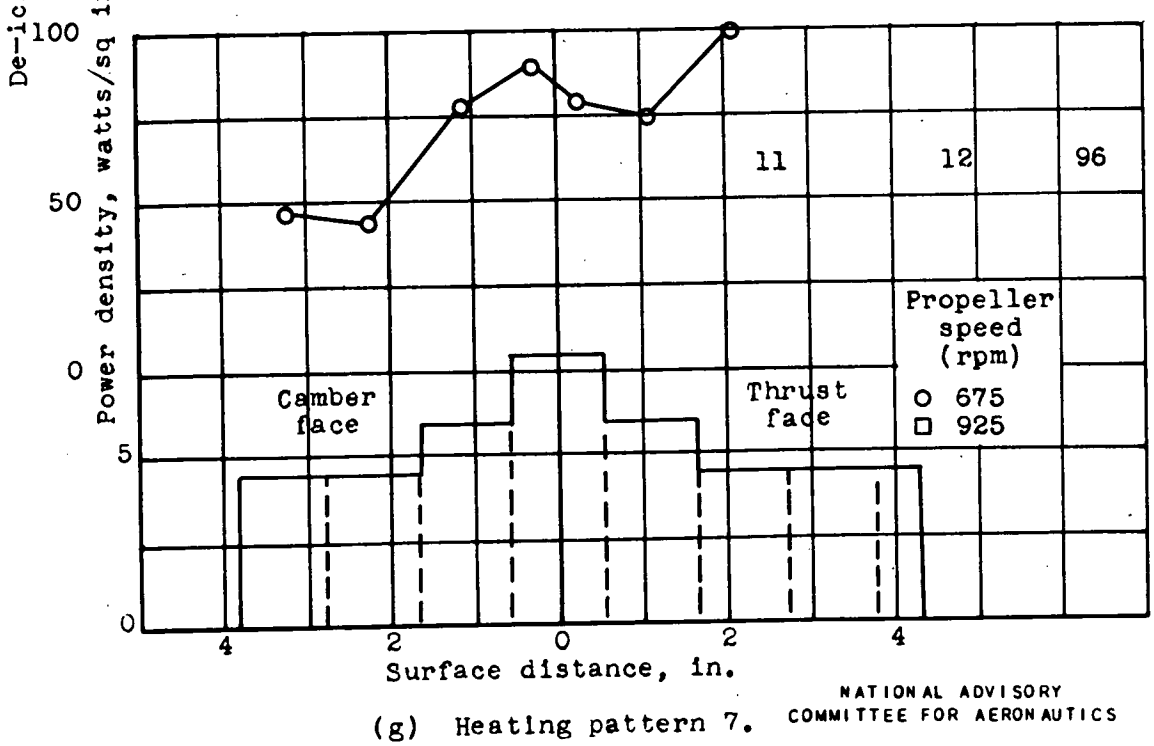


(g) Heating pattern 7.

NATIONAL ADVISORY COMMITTEE FOR AERONAUTICS

Figure 15. - Continued. Variation of de-icing effectiveness at various conditions.

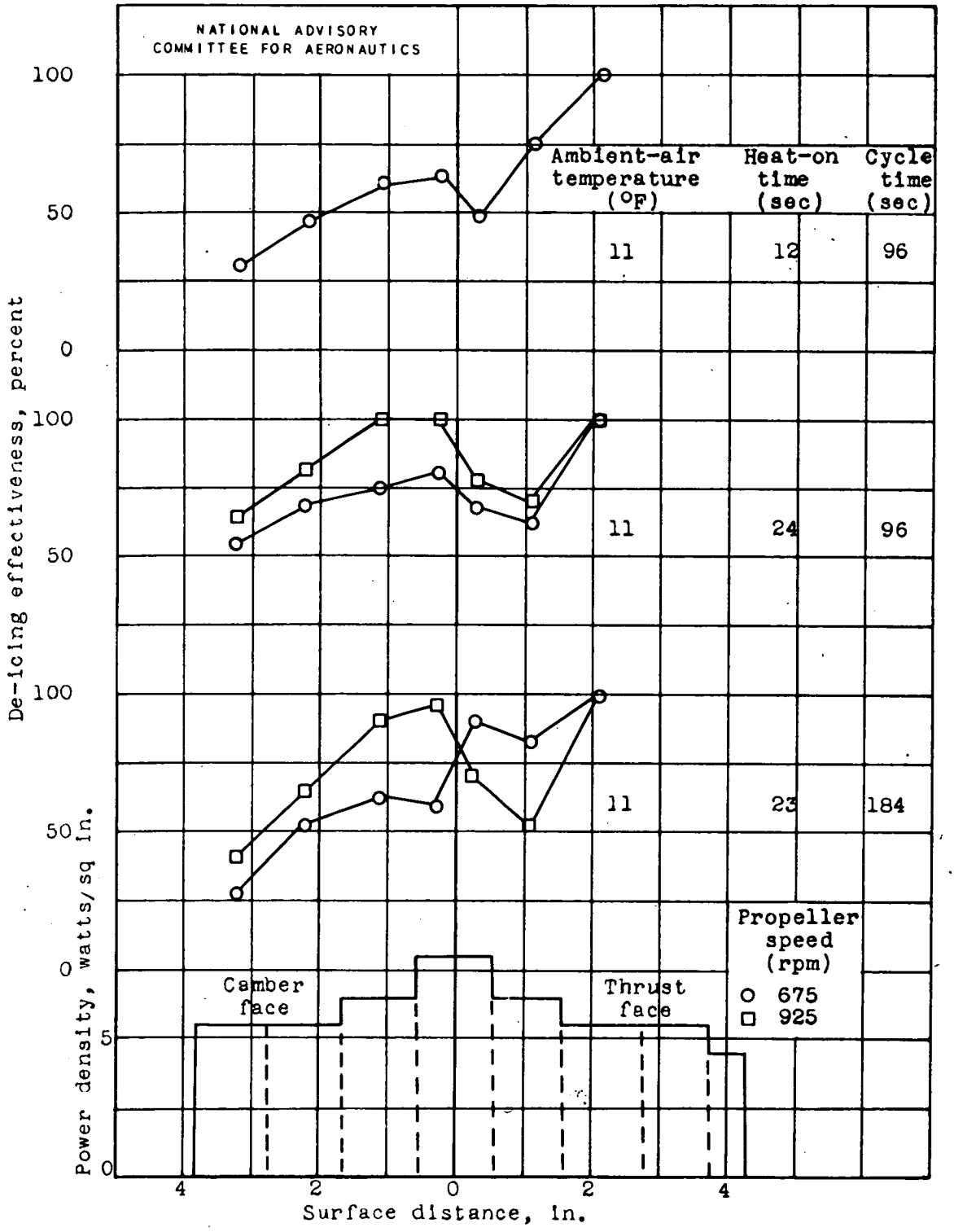


(h) Heating pattern 8.

Figure 15. - Continued. Variation of de-icing effectiveness at various conditions.

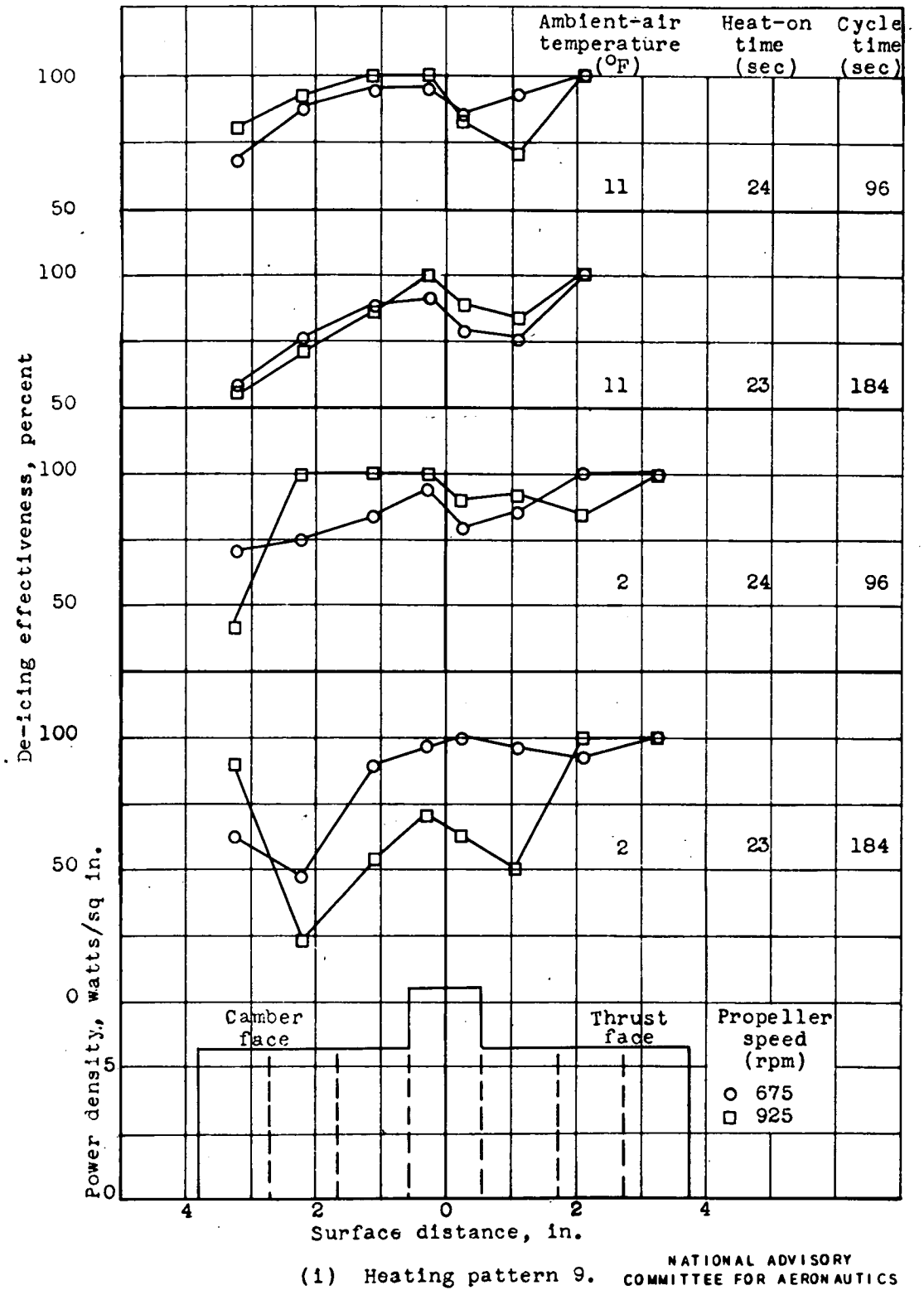


Figure 15. - Concluded. Variation of de-icing effectiveness at various conditions.

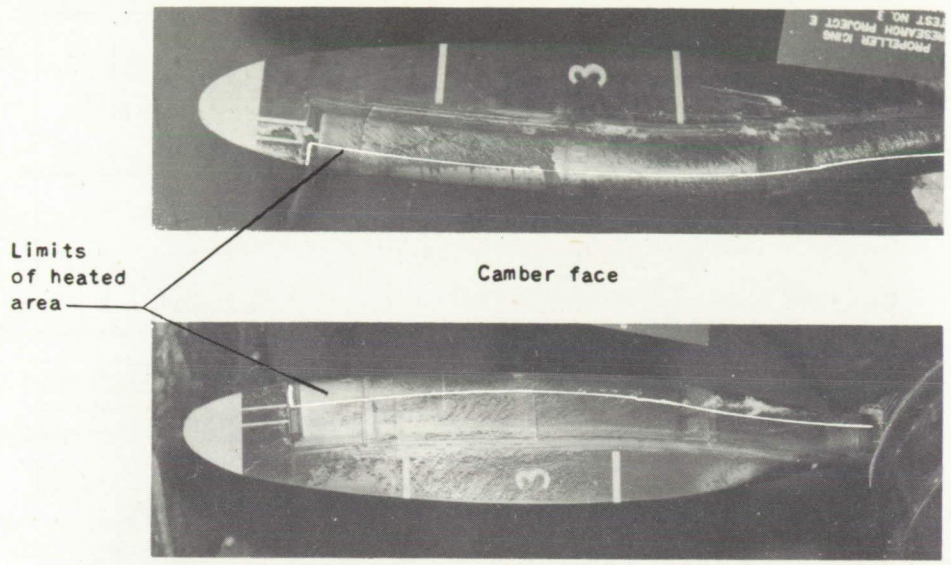


(a) Propeller speed, 675 rpm.

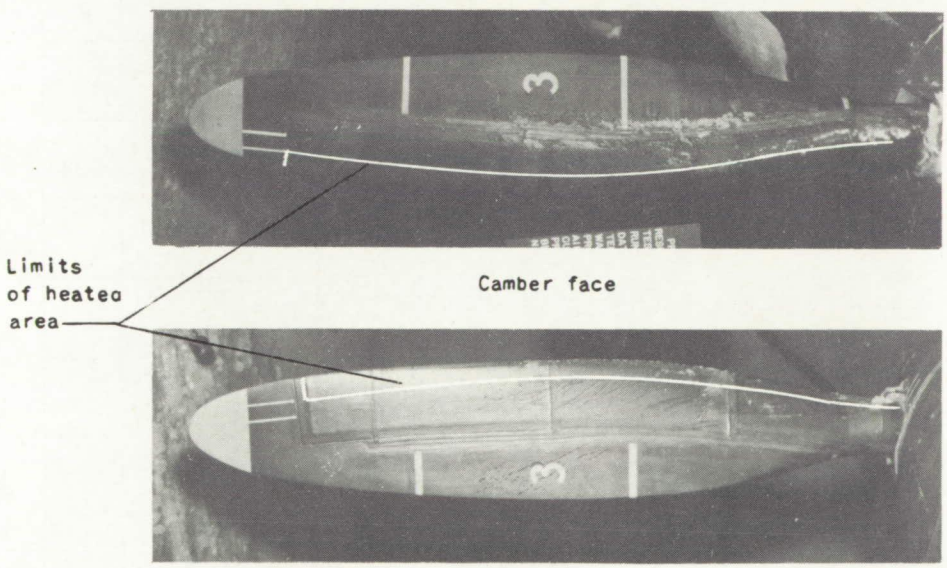


(b) Propeller speed, 925 rpm.

Figure 16. - Views of residual ice after cyclic de-icing with heating pattern 1. Ambient-air temperature, 21° F; heat-on time, 12 seconds; cycle time, 96 seconds.

Page intentionally left blank

Page intentionally left blank

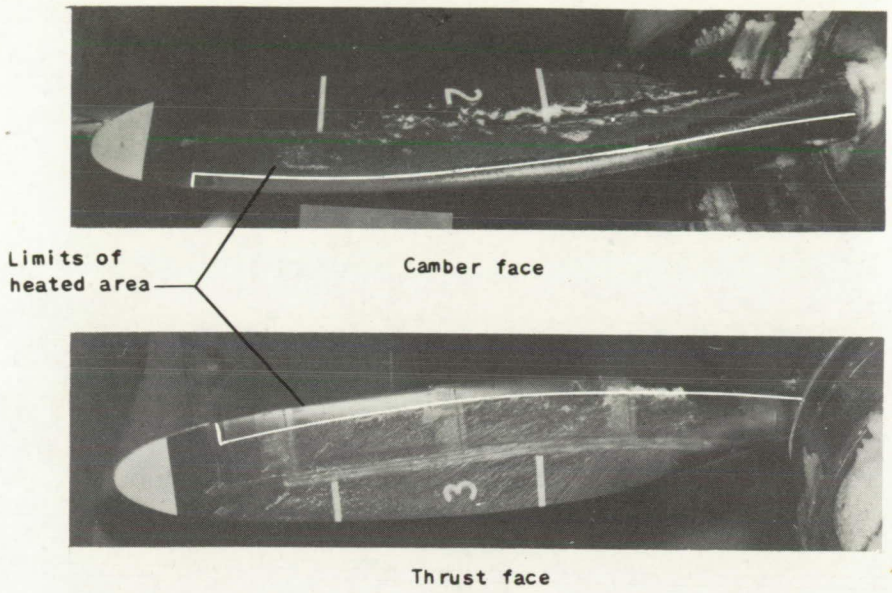


(a) Propeller speed, 675 rpm; ambient-air temperature, 21° F; heat-on time, 12 seconds; cycle time, 48 seconds.

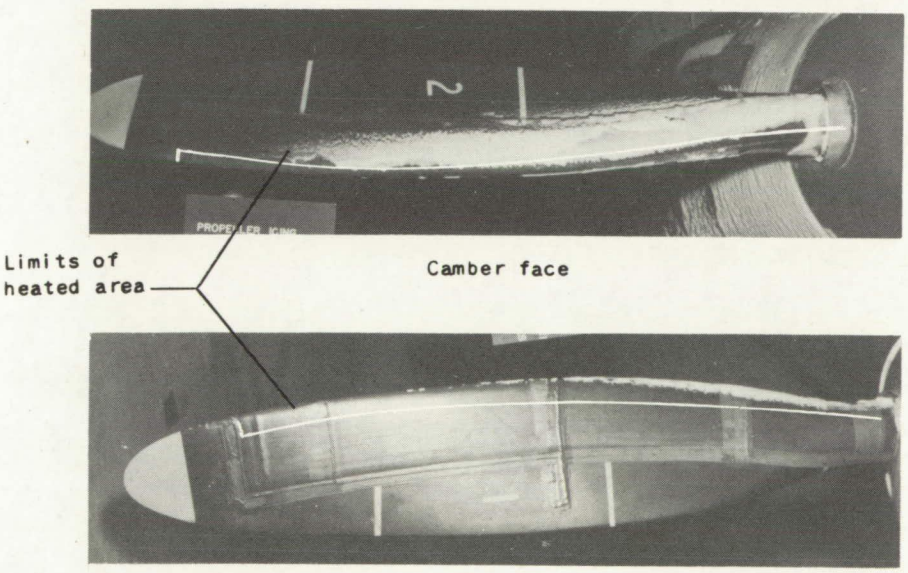


(b) Propeller speed, 925 rpm; ambient-air temperature, 11° F; heat-on time, 12 seconds; cycle time, 48 seconds.

Figure 17. - Views of residual ice after cyclic de-icing with heating pattern 2.

Page intentionally left blank

Page intentionally left blank

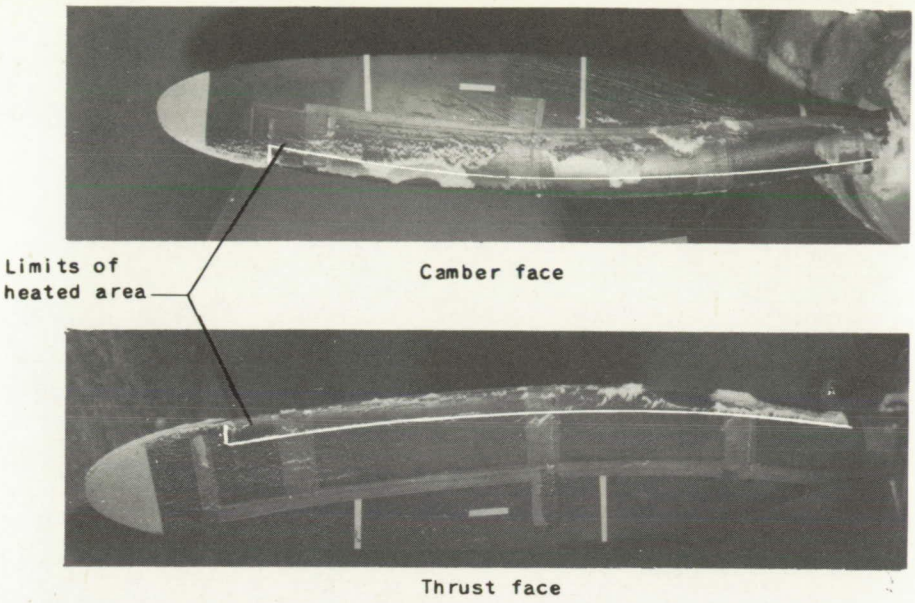


(c) Propeller speed, 675 rpm; ambient-air temperature, 21° F; heat-on time, 12 seconds; cycle time, 96 seconds.

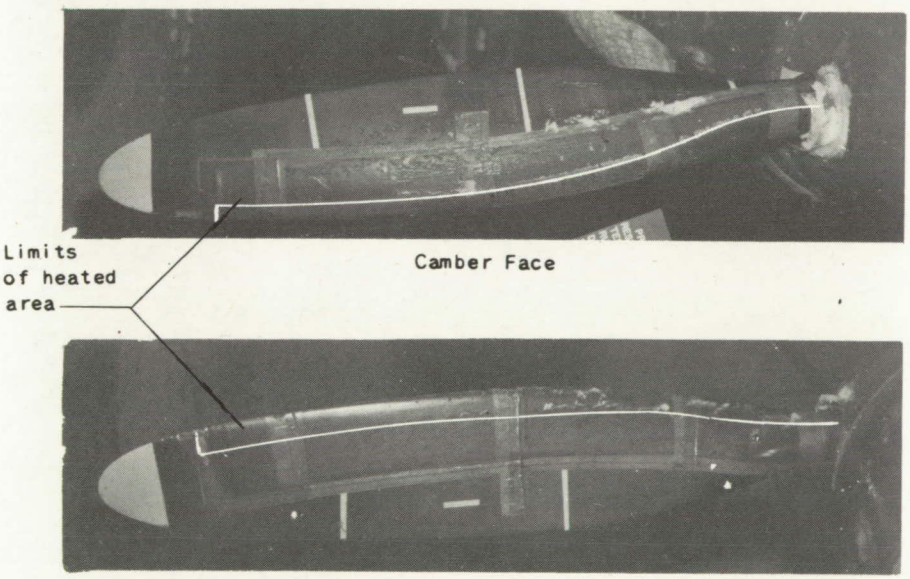


(d) Propeller speed, 925 rpm; ambient-air temperature, 21° F; heat-on time, 12 seconds; cycle time, 96 seconds.

Figure 17. - Continued. Views of residual ice after cyclic de-icing with heating pattern 2.

Page intentionally left blank

Page intentionally left blank

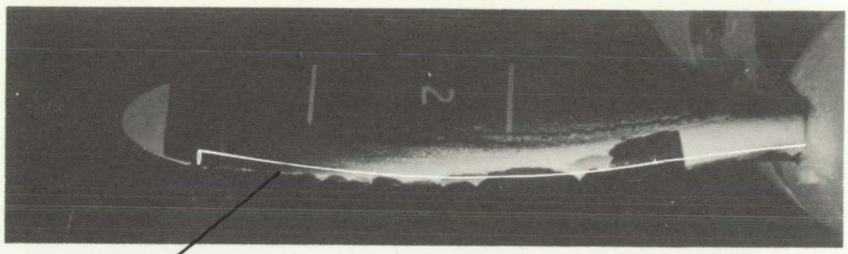


Limits of heated area

Camber face

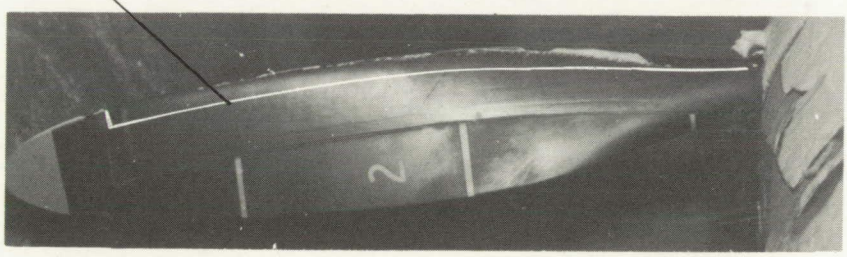


NACA C-19380 8-21-47

Thrust face

(e) Propeller speed, 675 rpm; ambient-air temperature, 2° F; heat-on time, 24 seconds; cycle time, 96 seconds.

Figure 17. - Concluded. Views of residual ice after cyclic de-icing with heating pattern 2.

Page intentionally left blank

Page intentionally left blank

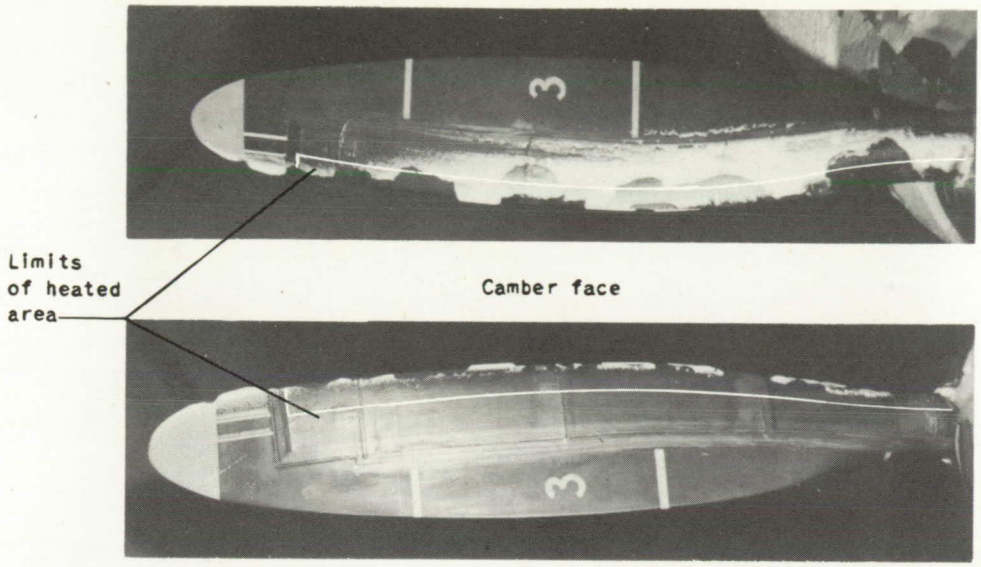


(a) Propeller speed, 675 rpm.

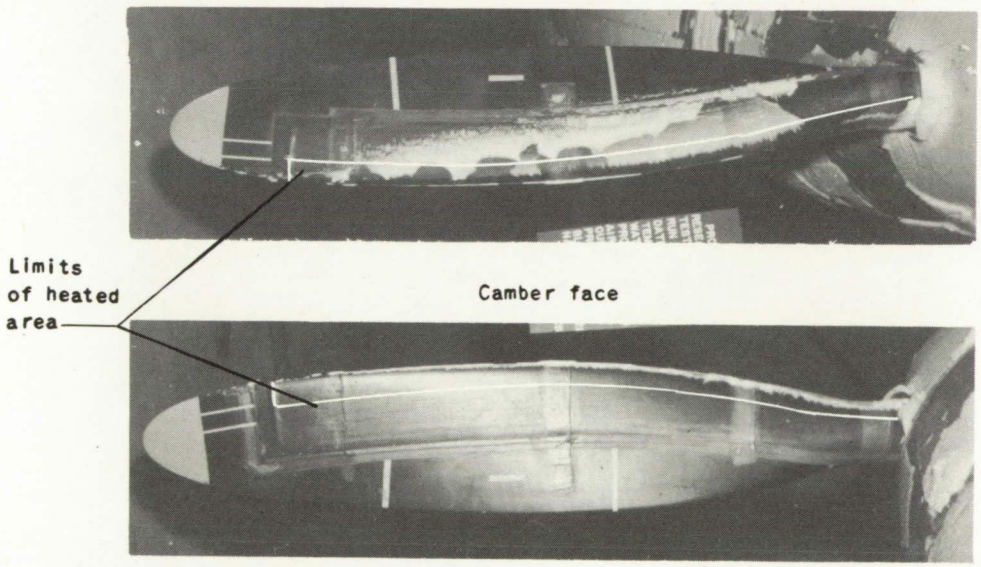


(b) Propeller speed, 925 rpm.

Figure 18. - Views of residual ice after cyclic de-icing with heating pattern 3. Ambient-air temperature, 11° F; heat-on time, 12 seconds; cycle time, 96 seconds.

Page intentionally left blank

Page intentionally left blank

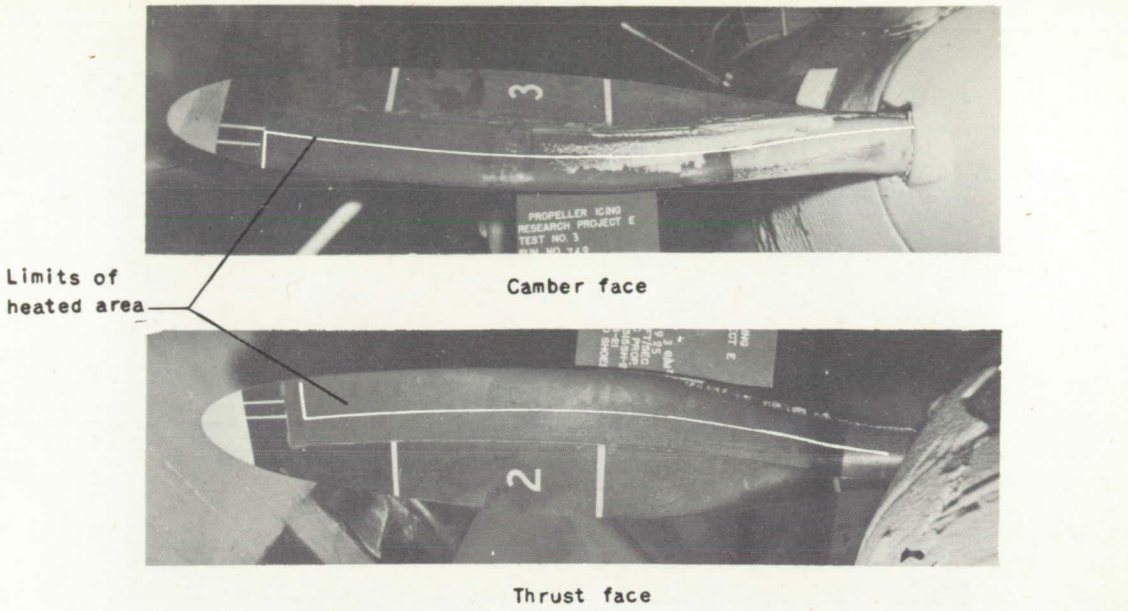


(a) Ambient-air temperature, 2° F; heat-on time, 24 seconds; cycle time, 96 seconds.

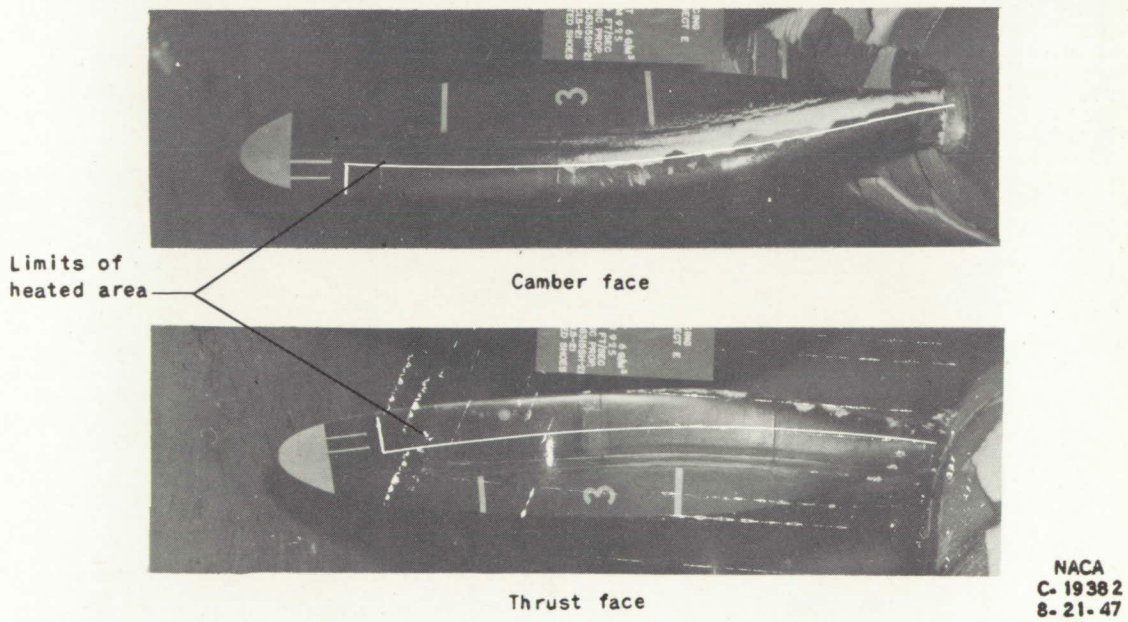


(b) Ambient-air temperature, 11° F; heat-on time, 24 seconds; cycle time, 96 seconds.

Figure 19. - Views of residual ice after cyclic de-icing with heating pattern 4. Propeller speed, 925 rpm.

Page intentionally left blank

Page intentionally left blank

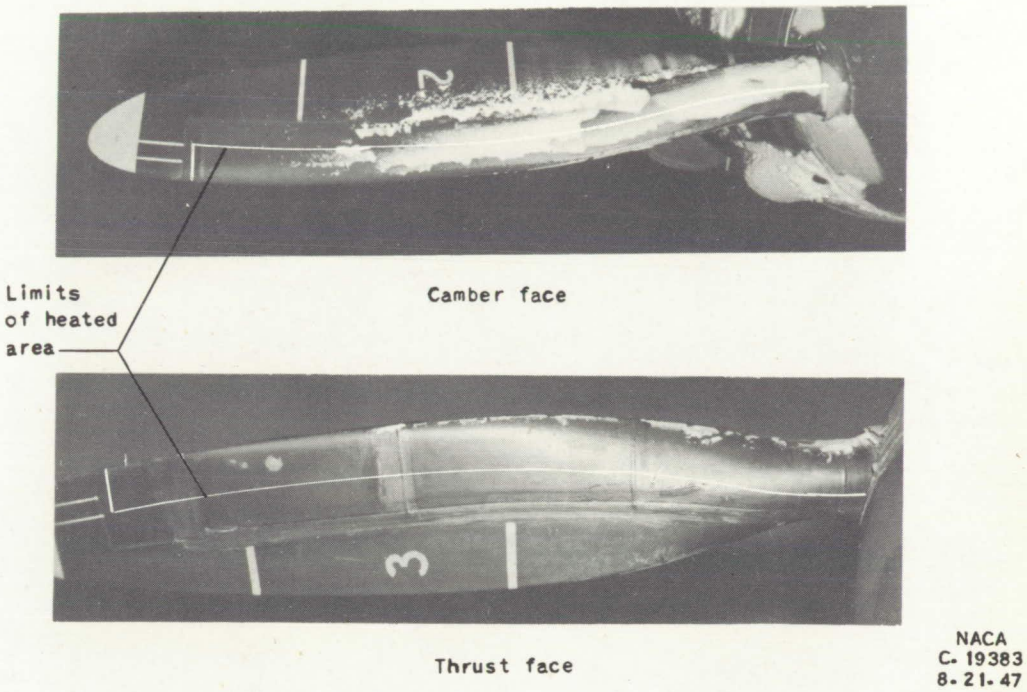


(c) Ambient-air temperature, 11° F; heat-on time, 23 seconds; cycle time, 184 seconds.

Figure 19. - Concluded. Views of residual ice after cyclic de-icing with heating pattern 4. Propeller speed, 925 rpm.

Page intentionally left blank

Page intentionally left blank

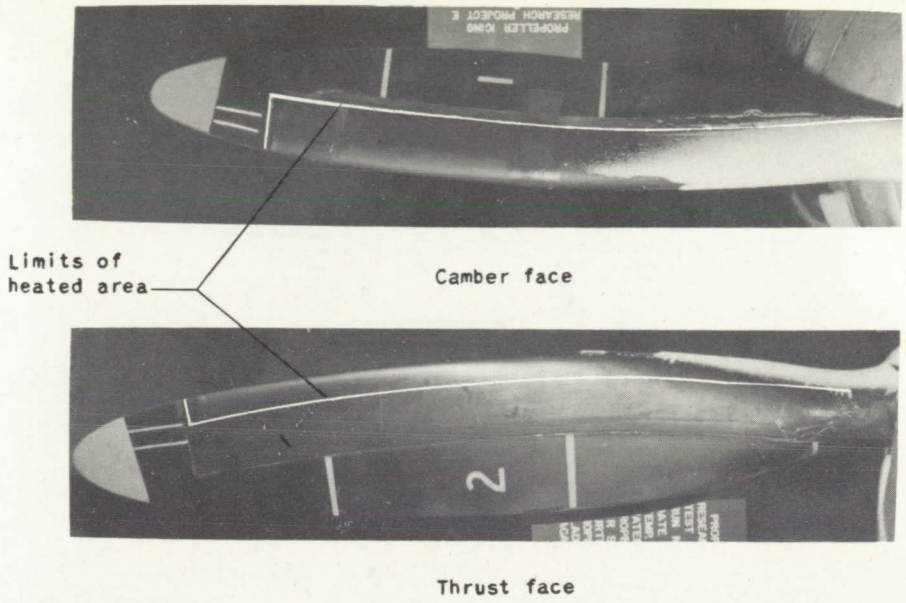


(a) Ambient-air temperature, 2° F; heat-on time, 12 seconds; cycle time, 96 seconds.

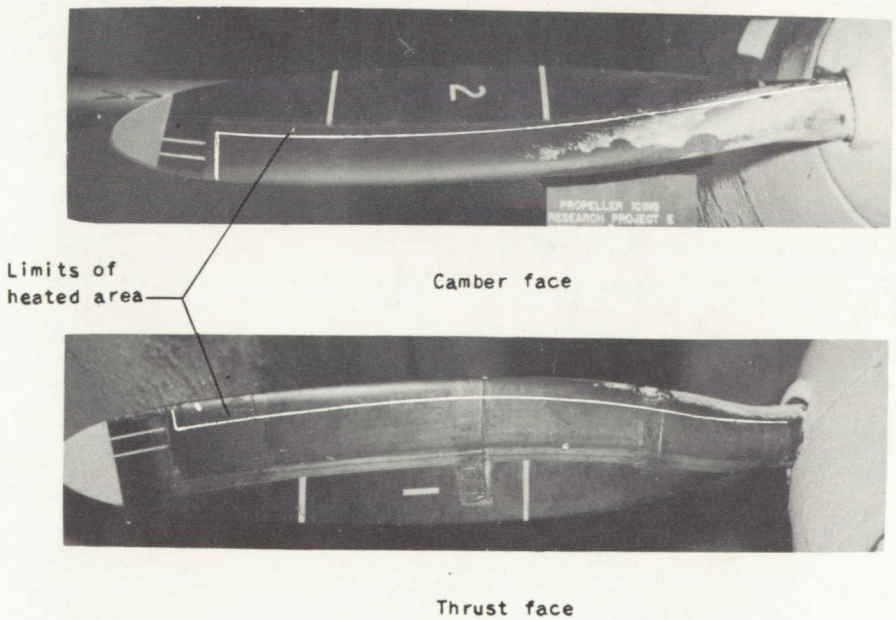


(b) Ambient-air temperature, 2° F; heat-on time, 24 seconds; cycle time, 96 seconds.

Figure 20. - Views of residual ice after cyclic de-icing with heating pattern 5. Propeller speed, 925 rpm.

Page intentionally left blank

Page intentionally left blank

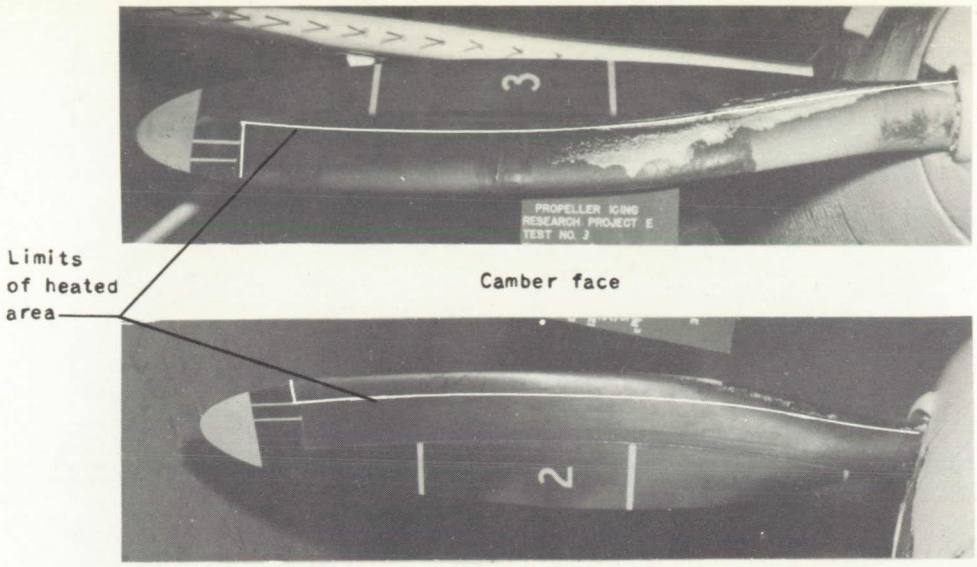


(c) Ambient-air temperature, 2° F; heat-on time, 23 seconds; cycle time, 184 seconds.

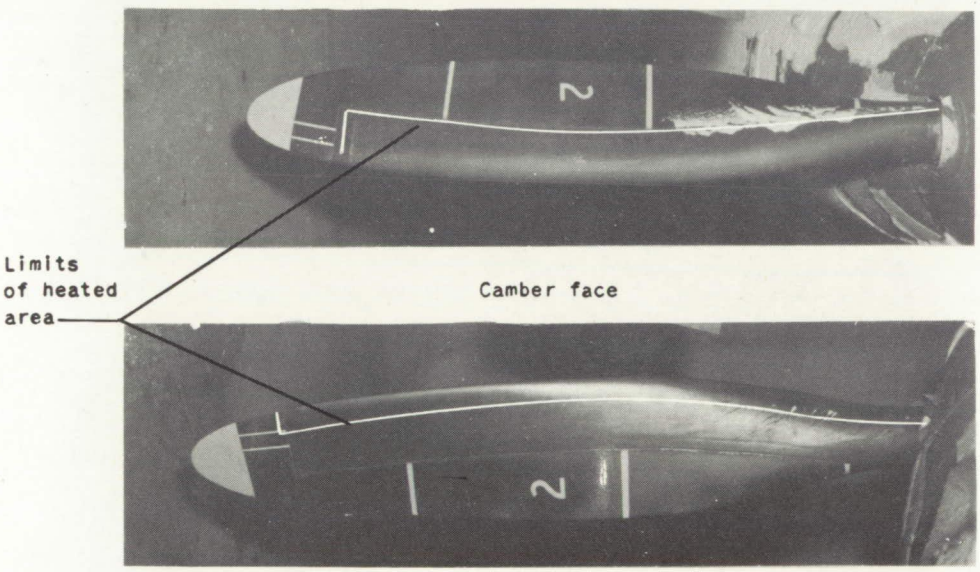


(d) Ambient-air temperature, 11° F; heat-on time, 23 seconds; cycle time, 184 seconds.

Figure 20. - Concluded. Views of residual ice after cyclic de-icing with heating pattern 5. Propeller speed, 925 rpm.

Page intentionally left blank

Page intentionally left blank

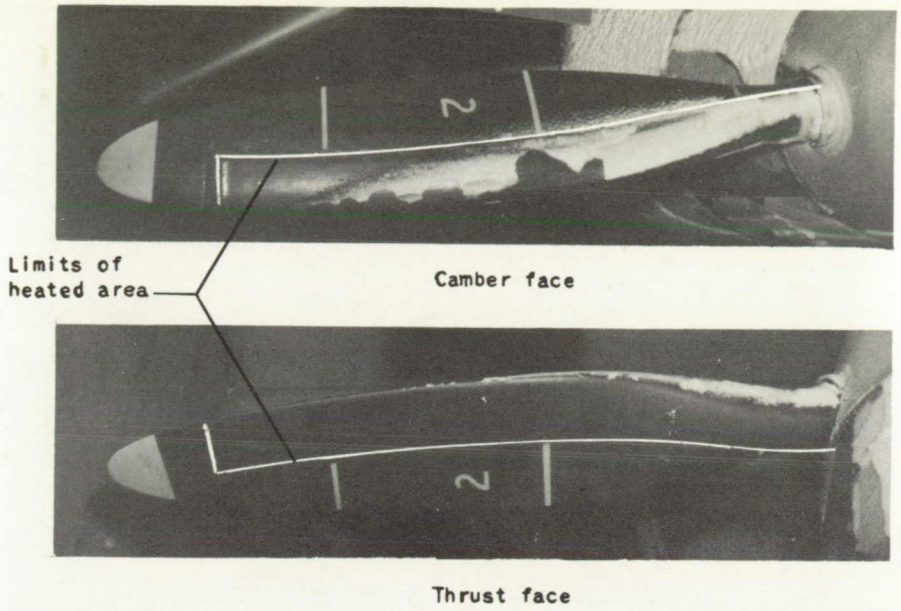


(a) Heating pattern 6.

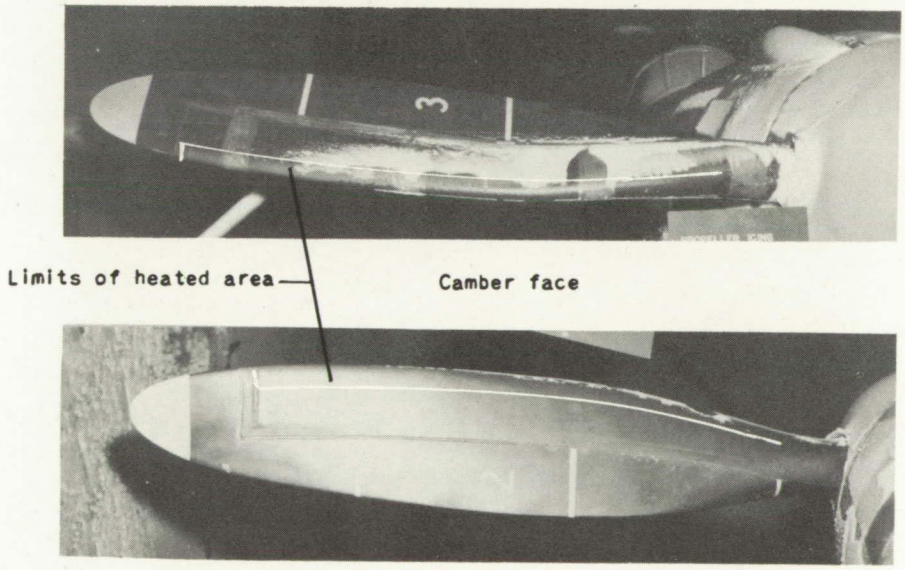


(b) Heating pattern 7.

Figure 21. - Views of residual ice after cyclic de-icing. Propeller speed, 925 rpm; ambient-air temperature, 11° F; heat-on time, 12 seconds; cycle time, 96 seconds.

Page intentionally left blank

Page intentionally left blank

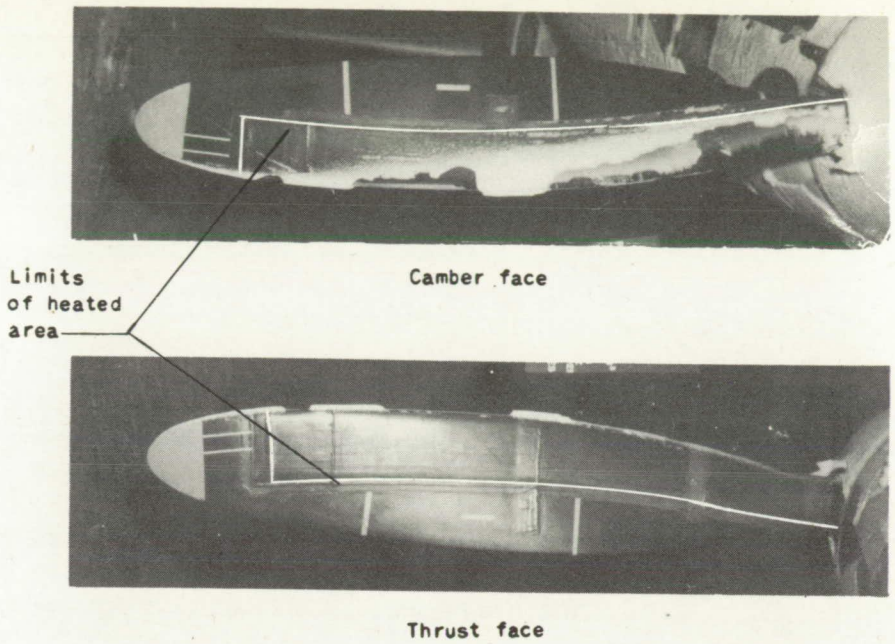


(a) Propeller speed, 675 rpm; heat-on time, 12 seconds; cycle time, 96 seconds.

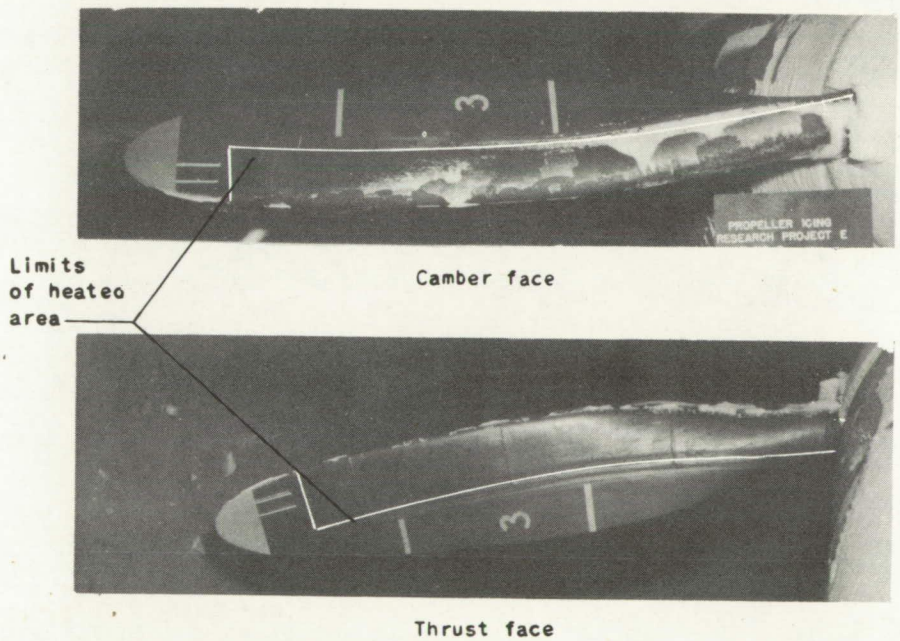


(b) Propeller speed, 675 rpm; heat-on time, 24 seconds; cycle time, 96 seconds.

Figure 22. - Views of residual ice after cyclic de-icing with heating pattern 8. Ambient-air temperature, 11° F.

Page intentionally left blank

Page intentionally left blank

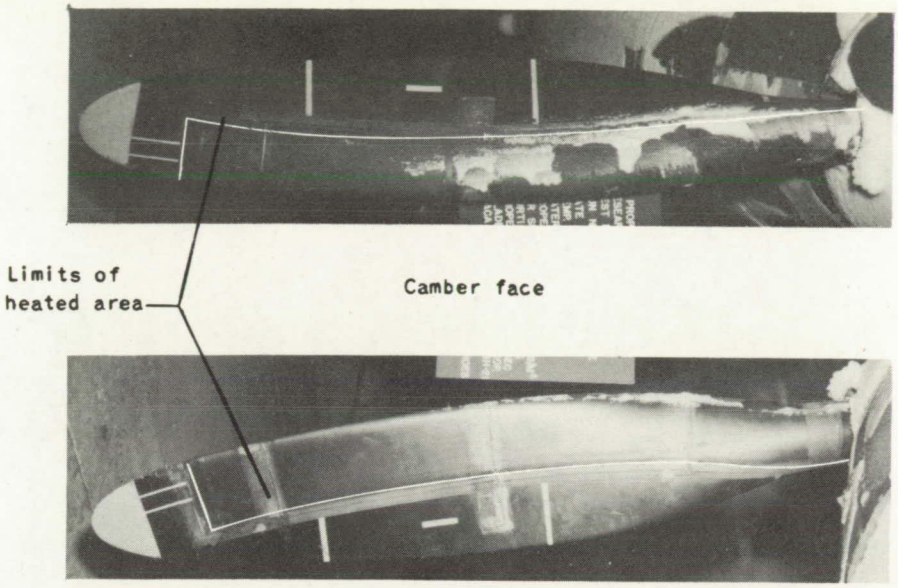


(c) Propeller speed, 925 rpm; heat-on time, 24 seconds; cycle time, 96 seconds.

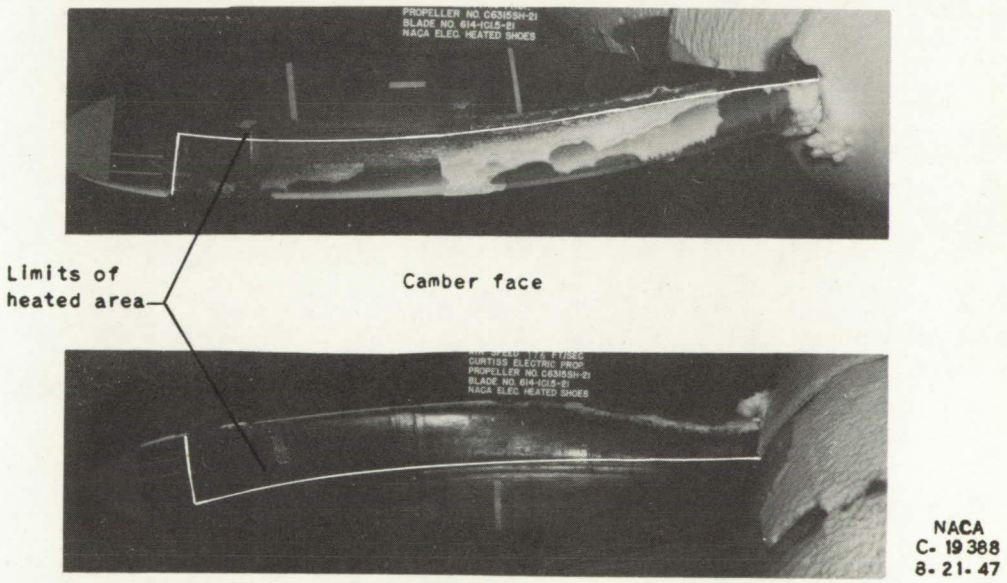


(d) Propeller speed, 675 rpm; heat-on time, 23 seconds; cycle time, 184 seconds.

Figure 22. - Continued. Views of residual ice after cyclic de-icing with heating pattern 8. Ambient-air temperature, 11° F.

Page intentionally left blank

Page intentionally left blank

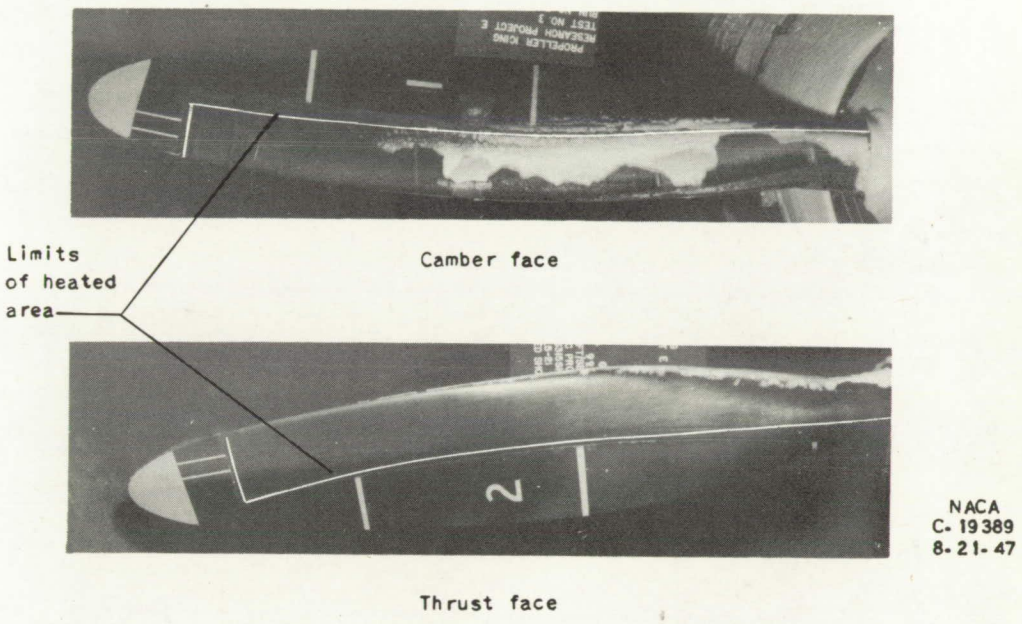


(e) Propeller speed, 925 rpm; heat-on time, 23 seconds; cycle time, 184 seconds.

Figure 22. - Concluded. Views of residual ice after cyclic de-icing with heating pattern 8. Ambient-air temperature, 11° F.

Page intentionally left blank

Page intentionally left blank

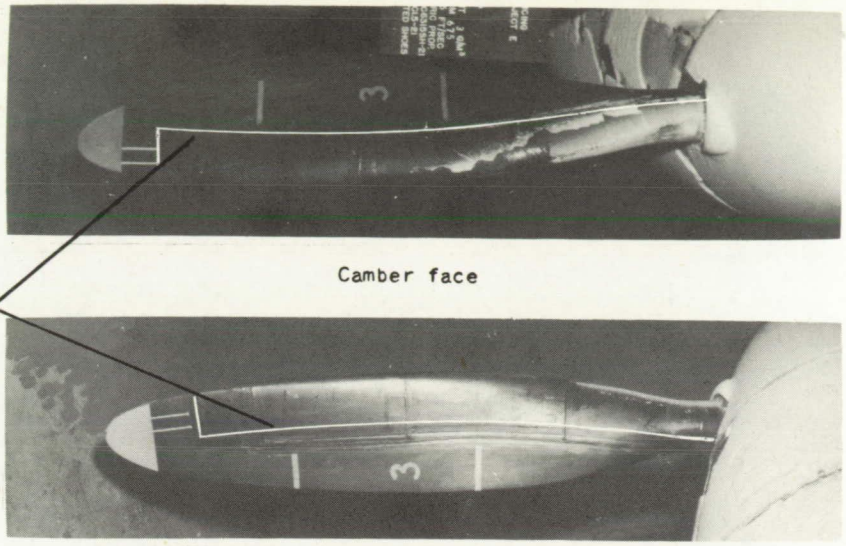


(a) Propeller speed, 675 rpm; ambient-air temperature, 2° F; heat-on time, 24 seconds; cycle time, 96 seconds.

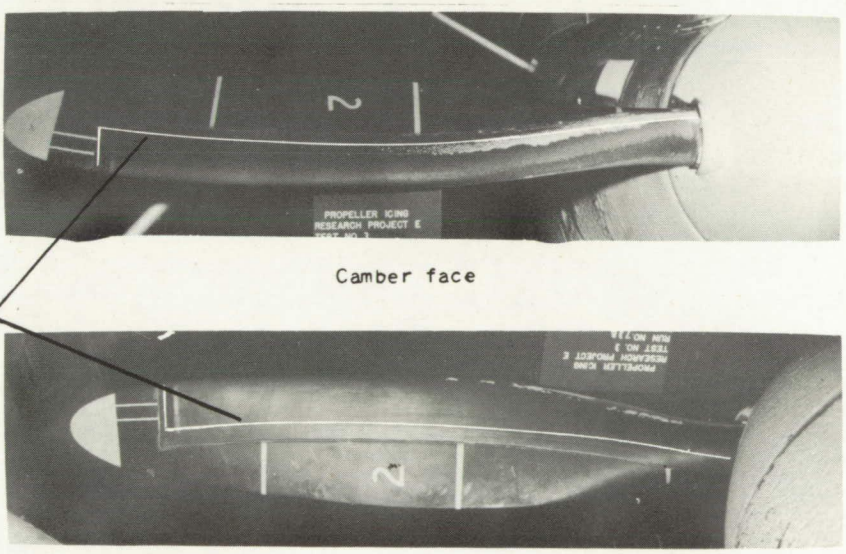


(b) Propeller speed, 925 rpm; ambient-air temperature, 2° F; heat-on time, 24 seconds; cycle time, 96 seconds.

Figure 23. - Views of residual ice after cyclic de-icing with heating pattern 9.

Page intentionally left blank

Page intentionally left blank

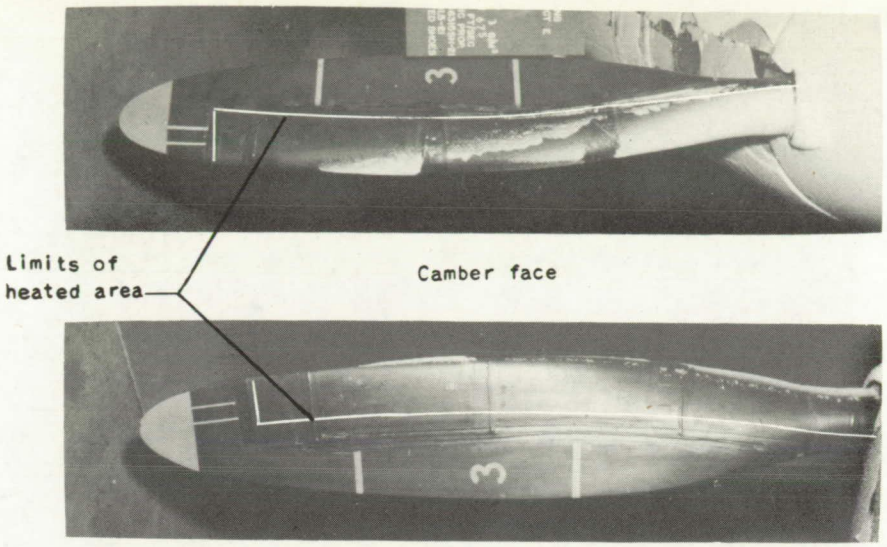


(c) Propeller speed, 675 rpm; ambient-air temperature, 2° F; heat-on time, 23 seconds; cycle time, 184 seconds.

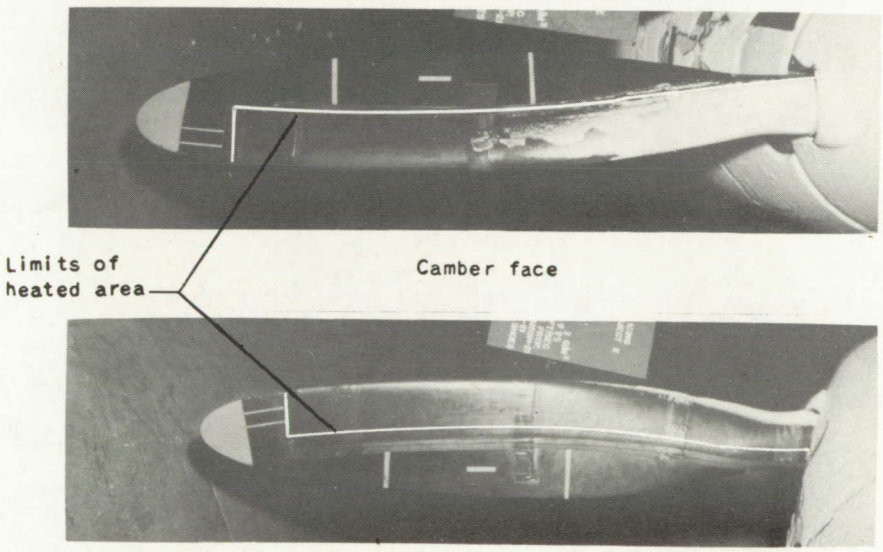


(d) Propeller speed, 925 rpm; ambient-air temperature, 2° F; heat-on time, 23 seconds; cycle time, 184 seconds.

Figure 23. - Continued. Views of residual ice after cyclic de-icing with heating pattern 9.

Page intentionally left blank

Page intentionally left blank

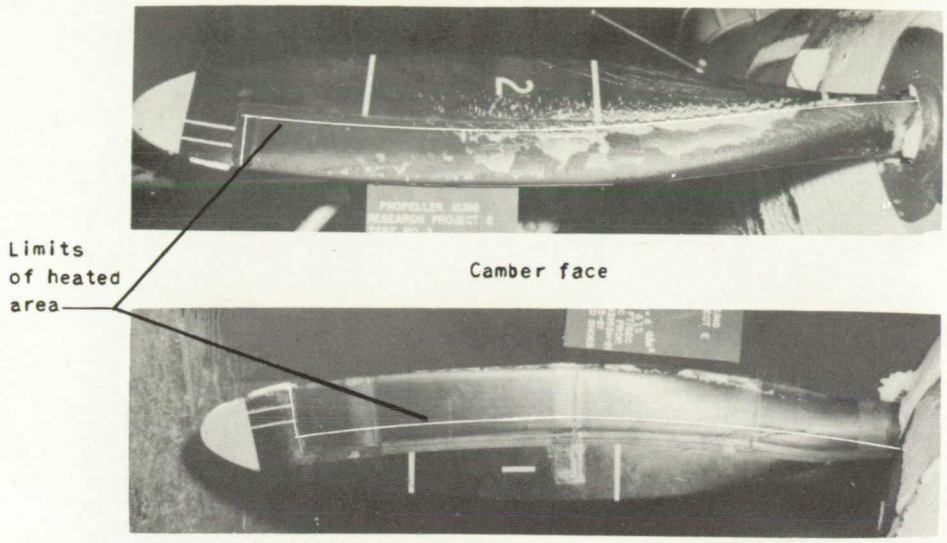


(e) Propeller speed, 675 rpm; ambient-air temperature, 11° F; heat-on time, 24 seconds; cycle time, 96 seconds.

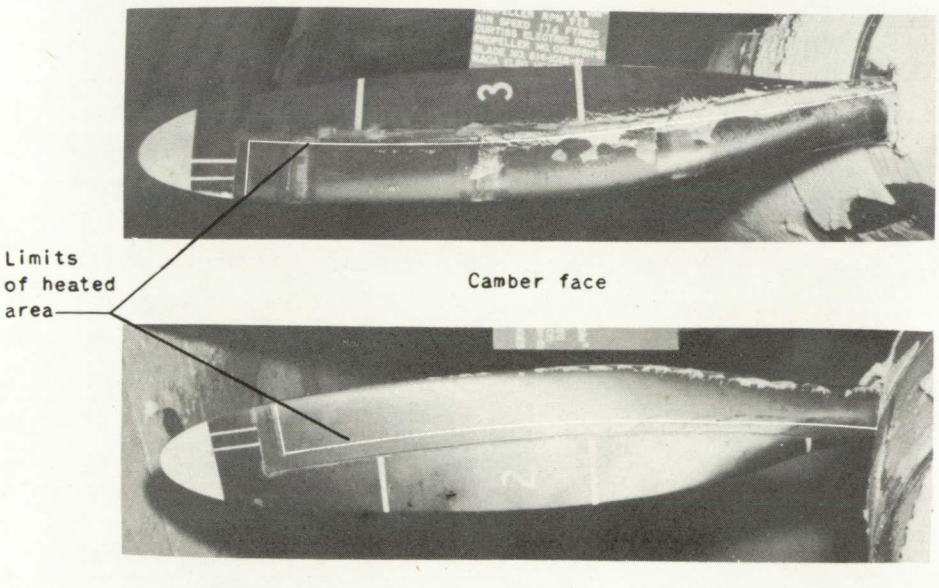


(f) Propeller speed, 925 rpm; ambient-air temperature, 11° F; heat-on time, 24 seconds; cycle time, 96 seconds.

Figure 23. - Continued. Views of residual ice after cyclic de-icing with heating pattern 9.

Page intentionally left blank

Page intentionally left blank

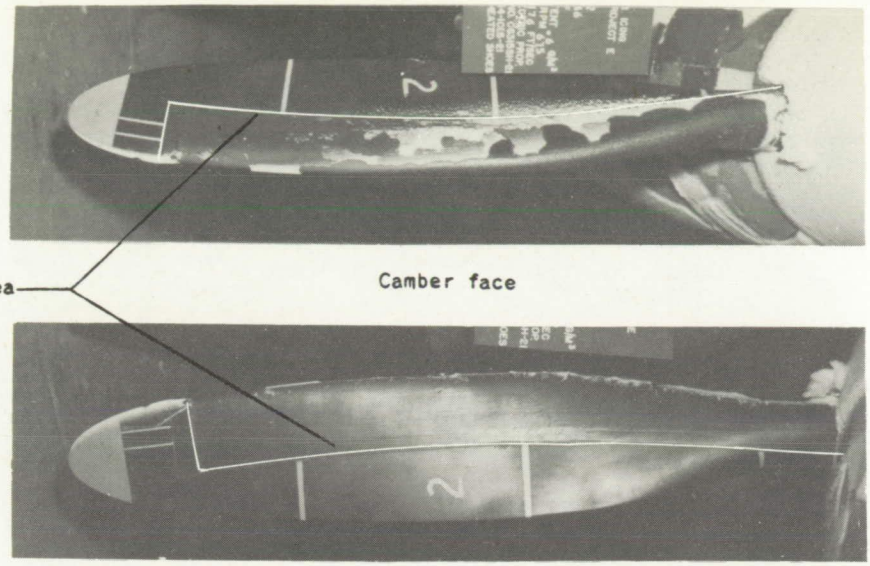

Limits of heated area

Camber face



Thrust face

(g) Propeller speed, 675 rpm; ambient-air temperature, 11° F; heat-on time, 23 seconds; cycle time, 184 seconds.

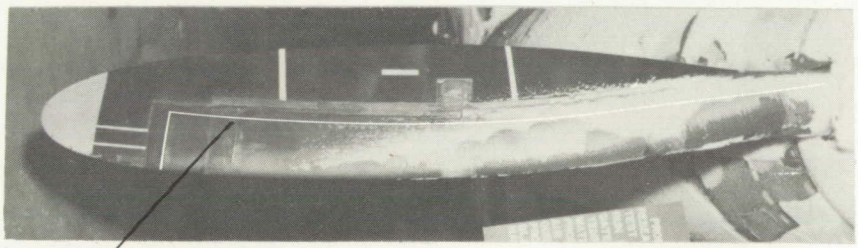

Limits of heated area

Camber face

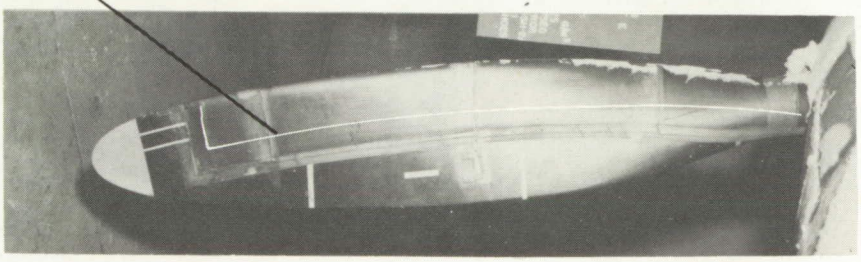

NACA C-19393 8-21-47

Thrust face

(h) Propeller speed, 925 rpm; ambient-air temperature, 11° F; heat-on time, 23 seconds; cycle time, 184 seconds.

Figure 23. - Concluded. Views of residual ice after cyclic de-icing with heating pattern 9.

Page intentionally left blank

Page intentionally left blank

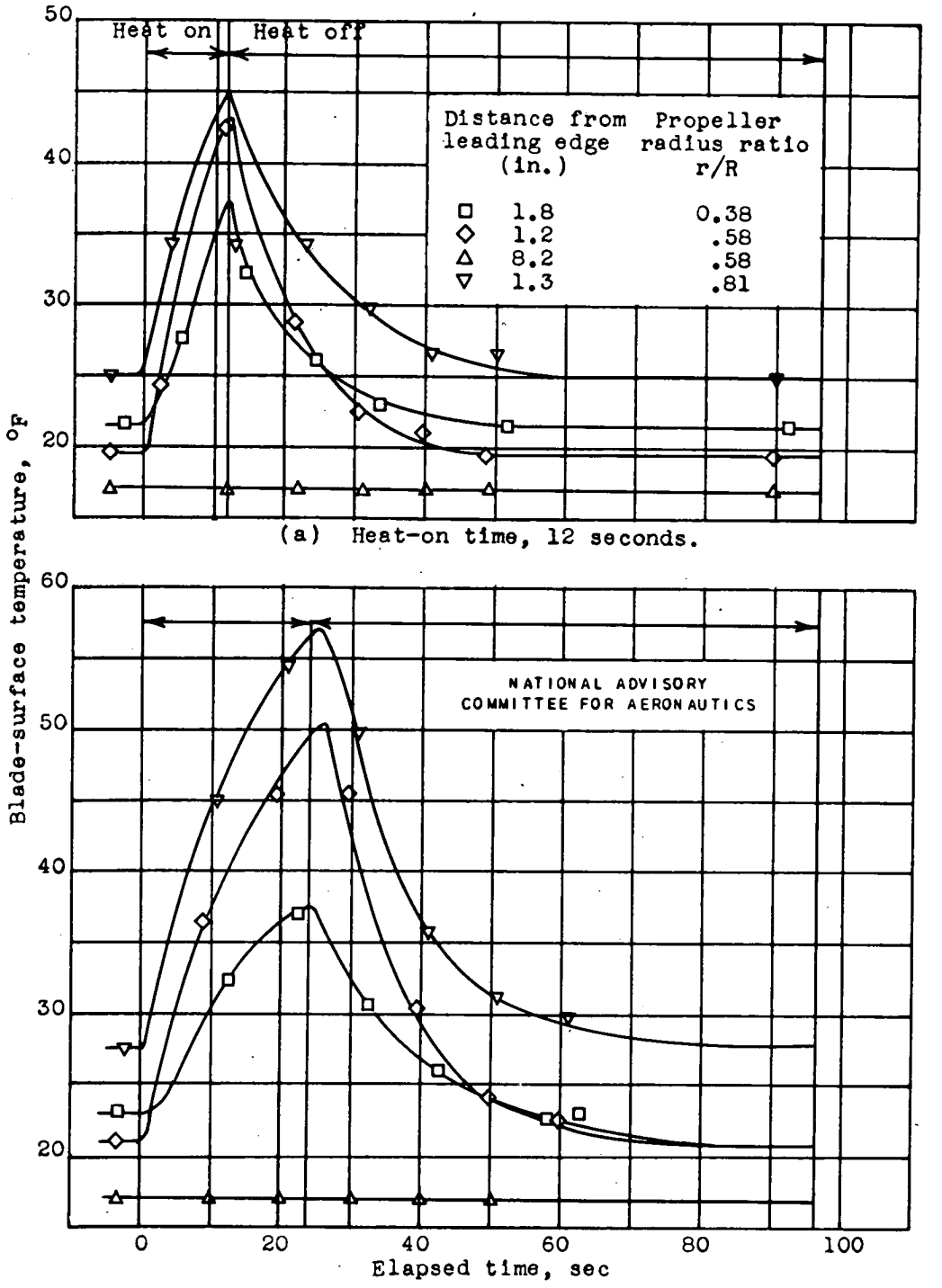


Figure 24. - Variation of blade-surface temperature with time on thrust face during cyclic de-icing. Heating pattern 5; propeller speed, 925 rpm; ambient-air temperature, 2° F; cycle time, 96 seconds.

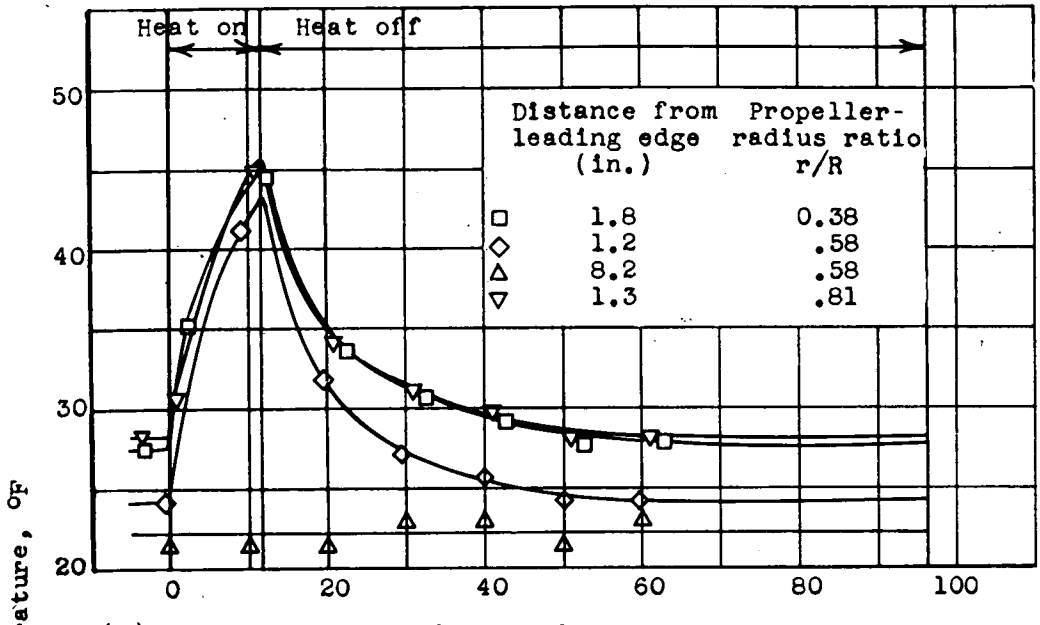


(a) Heating pattern 8; propeller speed, 675 rpm; heat-on time, 12 seconds; cycle time, 96 seconds.

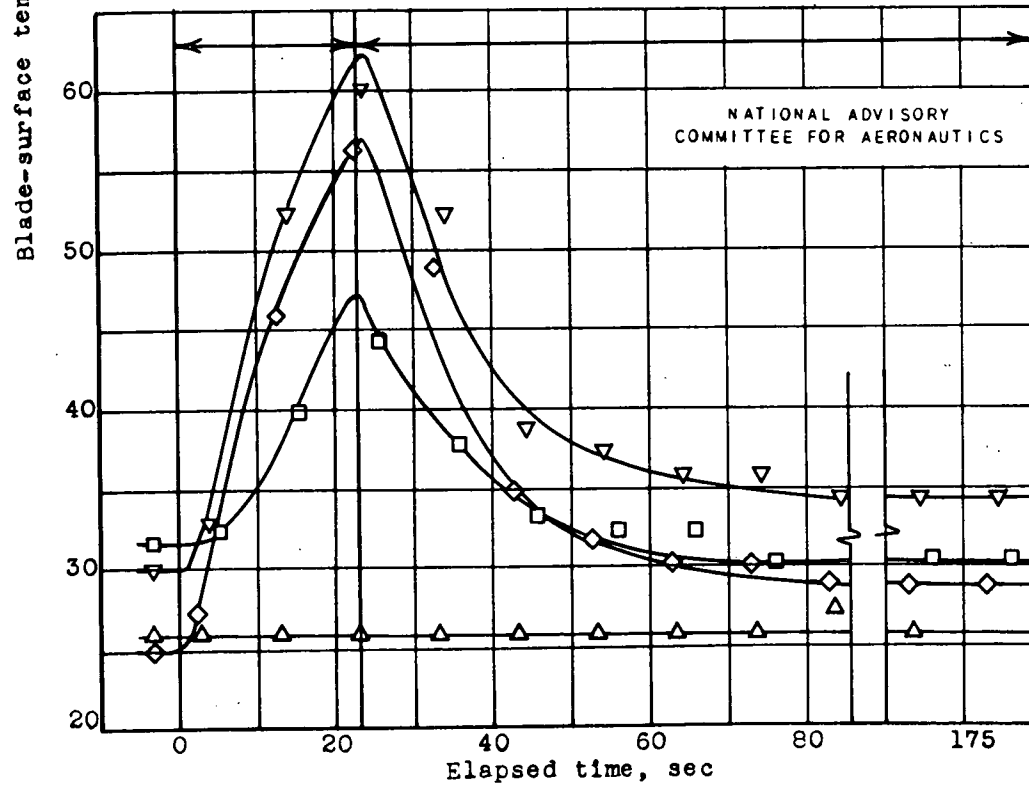


(b) Heating pattern 5; propeller speed, 925 rpm; heat-on time, 23 seconds; cycle time, 184 seconds.

Figure 25. - Variation of blade-surface temperature with time on thrust face during cyclic de-icing for two heating patterns. Ambient-air temperature, 11° F.

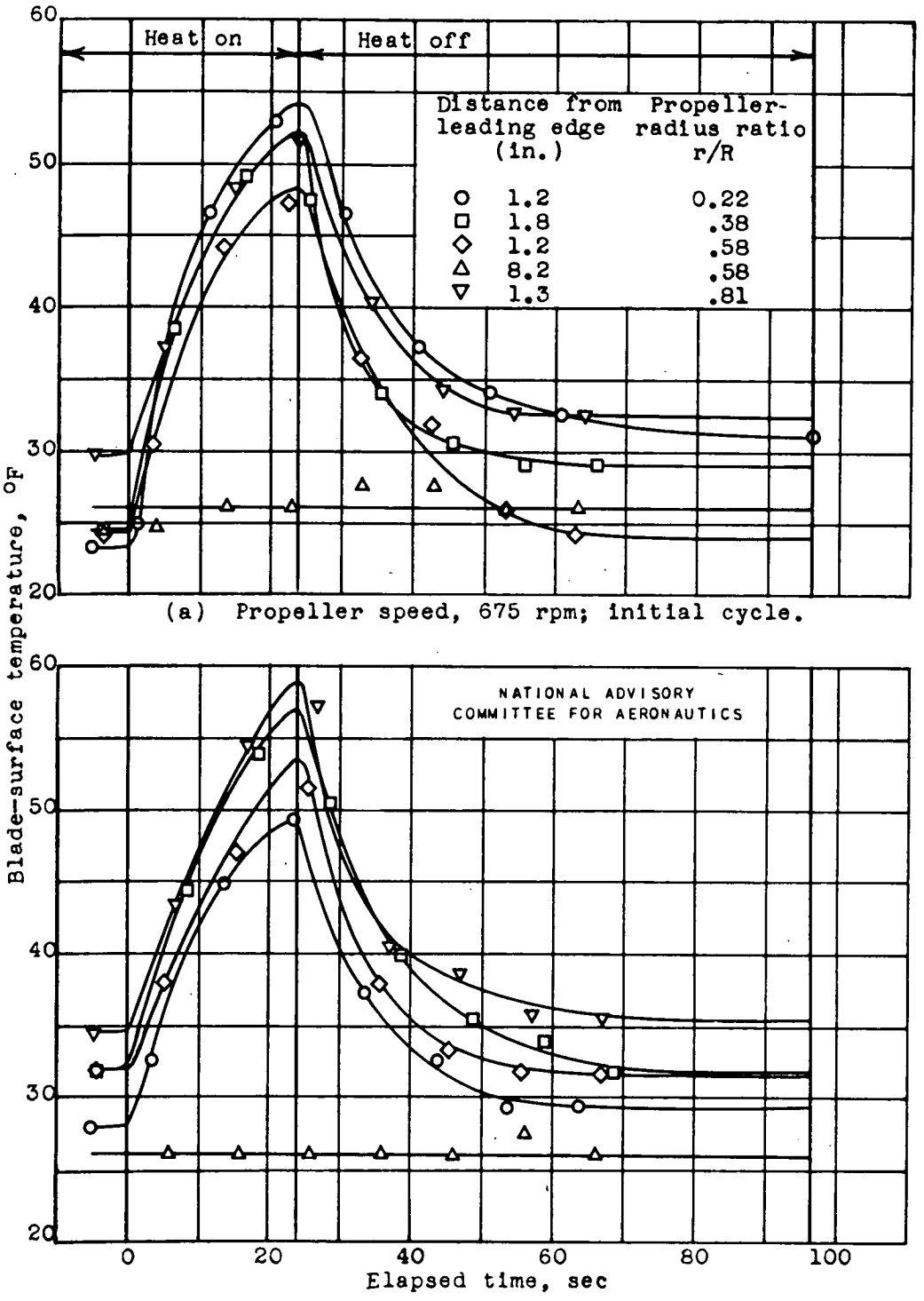


(a) Propeller speed, 675 rpm; initial cycle.

(b) Propeller speed, 925 rpm.

Figure 26. - Variation of blade-surface temperature with time on thrust face during cyclic de-icing. Heating pattern 8; ambient-air temperature, 11° F; heat-on time, 24 seconds; cycle time, 96 seconds.

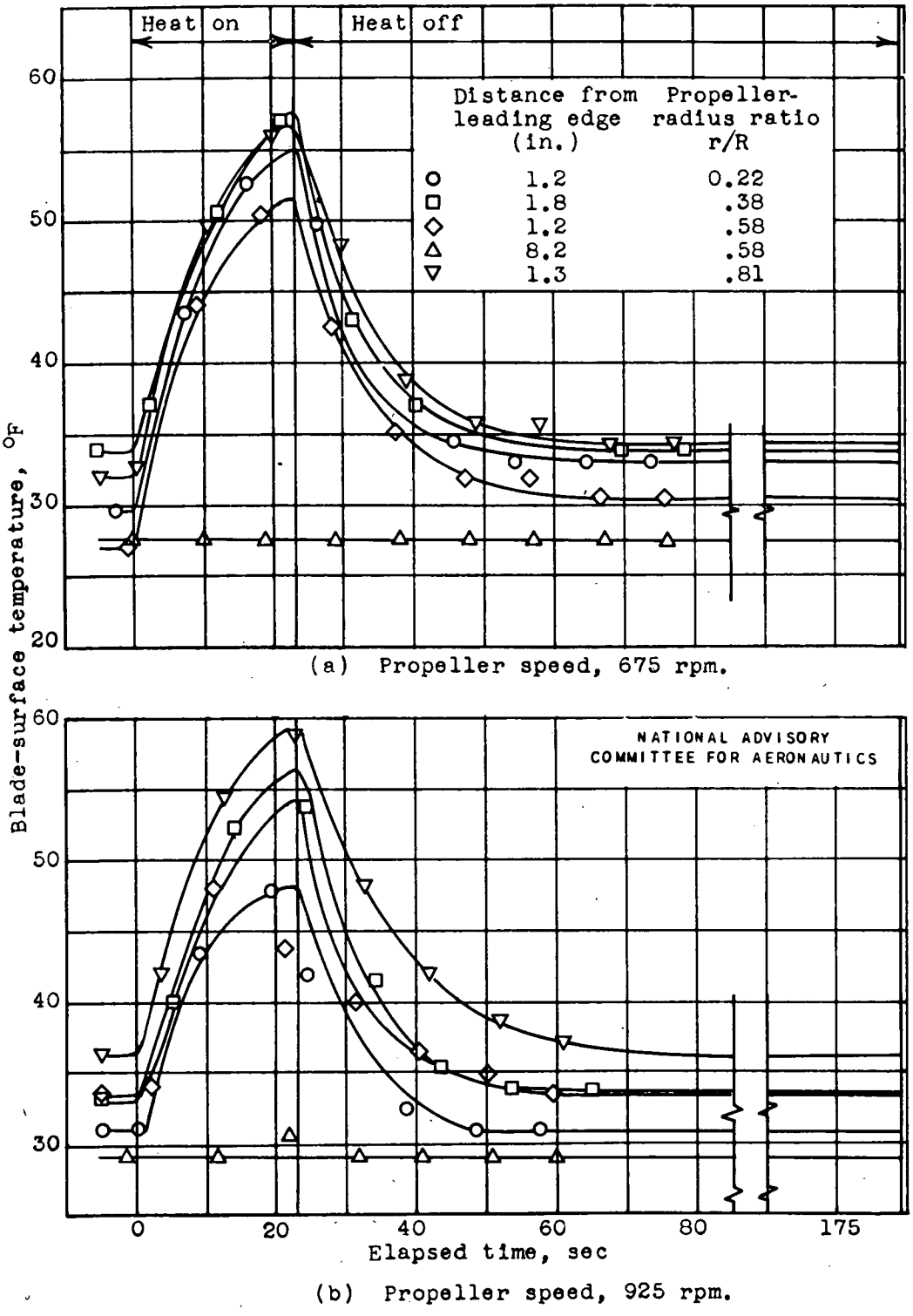


Figure 27. - Variation of blade-surface temperature with time on thrust face during cyclic de-icing. Heating pattern 8; ambient-air temperature, 11° F; heat-on time, 23 seconds; cycle time, 184 seconds.

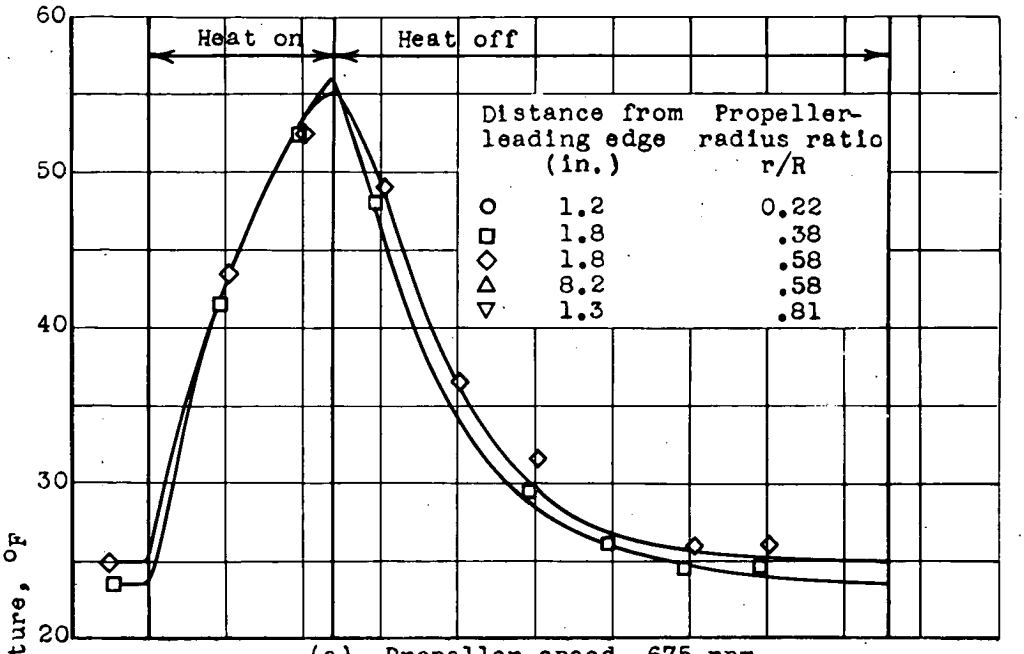


(a) Propeller speed, 675 rpm.

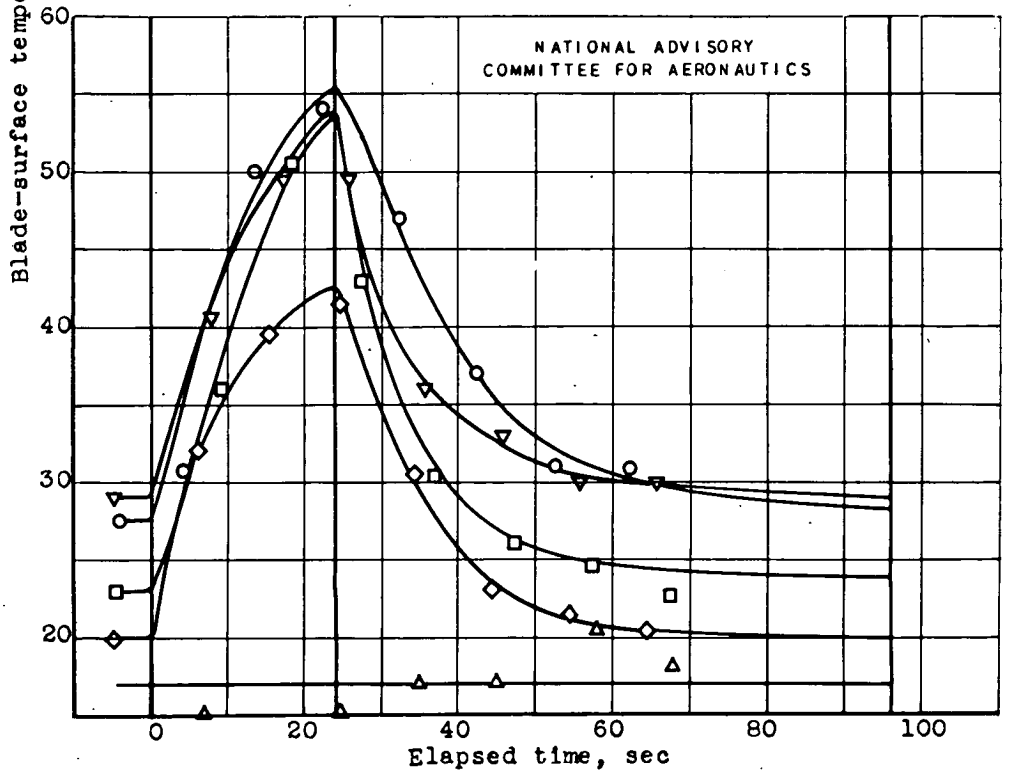


(b) Propeller speed, 925 rpm.

Figure 28. - Variation of blade-surface temperature with time on thrust face during cyclic de-icing. Heating pattern 9; ambient-air temperature, 2° F; heat-on time, 24 seconds; cycle time, 96 seconds.

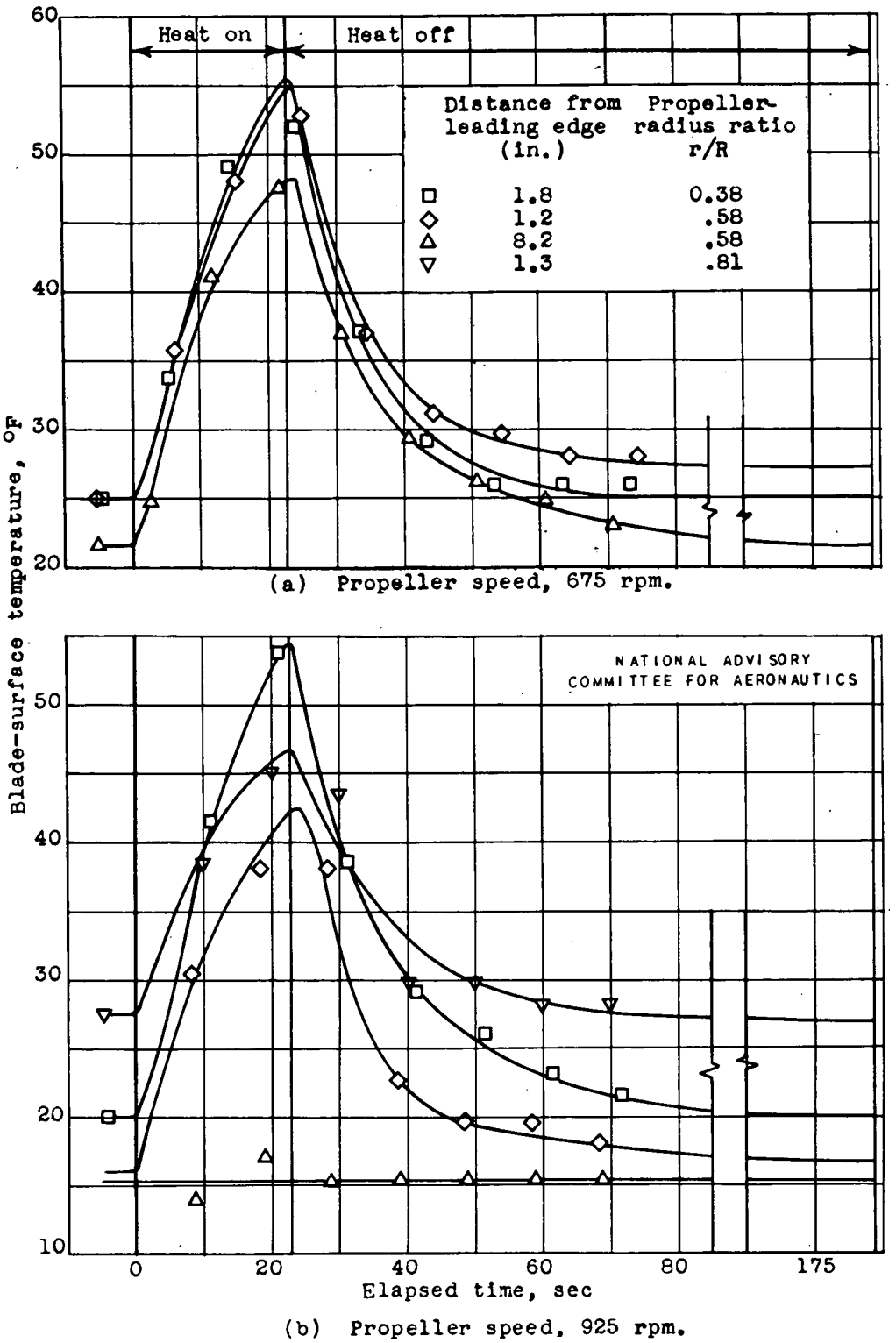


Figure 29. - Variation of blade-surface temperature with time on thrust face during cyclic de-icing. Heating pattern 9; ambient-air temperature, 2° F; heat-on time, 23 seconds; cycle time, 184 seconds.

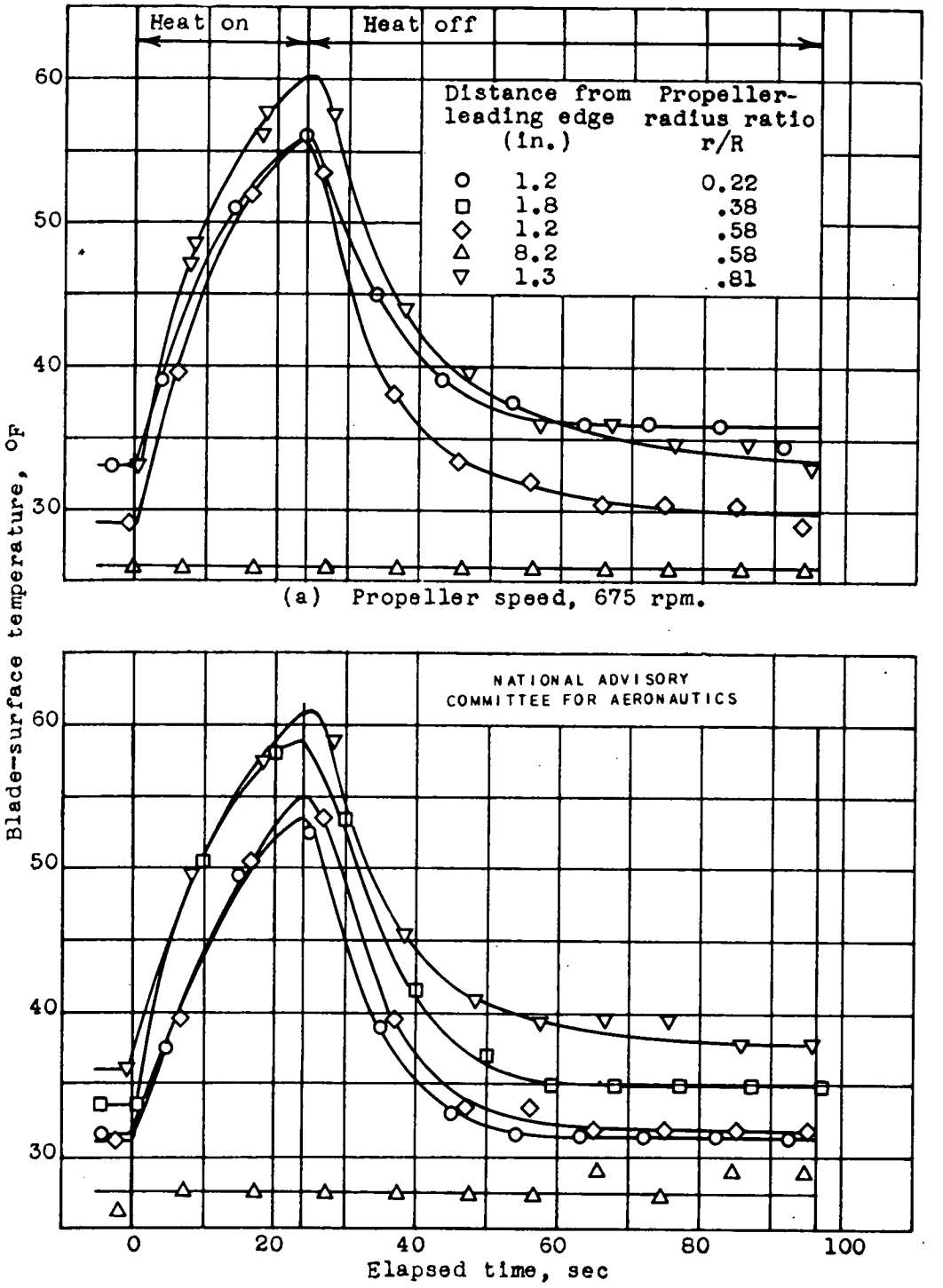


Figure 30. - Variation of blade-surface temperature with time on thrust face during cyclic de-icing. Heating pattern 9; ambient-air temperature, 11° F; heat-on time, 24 seconds; cycle time, 96 seconds.

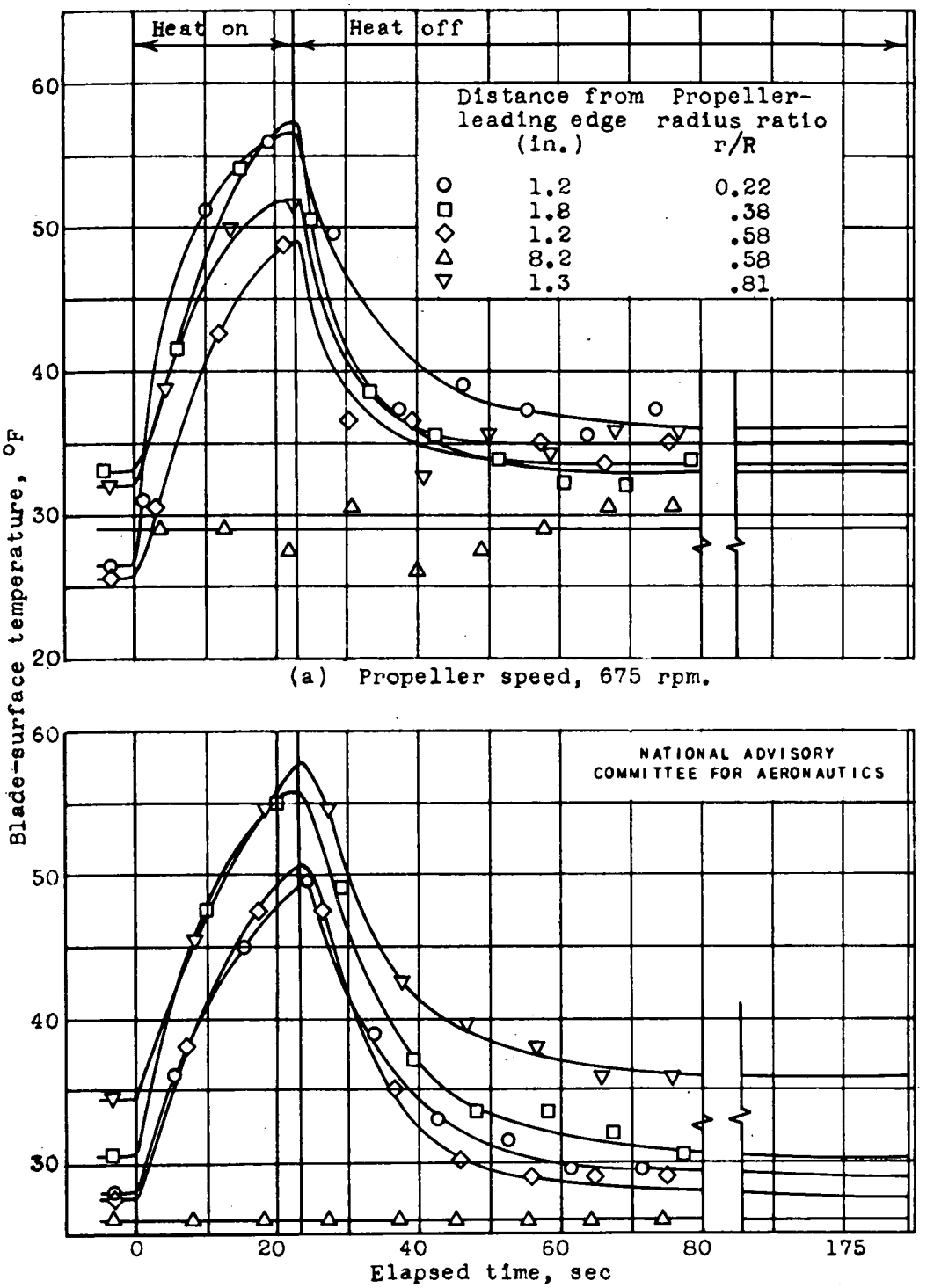


Figure 31. - Variation of blade-surface temperature with time on thrust face during cyclic de-icing. Heating pattern 9; ambient-air temperature, 11° F; heat-on time, 23 seconds; cycle time, 184 seconds.

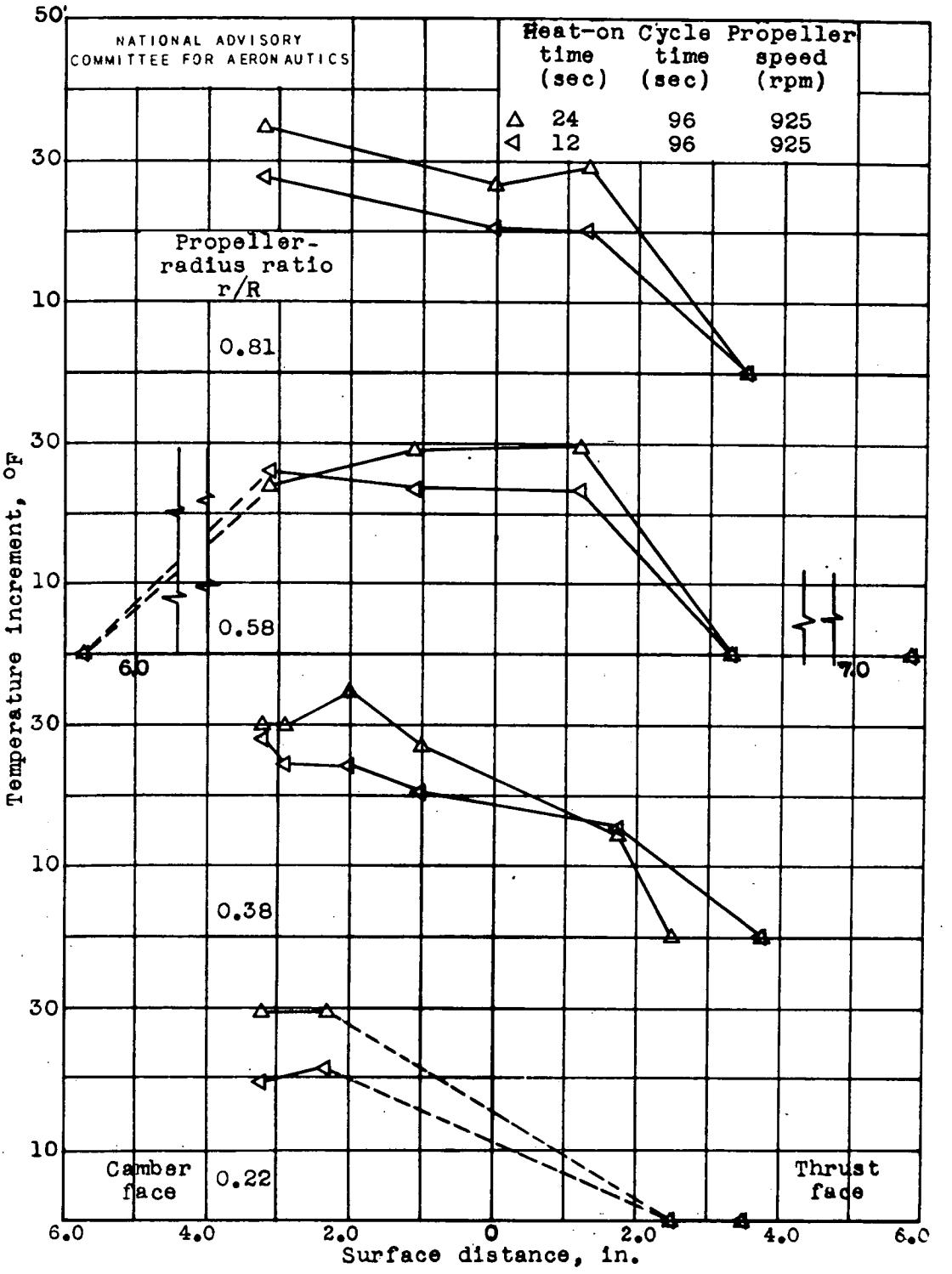


(a) Heating pattern 5; ambient-air temperature, 2° F.

Figure 32. - Variation of blade-surface temperature increment with chordwise surface distance.

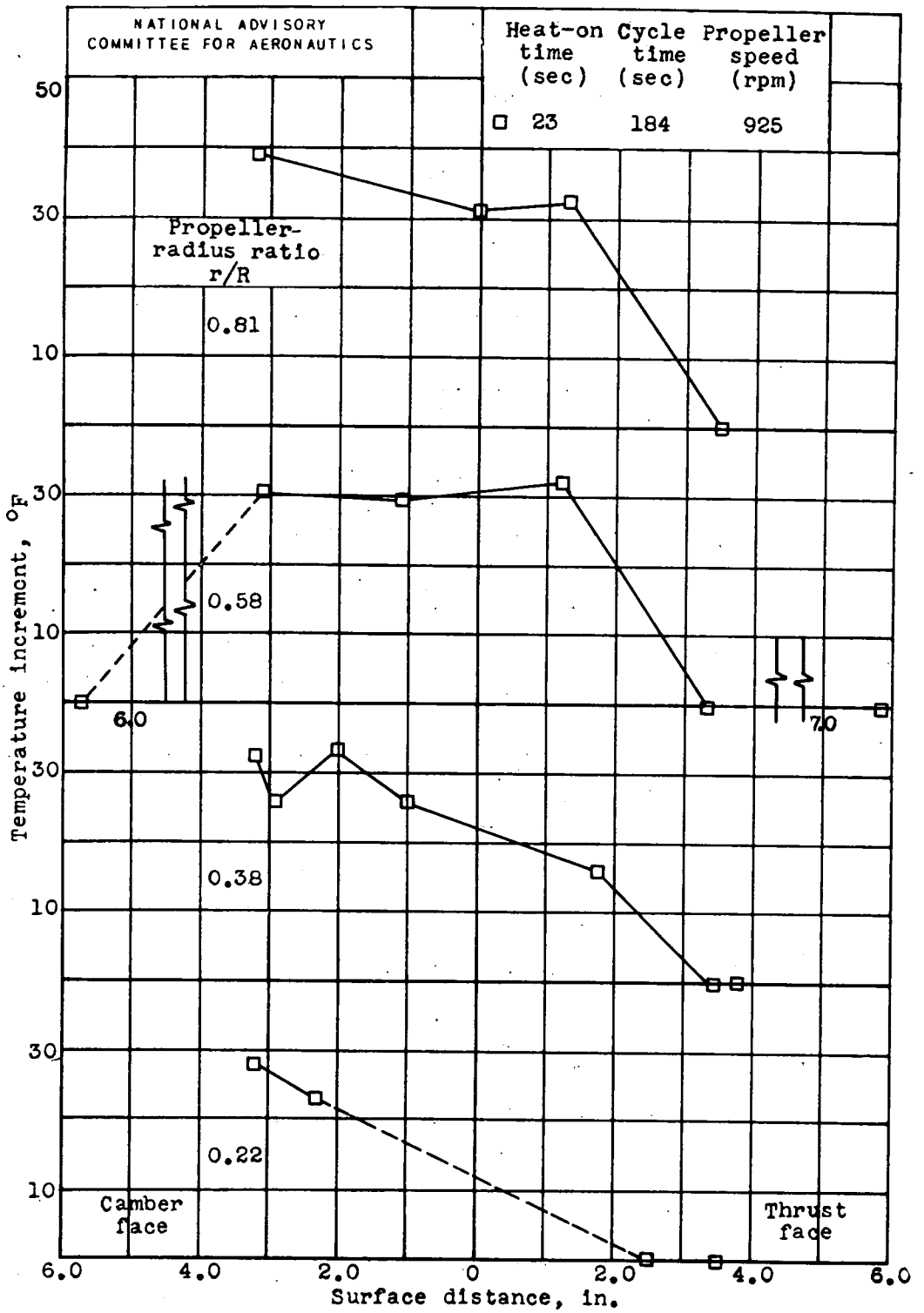


(b) Heating pattern 5; ambient-air temperature, 11° F.

Figure 32. - Continued. Variation of blade-surface temperature increment with chordwise surface distance.

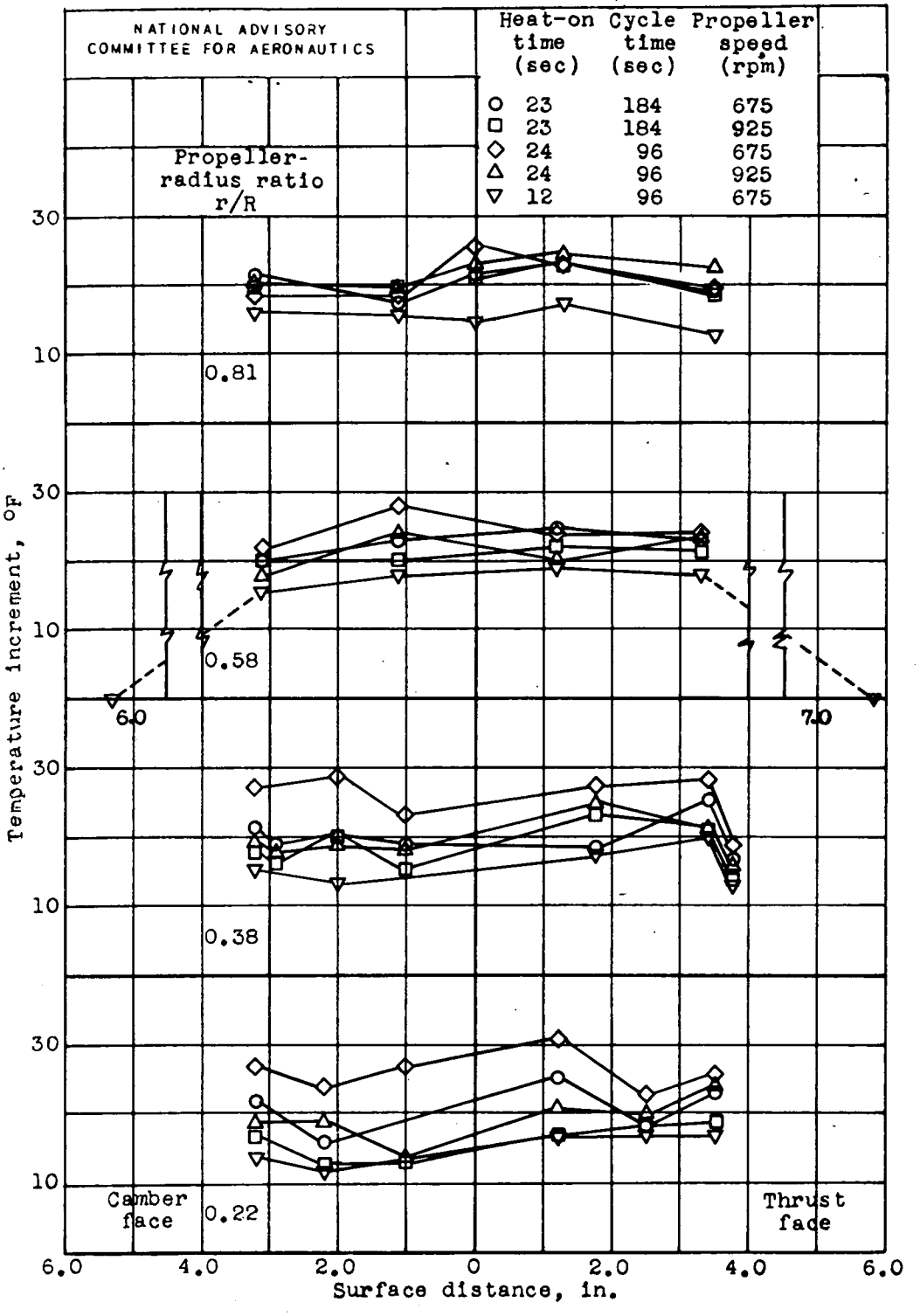


(c) Heating pattern 8; ambient-air temperature, 11° F.

Figure 32. - Continued. Variation of blade-surface temperature increment with chordwise surface distance.

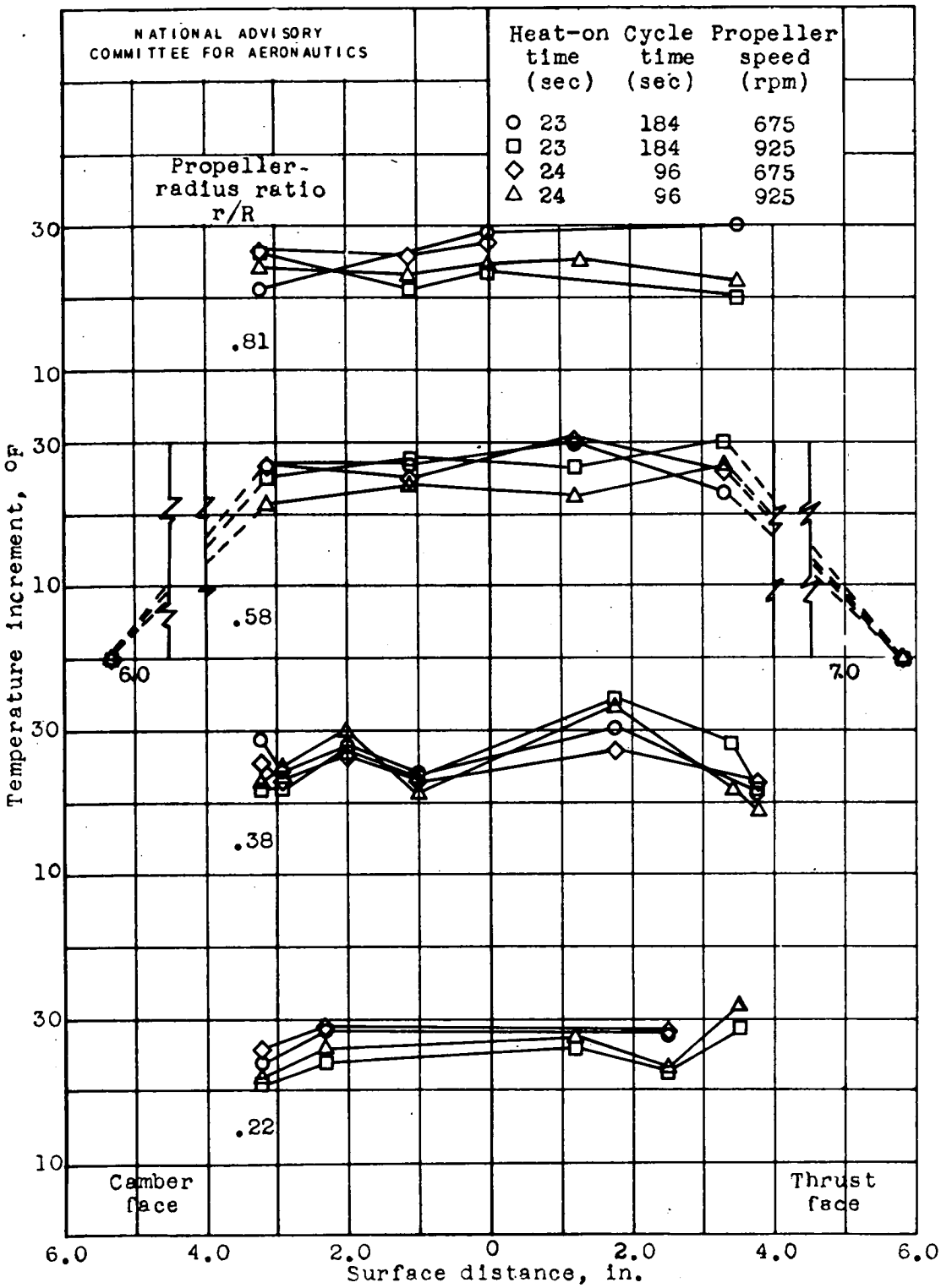


(d) Heating pattern 9; ambient-air temperature, 2° F.

Figure 32. - Continued. Variation of blade-surface temperature increment with chordwise surface distance.

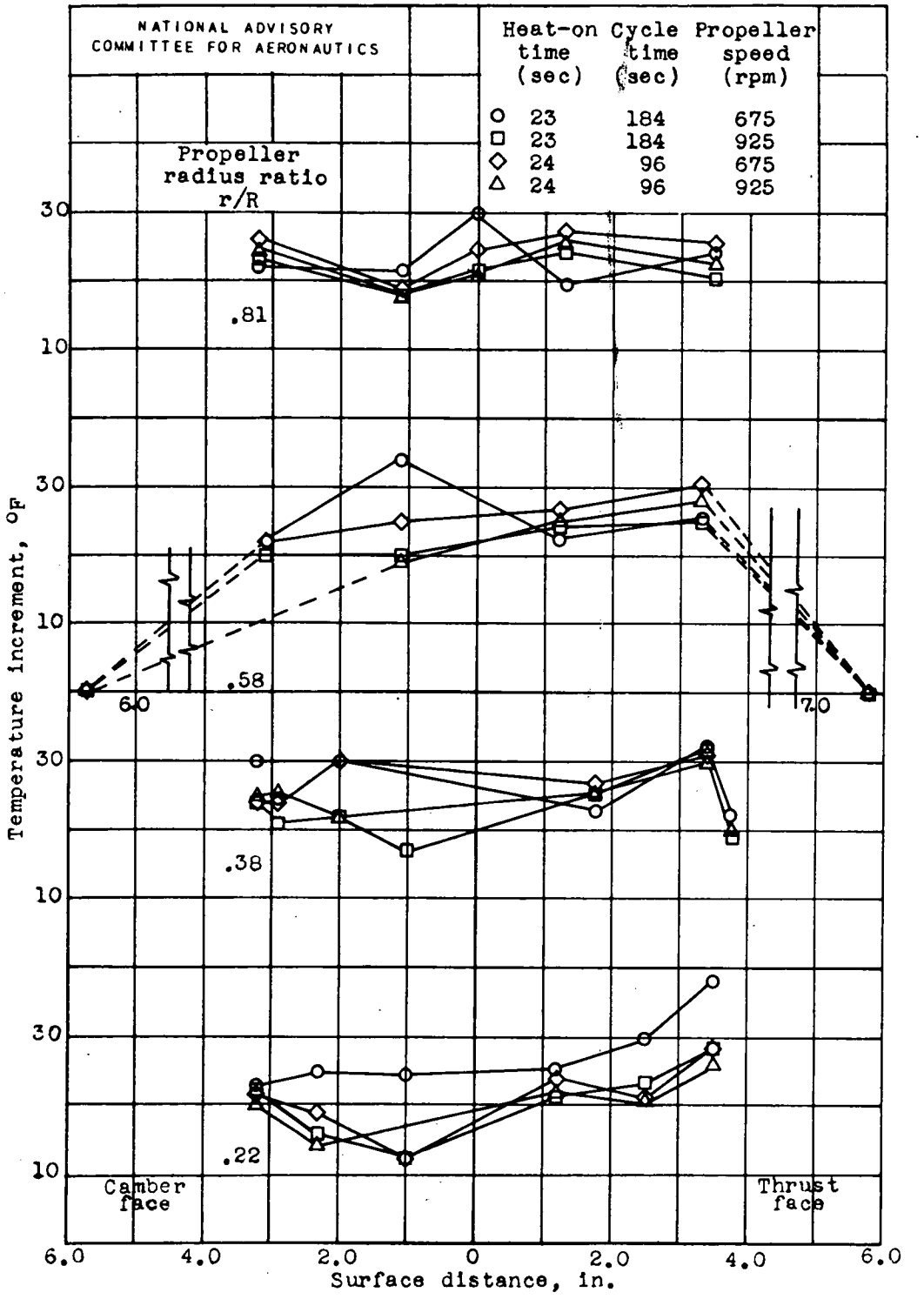


(e) Heating pattern 9; ambient-air temperature, 11° F.

Figure 32. - Concluded. Variation of blade-surface temperature increment with chordwise surface distance.

Page intentionally left blank

Page intentionally left blank

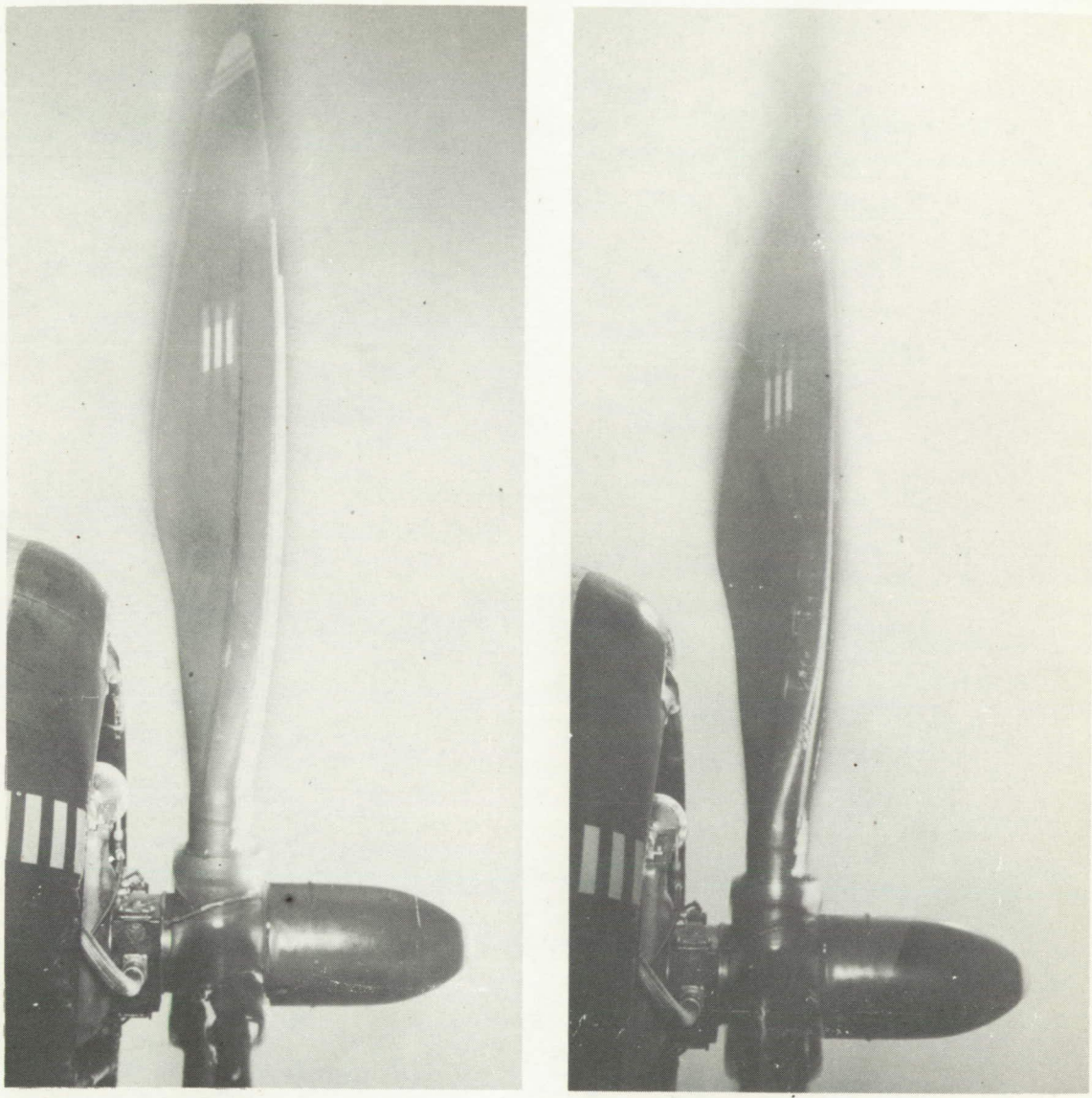

(a) Ice formation obtained after 8 minutes of icing.

(b) De-icing obtained at 1470 watts per blade.

NACA
C-19395
8-21-47

Figure 33. - Icing and de-icing obtained in flight at true airspeed of 190 miles per hour. Propeller speed, 955 rpm; ambient-air temperature, -10° F; liquid-water concentration, 0.1 gram per cubic meter; blade angle, 35°; droplet size, 11 microns.

Page intentionally left blank

Page intentionally left blank

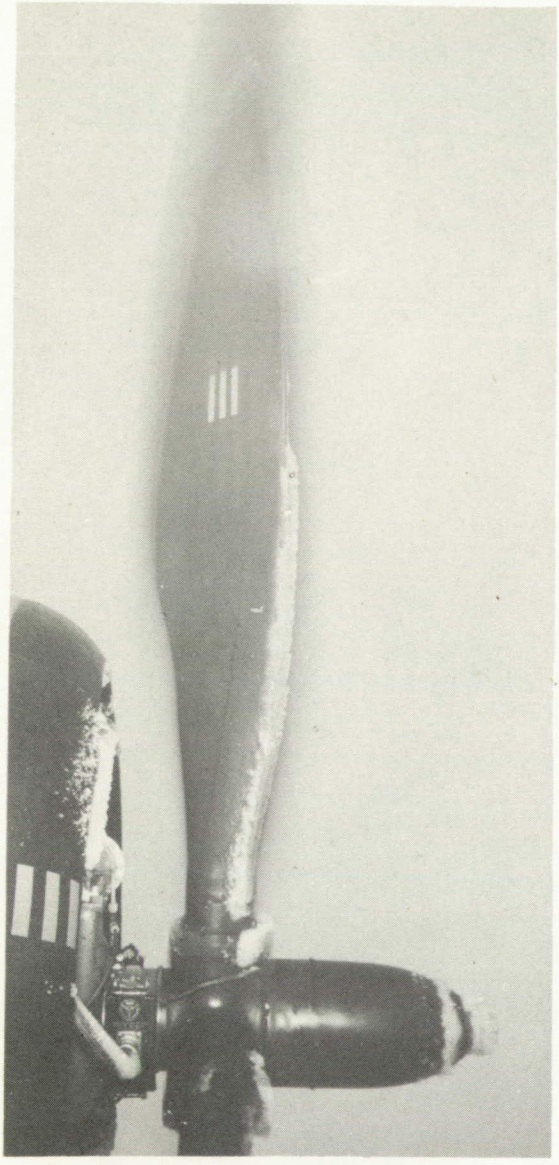

(a) Ice formation obtained after 16 minutes of icing.

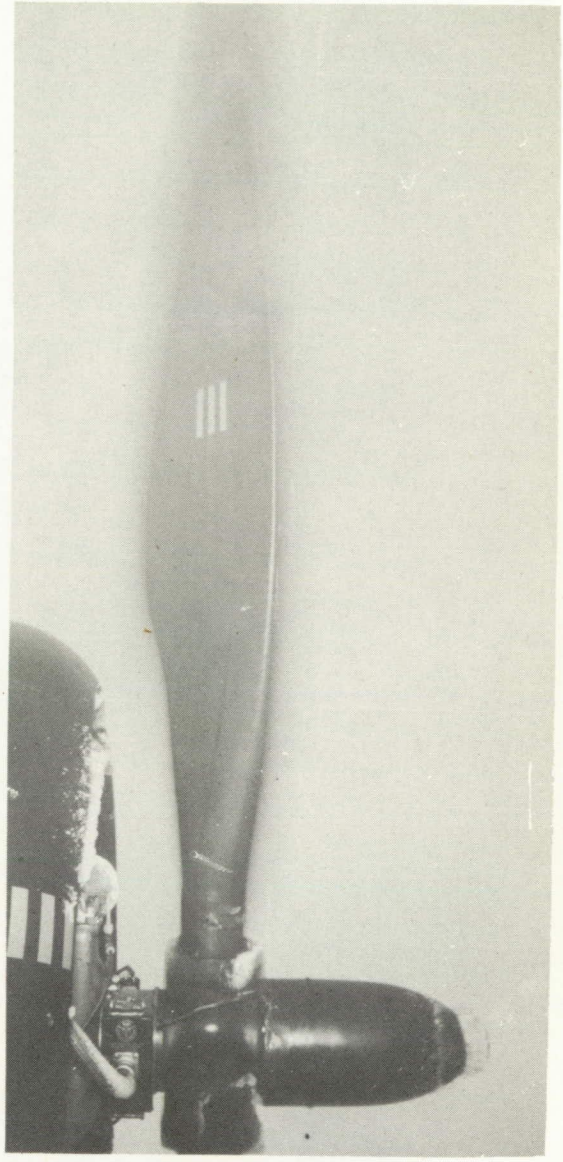

(b) De-icing obtained at 1470 watts per square inch.

NACA
C-19394
8-21-47

Figure 34. - Icing and de-icing obtained in flight at true airspeed of 213 miles per hour. Propeller speed, 1070 rpm; ambient-air temperature, 25° F; liquid-water concentration, 0.2 gram per cubic meter; blade angle, 34°; droplet size, 18 microns.